Photocopy and Use Authorization

In presenting this thesis in partial fulfillment of the requirements for an advanced degree at Idaho State University, I agree that the Library shall make it freely available for inspection. I further state that permission for extensive copying of my thesis for scholarly purposes may be granted by the Dean of the Graduate School, Dean of my academic division, or by the University Librarian. It is understood that any copying or publication of this thesis for financial gain shall not be allowed without my written permission.

_____

Kean Martinic

_____

Date

The Appropriateness of Electron Accelerators as Applied to Space Reactors, A LEU Adaptation of the Kilowatt Reactor Using Stirling Technology (KRUSTY)

by

Kean Martinic

A thesis

Submitted in partial fulfillment

of the requirements for the degree of

Master of Science in the Department of Nuclear

Engineering

Idaho State University

Fall 2021

To the Graduate Faculty:

The members of the committee appointed to examine the thesis of Kean Martinic find it satisfactory and recommend that it be accepted.

_____

Dr. George Imel,

Major Advisor

_____

Dr. Carlos Maidana,

Committee Member

_____

Dr. Erdinch Tatar,

Committee Member

Acknowledgements:

I would like to thank Dr. Imel for his patience and guidance throughout my thesis research. Dr. Imel played a vital role in my understanding of the mathematics involved in this thesis and provided thought provoking insight along the way. Thanks again for allowing me to pursue my own research topic. I look forward to discussing the future direction of this continued research.

A big thanks to Dr. Maidana for supplementing my research with relevant literature. Dr. Maidana kept me updated on the latest uses of electron accelerator driven systems and ensured I was versed in the major takeaways from previous EADS experiments. Dr. Maidana also provided insight into particle beam terminology, dynamics and optimization helping ensure this thesis considered these parameters appropriately. I hope to continue to remain under your mentorship throughout the rest of my education.

Additional thanks to the following individuals:

Dr. Eddie Tatar of Idaho State for discussing the rationality of pion influence in photonuclear influences.

Dr. Chad Pope of Idaho State for letting me borrow his original Lamarsh textbook and taking the time to discuss my research with him over the years. An extremely pleasant individual.

Kermit Bunde for educating me in MCNP and answering the many questions I had along the way. My parameterization would not have been nearly as comprehensive/accurate without him.

Dr. Stephen Johnson of Idaho National Lab for validating the need for this type of research.

Dr. Dan Dale of Idaho State for discussing the intricacies of photonuclear physics with me.

Dr. Ian Perry of Cambridge for providing fascinating insight into meson dynamics.

Dr. Theodore Sande of MIT for discussing the relation of nucleus excitation energies and giant dipole resonances.

Dr. Ryan Bodenstein of Jefferson National Lab for reviewing my ideology on accelerator power deduction and for providing clarity regarding the parameters relating to beam power.

Emory Colvin of Oregon State for teaching me about ORIGEN and how to appropriately interface it with MCNP given my simulated scenarios. My depletion analysis wouldn't have been correct without his assistance.

Wesley Yockey of Idaho State for allowing me to use his computer to run countless simulations faster than my own CPU would permit.

Dr. Milan Martinic of University of Wisconsin, Dad, despite no longer being a practicing physicist your relentless encouragement and insight on academia really helped me get to this point.

TABLE OF CONTENTS

LIST OF FIGURES

LIST OF TABLES

LIST OF DEFINITIONS

Accelerator Driven System: (ADS), An energy amplification in which a beam of high energy particles stimulate nuclear reactions; resulting in the sufficient production of energy to power the driving accelerator while leaving some additional gain.

Depletion: The loss of fissionable atoms within the fuel due to burn up.

Highly Enriched Uranium: (HEU), Uranium that is >20% weight percent U-235.

Kilowatt Reactor Using Stirling Technology: (KRUSTY), A comparatively small, fast fission reactor designed for space applications, consisting of a single fuel rod, reflector and heat pipes.

Longevity: The amount of operational time of a reactor without the need for refueling or human maintenance.

Low Enriched Uranium: (LEU), Uranium that is ≤20 weight percent U-235.

Mathematica: A software developed by Wolfram Research used to perform the computation of advanced mathematics and plotting of 3-dimensional functions.

Monte Carlo Neutral Particle Transport: (MCNP), A software developed by Los Alamos National Laboratory used to simulate the photonuclear irradiation of U-8Mo and sample data regarding neutron production and flux.

Novel Compact Electron Accelerator: (NCEA), A comparatively small device which generate, collimates and increases the kinetic energy of electrons.

Oak Ridge Isotope Generation Code: (ORIGEN), A software developed by Oak Ridge National Laboratory used to simulate depletion, decay, activation and emission of various isotopes.

Photonuclear: A process in which an x-ray produced through the interaction between a high energy electron and an electron cloud, is absorbed by a isotope resulting in the ejection of neutrons from that isotope’s nucleus.

Tally: A term referring to the mechanism used by MCNP to sample pre-specified data.

The Appropriateness of Electron Accelerators as Applied to Space Reactors, A LEU Adaptation of the Kilowatt Reactor Using Stirling Technology (KRUSTY)

Thesis Abstract—Idaho State University (2021)

An electron accelerator is proposed as a mechanism to optimally alleviate space based reactors from highly enriched fuels. Viability for this concept was evaluated through an examination into the effects on system size, power and longevity. Using MCNP6.2, the "Kilowatt Reactor Using Stirling Technology" was recreated and a parametric study was performed to determine the appropriateness of driving a low enriched uranium core to 5kWth with an electron beam. Results revealed that when considering beam energies from 10-150 MeV, a 50MeV beam provided the most stimulation per cost of accelerator power. Extrapolated results found the most affordable reduction in enrichment to be to 70% with use of a 1kW beam. A longevity analysis was then performed using ORIGEN on a 20% LEU system driven by a 50MeV beam, which found accelerator usage decreased system power by ~97% over 30days.

Key Words:

Accelerator Driven System, Depletion, Highly Enriched Uranium, Kilowatt Reactor Using Stirling Technology, Longevity, Low Enriched Uranium, Mathematica, Monte Carlo Neutral Particle Transport, Novel Compact Electron Accelerator, Oak Ridge Isotope Generation Code, Photonuclear, Tally.

Chapter 1: Introduction

'Fission surface power' refers to the concept of using nuclear reactor technology on extraterrestrial voyages as a more compact and reliable means of establishing long term power. Following the concept's initial implementation in 1965 with the System's for Nuclear Auxiliary Power-10A satellite, a system that prematurely failed only 45 days into its mission, little has been since done to perpetuate the use of fission surface power. Within recent years a shift in focus towards less massive designs, microreactors, has revitalized the concept leading to a plethora of designs emerging to compete in the reactor space race. In March of 2018 the *Kilowatt Reactor Using Stirling TechnologY* (KRUSTY), was successfully assembled and terrestrially tested; being acclaimed as "the first nuclear-powered operation of any truly new reactor design in the United States in over 40 years.[1]" Despite this, the practicality of KRUSTY's design comes into question when one considers the design's 93% enriched uranium core and the United States' signatory status on the International Nonproliferation Treaty which as of 2001 has implemented the goal of no longer using highly enriched uranium (HEU, >20%) in any future reactor designs. KRUSTY creator Dr. David Poston acknowledges the economic/political concerns of HEU[2] and individuals more familiar with the logistics involved, like Dr. Steve Johnson, the Director of the Space Power Division at the Idaho National Laboratory believe it will take "little short of a presidential decree for KRUSTY's HEU design to make it into space.[3]" Thus it comes as no surprise that the National Aeronautics Space Agency's development of a design truly optimal for fission surface power is something still in the works today.

The intent of this research is to investigate an electron accelerator's compatibility with fission surface power by evaluating the technology's ability to reduce enrichment without compromising reactor size or longevity. The aforementioned fission surface power design, KRUSTY, has been

selected for the proposed theoretical modification as previous attempts to reduce its enrichment have resulted in designs 187% heavier than its highly enriched counterpart (Figure 1)[4]. Using MCNP6.2, LEU versions of KRUSTY (5-20%) consistent in size with the 5kWt HEU counterpart are modeled and have their neutronics analytically verified. The interfacing of a 10-150MeV electron accelerator onto the described LEU versions of KRUSTY is additionally simulated and beam intensity is parameterized as a function of core flux to identify the minimum operational conditions needed to achieve a net gain of 4-5kWt. Lastly to ensure that the core's irradiation by such a beam does not jeopardize KRUSTY's intended duration of independent operation, a computational depletion analysis concerning photonuclear production's toll on the fuel is performed.

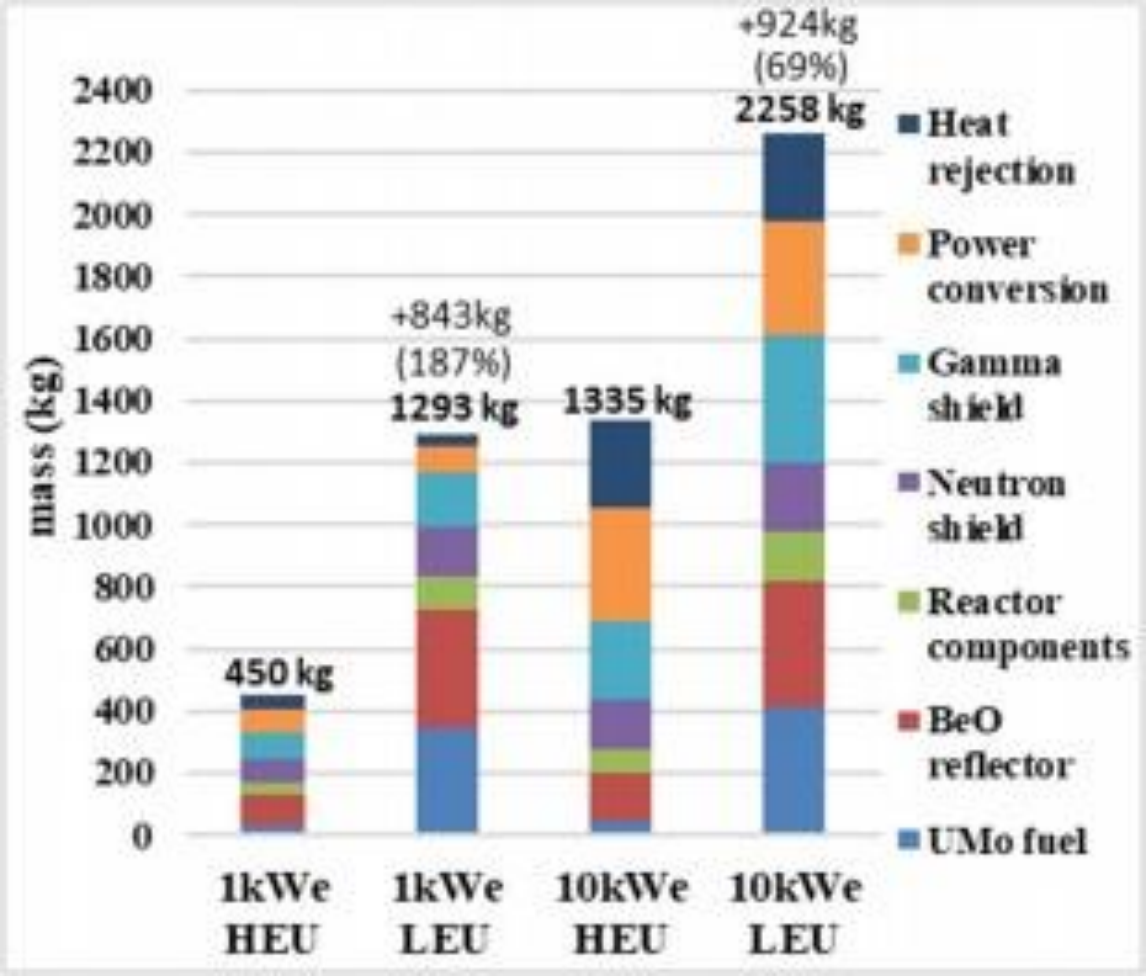

Figure 1: Mass of KRUSTY for different powers & enrichments

Chapter 2: Kilowatt Reactor Using Stirling TechnologY

KRUSTY:

KRUSTY is a $20M NASA funded fast fission reactor, heavily designed with uptime longevity for space travel in mind. The budget allocated to this reactor has been largely consumed by the manufacturing of the HEU fuel and the mandated security of said fuel[5]. In its 5kWt iteration, KRUSTY is a ~2m tall reactor which uses fuel cast in a cylindrical ingot (Figure 2) modified to accommodate the presence of a centered material and 8 heat pipes. In its HEU configuration, the fuel composition is an UMo alloy, where the uranium is ~93% enriched (28 kilograms total) and the molybdenum contributes to ~8% of the alloy's weight. Designed for spaceflight, the KRUSTY core design includes a single mobile component, a B_4C control rod that occupies a 4cm annulus spanning throughout the core. The core and heat pipes are then axially and radially surrounded by a 15.5cmm thick BeO reflector. KRUSTY's low operational power of 5kWt, allows reactor to maintain full power for ~15+ years at 0.1% burnup[6], implying little need for reactivity control over the duration of the reactor's life after the reactor's initial startup. Having undergone successful testing at both the Nevada National Security Site and NASA's Glenn Research Center in 2017, KRUSTY is considered the "First truly innovative, new reactor design the US has seen in 40 years." KRUSTY cofounder, Marc Gibson stated the results of these tests proves "the system (reactor and associated safety systems) behaves the way we designed it to work; no matter what environment we expose it to, the reactor performs very well.[7] This perception of KRUSTY as a landmark innovation appropriately makes it the subject of criticism and speculated improvements. Specifically, innovative techniques for reducing the fuel's enrichment to that of LEU levels without greatly compromising reactor size are the most desired as these will offer more plausible avenues for getting the KRUSTY design into space and have not been explicitly explored by

those invested in the project. Since the conclusion of testing on KRUSTY in 2018, there have been talks of NASA implementing a kilowatt power lunar system but none that explicitly imply KRUSTY will be that system as such projects will focus on LEU systems[8], leaving the impression that logistical hurdles are the sole adversaries in KRUSTY's lunar use coming to fruition.

In the years following KRUSTY's testing, co-founder David Poston has made many efforts of outreach to discuss the success of KRUSTY with different bodies of the scientific community. Presentations and reports on this front have revealed several of the dimensional and material intricacies of the KRUSTY design (Figure 3). These provided details allowed for this research to conduct computational analysis on a LEU system that had the same structural environment as the original KRUSTY system, (Figure 4).

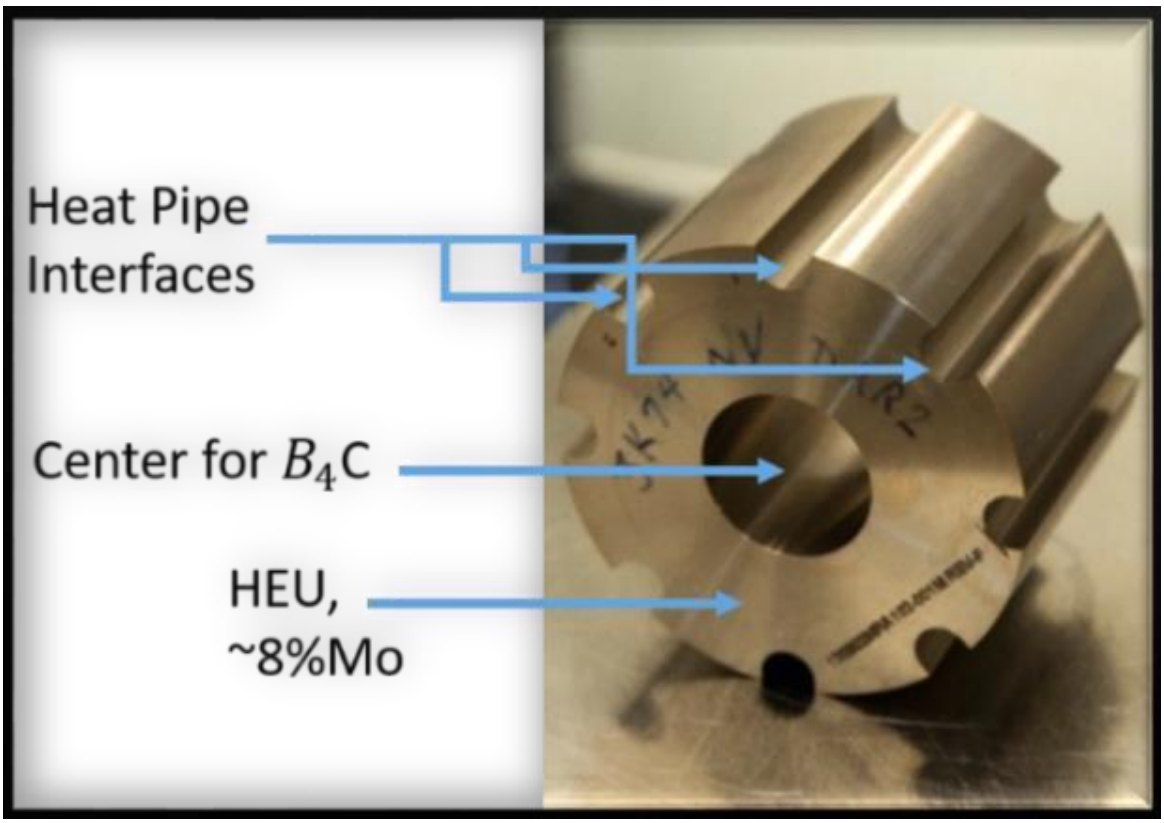

Figure 2: KRUSTY core geometry

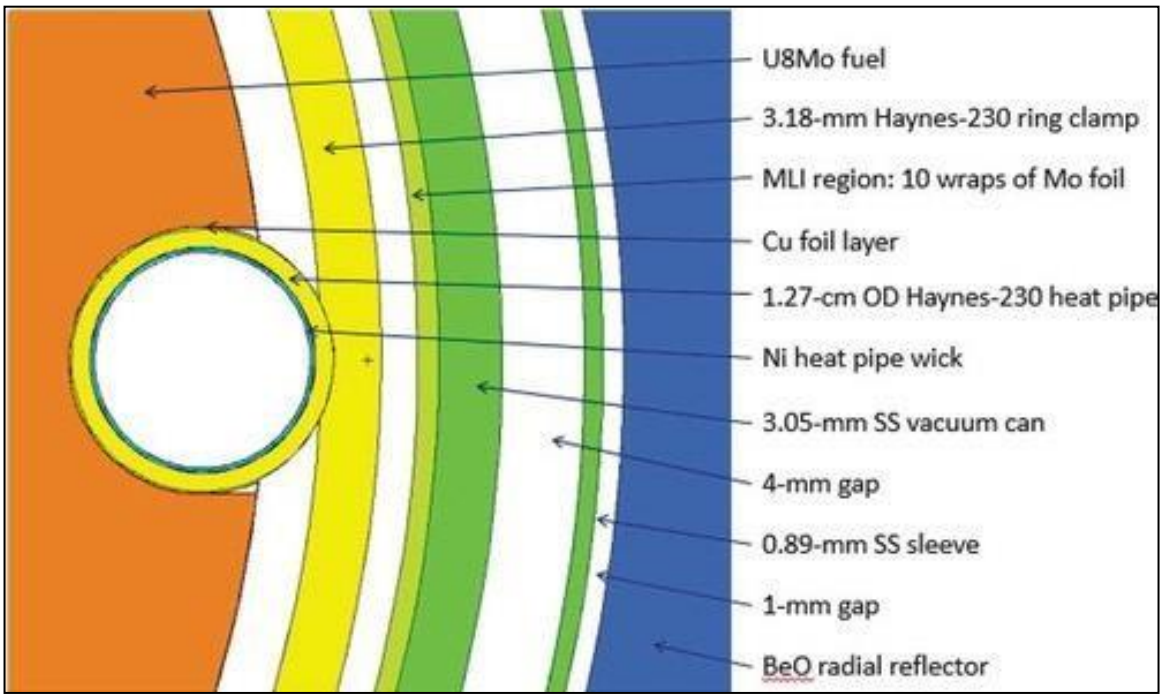

Figure 3: KRUSTY Material Schematics

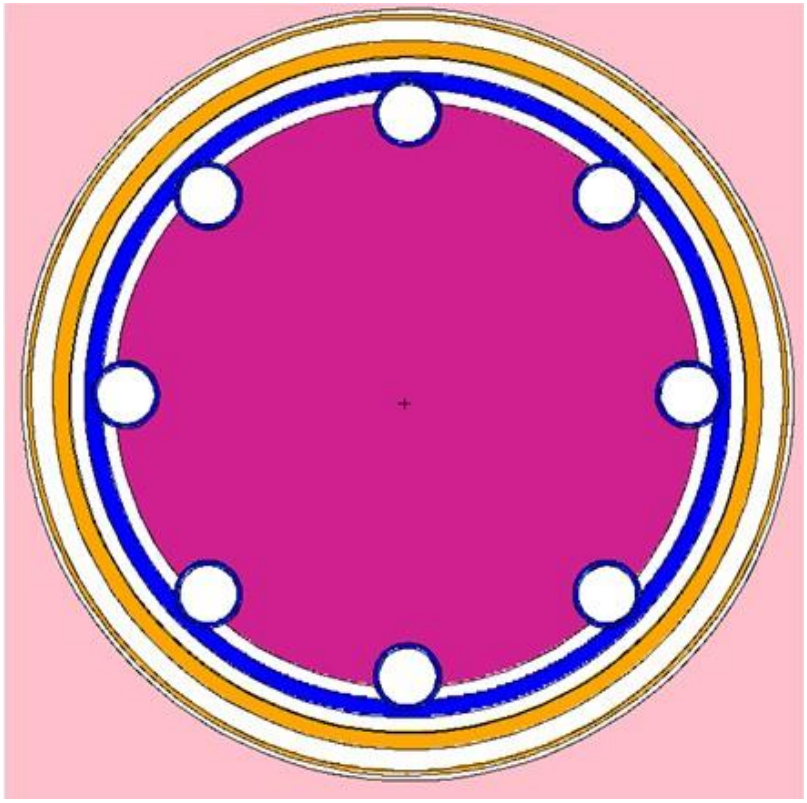
Figure 4: Recreated KRUSTY core

Chapter 3: Use and Implementation of the Photonuclear Effect

The Photonuclear Effect

The photonuclear effect refers to a nuclear process where high energy electromagnetic radiation incident upon a nucleus is absorbed prompting a collective oscillatory excitation of the internal nucleons (known as the giant dipole resonance[9]); effectively exciting the nucleus[10]. This excitation results in an increase in the dipole moment of the nucleus which in turn leads to its instability that is relaxed by decay via ejection of a subatomic particle. In isotopes, the ejected particle is commonly a neutron due to it requiring a smaller energy to escape the strong nuclear force potential well (compared to a proton which has to overcome an additional coulomb barrier, Figure 5[11]); multiplicities of which are dependent on the energy of the incident photon. In the event excitation achieves or exceeds that of the nucleus' fission barrier, photofission will occur also resulting in the release of neutrons[12 13]. Production of neutrons via photonuclear interactions are sourced by 3 types of events: (γ, n), (γ, 2n) and (γ, Fiss).

When a system is driven by an electron accelerator, photonuclear reactions are achieved by the bremsstrahlung process, a process involving high energy electrons passing through a target material. As the electrons enter the electron cloud of the target atom, various electromagnetic braking and scattering events occur and while the electron experiences acceleration, work must be done by the electron's field to correct its position relative to its outer, previous electric field, generating a pulse of electromagnetic radiation[14] (in the form of an x-ray) Figure 6, with momentum conserved (within a continuous energy spectrum limited to the incident energy of the electron[15]). Such an x-ray is then ideally (if within the range of resonance energy, typically 30MeV for U235[16]) absorbed by the nucleus exciting its giant dipole resonance (in a process conceptually similar to a reverse gamma decay). The induced excitation increases the energy of the nucleons

and causes their respective positive charges to separate, ultimately resulting in the ejection of neutrons, hence the (γ, n), (γ, 2n) reactions.

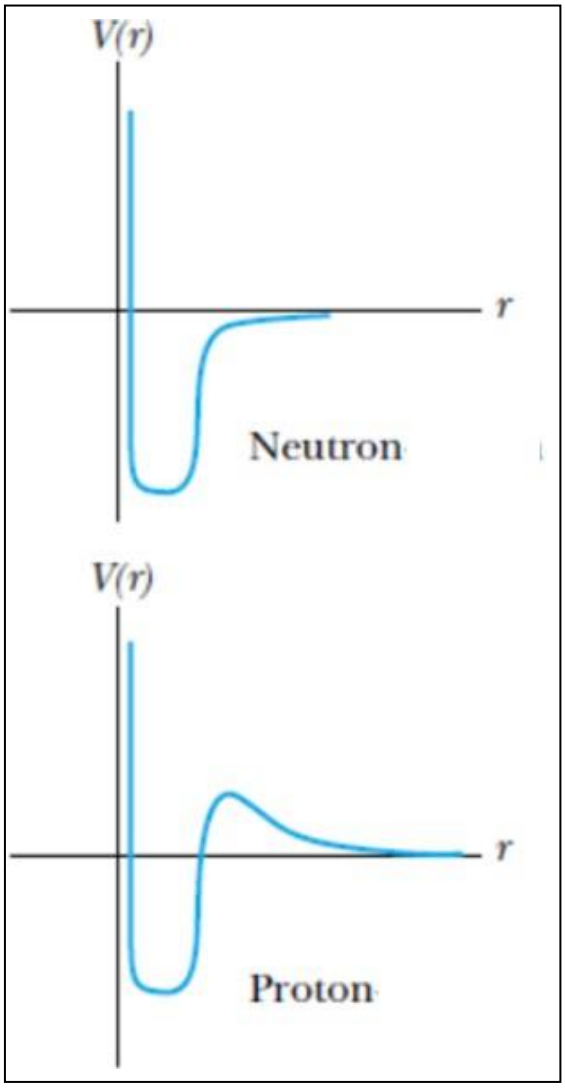

Figure 5: Nuclear forces as a function of distance

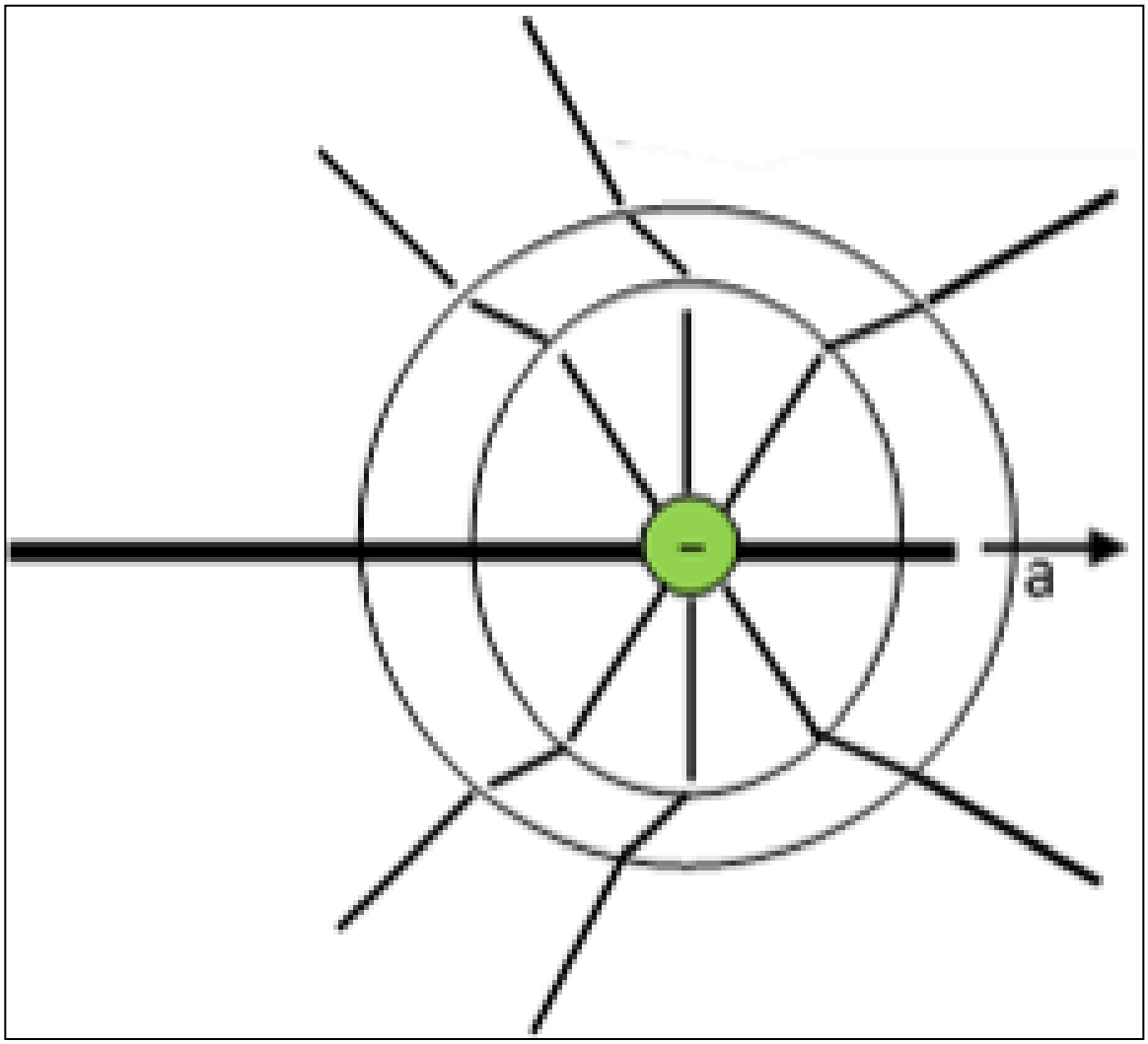

Figure 6: Depicts the gradual change of the electric field around an accelerating electron

Electron Accelerators vs Proton Accelerators:

Given all 3 photonuclear reactions, the average neutron production for a 100MeV electron incident upon uranium (of natural composition) target is ~0.11n/e^{17}. The cost of neutron production per incident electron (~900MeV) is then significantly greater than that of the average neutron cost when using an incident proton ("spallation," ~30MeV). An important feature to note is the difference in relative power cost of an electron accelerator compared to that of a proton accelerator, where the electron accelerator is fundamentally cheaper. Considering the 2 costs at play, an evaluated investment cost can be derived for both high energy electrons and protons, and these investment costs suggest that the low neutron efficiency of photonuclear is cost effective for low end neutron fluxes while vice versa is true for protons. While exact values are in reference to naturally enriched uranium, Figure 7 validates that regions do in fact exist for which a neutron source strength is more cost effective when produced by an electron accelerator as opposed to a proton accelerator and that these regions can overlap at lower levels.

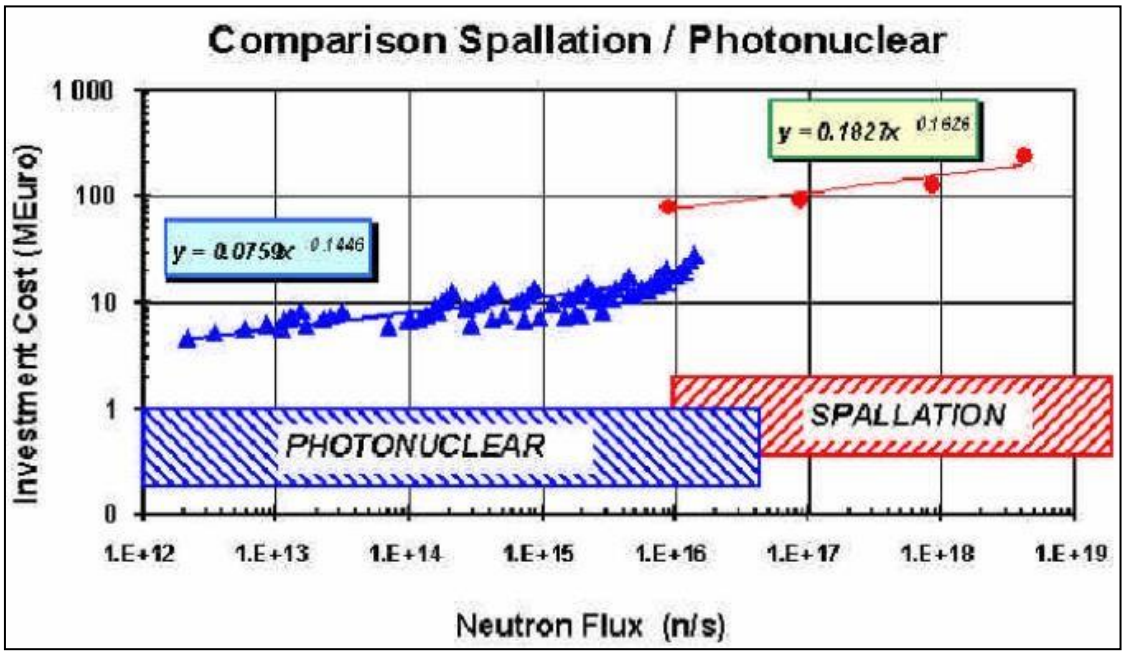

Figure 7: Displays a region of efficiency for electron accelerators.

The relative size of a photonuclear system in comparison to that of a spallation system is typically much less complex in terms of ADS configurations. If mass is an object's resistance to acceleration, then it reasons that there is a larger investment needed to achieve a particle of high kinetic energy. This larger investment must also be accompanied by a physically larger apparatus as well and this can be gleamed from Figure 8[18] which shows the relativistic velocity as a function of kinetic energy. Notice that after what corresponds to ~1meter (0MeV-10MeV) the electron's velocity has achieved max, near light speeds whereas the proton's relativistic and corrected (dashed) velocity undergoes more gradual changes in magnitude. Thus the hardware for an electron beam need only consist of an injector used to initially accelerate the electron while the hardware necessary to maintain proton acceleration will have to consist of several sections calibrated for the various velocities of the proton. For space applications of supplemental neutron fluxes, the use of an electron accelerator is objectively superior in that it offers a more compact design with greater efficiency. For the reader's viewing, an example of a 1 MeV compact electron injector design is provided in Figure 9[19] emphasizing the size needed for an electron linac to achieve what would take a proton accelerator a few meters[20].

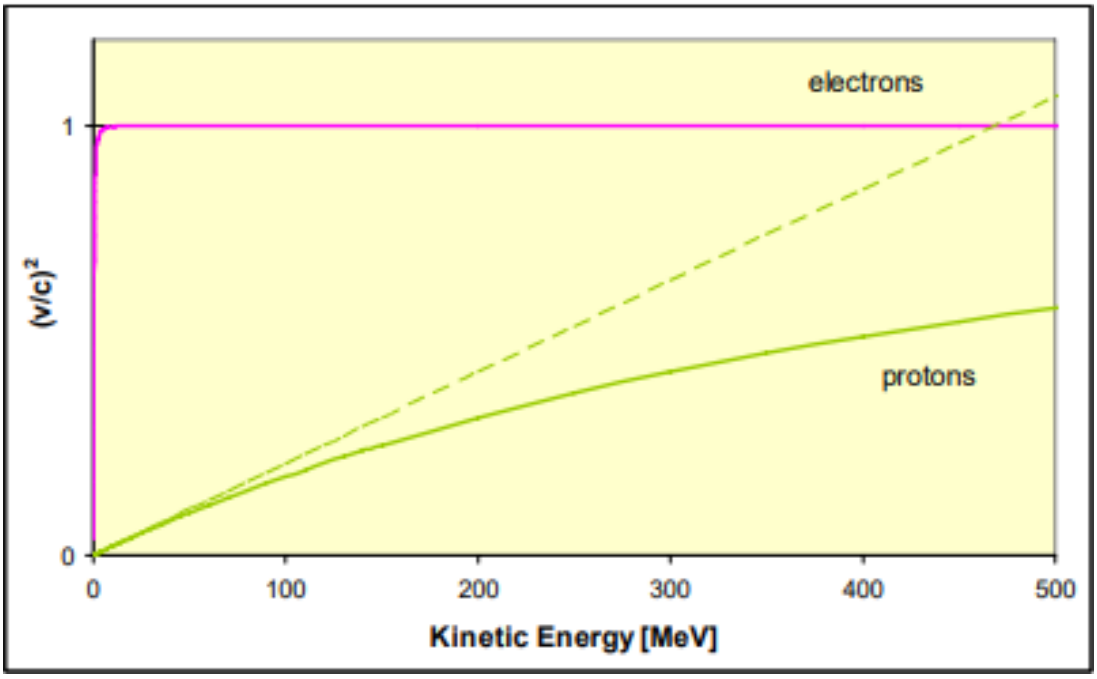

Figure 8: Squared relativistic velocity VS kinetic energy (Dashed line is relativistic corrected for proton)


Figure 9: 1 MeV novel compact electron accelerator

Historical Use of EADS:

The feasibility of the use of electron accelerators to drive nuclear systems was explored in the early 2000s as part of the Reactor-Accelerator-Coupled-Experiments (RACE) project funded by the US Department of Energy's Advanced Fuel Cycle Initiative. In a collaborative effort between Idaho State University's Idaho Accelerator Center and both University of Texas Austin and Texas A&M University, the RACE project saw the development of several electron linac-reactor (ranging from subcritical assemblies to 1MW TRIGAs) systems. RACE apparatii consisted of a photoneutron source in the form of a linac (operationally ranging up to 1kW beam of 40MeV electrons) interfaced with a tungsten alloy or uranium target surrounded with a water moderated, reflector contained LEU alloy assembly of 150 plates; results of which yielded $2x10^{-3}$ neutrons per electron[21]. Further analysis on the ISU-RACE system suggested that the interfacing of an incident beam with a target's flat surface results in a backscatter flux of electrons, photons and neutrons produced in the target that greatly contributed to the flux sampled over the target's entirety (forwards, backwards and radial); implying that target optimization requires an alteration of its geometry[22]. Similar designs were pursued 10 years later by the Kharkov Institute of Physics and Technology which employed a 100MeV, 100kW electron beam interfaced with both tungsten and uranium targets as a means to drive a subcritical, water moderated, LEU assembly at powers on the order of MWs. KIPT studies found that while neutron multiplicities produced by the uranium target exceeded that of the tungsten (due to the material's ability to support both photo and neutron fission events), the uranium target's longevity was less than that of the tungsten due to additional swelling caused by the fission projects[23]. In present day, the use of EADS has been stigmatized as only effective when driving LEU assemblies of near critical multiplication factors at MW power levels. To remedy this perception, the Michigan company Niowave, has been

experimenting with revitalizing the concept via the employment of liquid target systems surrounding LEU assemblies. While initial testing on an assembly consisting of a stagnant natural uranium target surrounded by10kg of LEU fuel pins found that a 40MeV, 530kW electron beam was only able to drive the surrounding system to a power 210kW, follow up studies using weaker 40MeV, 500W beams anda PbBi eutectic fluid flowing in channels both surrounding and through the core are being investigated with higher hopes of more efficient beam to reactor power ratios[24].

Chapter 4: Computational Parameterization

MCNP Conceptual Functionality and Procedure of Research:

The simulations used for this research were computed using the Los Alamos National Laboratory's MCNP6.2. The Monte Carlo N-Particle Transport software that allows for the statistical tracking of various particles (neutrons, protons, electrons, photons) throughout their interactions with predefined material. Particle-material interactions of all types are primarily expressed as energy dependent probabilities (compiled in a cross sectional libraries) and for each particle there exist some interaction (absorption) capable of ending the particle's transport; likewise there exists some position for the particle with a higher probability of permitting leakage from the system. Particle lifetimes are inferred through the use of pseudorandom number generators that provide the deciding values for what is analogous to a random walk. In the context of this research seemingly random numbers were produced using a Lehmer 48bit generator initiated with various seed values responsible for starting the transport of the first particle history in a given run. Seed values varied to allow for different 'pathways' to be taken during transport simulations of the same conditions and yielded results that were averaged to deduce an answer consistent with that of truly random statistics for a predefined value of allotted particles histories tracked. While time dependent, MCNP normalizes the values sampled to a snapshot of the operational system to yield data in units of per source particle per second. It is with this in mind that the following procedural flow chart, Figure 10**,** was conceptualized to conduct this research:

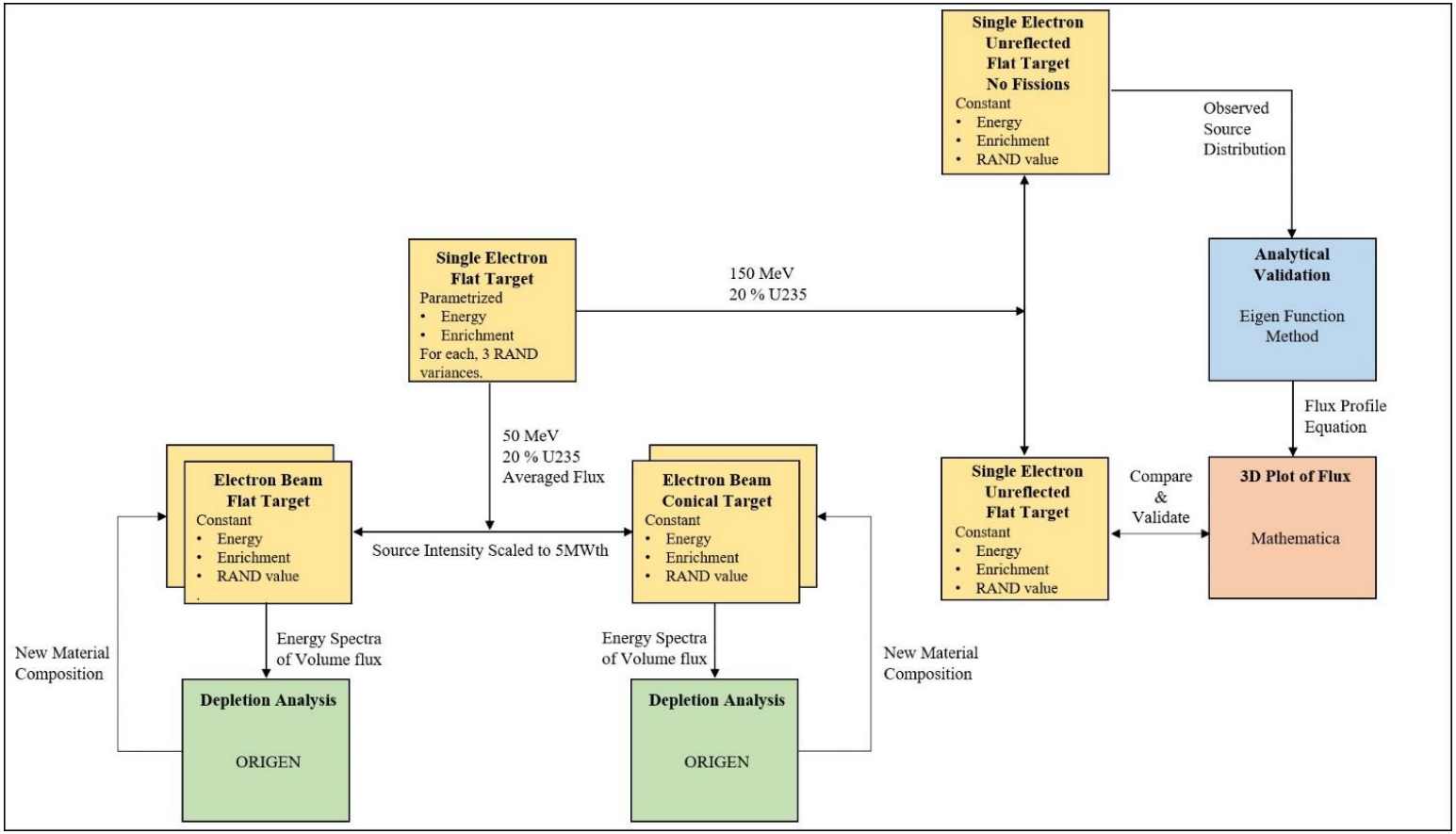

Figure 10: Procedural Flow Chart

The use of MCNP for this research was primarily allocated to the 1st box of Figure 10, in where a parametric study consisting of 48 input decks was performed but continued use of MCNP spans to all boxes of the beige color. Using both geometric and material data provided for KRUSTY's 5kWt design[25] [26], KRUSTY's core, heat pipes (including their various material wrappings), axial and radial neutron shielding and radial gamma shielding were modeled. As the goal of this research is to investigate the reduction of enrichment in KRUSTY's singular fuel 'cylinder,' through the implementation of a NCEA, the modeled core fuel was reduced to LEU levels that were parameterized from 5-20%. Consideration to both the desired placement of the proposed NCEA and findings from the previously covered electron-ADS studies, suggested KRUSTY's central B_4C control rod had little relevance in this research and thus neither the control rod nor its original cavity were modeled. Instead, this model treats the system's "target" and "core" as synonymous and alters the cavity intended to house the control rod to be completely filled with LEU. Beneath the reactor, a 1cm annulus was left in the lower axial shielding as a port for a NCEA to interface with. The initially simulated electron source is a single electron incident upon the completely filled core. For each of the four enrichments simulated (5%, 10%, 15%, 20%), the incident energy of the electron is varied from 10 to 150MeV (10MeV, 50MeV, 100MeV, 150MeV). For each scenario of a given fuel enrichment and incident electron energy three different inputs were run using different values fed to the random number generator.

Following the results of the parameterization, two further analyses are performed using a 150MeV electron energy and 20% enrichment. An analytical validation of the neutron flux profile observed through results of the parametric study was conducted using Mathematica as a means to provide additional confirmation to the perceived functionality of the MCNP software. After the

additional confirmation of the results obtained through the initial parameterization, a method for depletion analysis is proposed on two geometric variations of the fuel's core to determine the effects of the neutron flux produced by the electron source (now scaled to power) on the system's longevity.

Initial MCNP Data Sampled:

In all 48 parameterizing scenarios three primary tallies were used to sample data about the fuel. Values pertaining to the neutron flux about the fuel's surfaces were collected via an F2 tally which sampled over the three surfaces of the fuel 'cylinder' cell (top, radial, and flat bottom) and reported results in units of $\frac{1}{cm^2}$. The neutron flux over the fuel's volume was sampled using an F4 tally and reported results in units of $\frac{1}{cm^2}$. The kinetic energy deposited into the fuel via the resulting neutrons and fission products produced was sampled over the fuel's volume using an F6 tally, reporting results in units of $\mathrm{MeV/gram}$. The use of both F4 and F6 tallies about the fuel's volume is done as a means of redundancy to confirm MCNP's ability to accurately report the fuel's operational power given a specific scenario's conditions. Recall that reactor power can be described by the rate of energy released in fissions over all core volume or in terms of variables, Equation 1:

EQ1: $$P_{core} = E_R \cdot \Sigma_f \cdot \phi \cdot V$$

Where the rate of fission is given by the product of the macroscopic cross section of fission and the neutron flux. Using what is known as a "tally multiplier" one can define their input deck to such request that MCNP scale the F4 tally by the energy released per fission, atom density, microscopic cross section of fission and volume of a given material, to yield a tally result in units of MeV. Use of a tally multiplier is superior to that of a hand calculation to scale the traditional F4 tally result, as MCNP can reference provided cross sectional libraries to determine the exact microscopic cross section of fission for a particle of a given energy whereas a manual calculation would be mono-energetic[27]. Thus, being a result crucial to the determination of the operational parameters required for an electron accelerator beam to drive the system to the desired power of

5kW, the use of two different tallies to deduce the operational power due to a single electron is necessary for confirmatory purposes. The findings of these tallies are represented in Figures 11-16; Figures 11-13 pertain to the surface fluxes of the fuel at enrichments of 5-15% and are reserved for Appendix A.

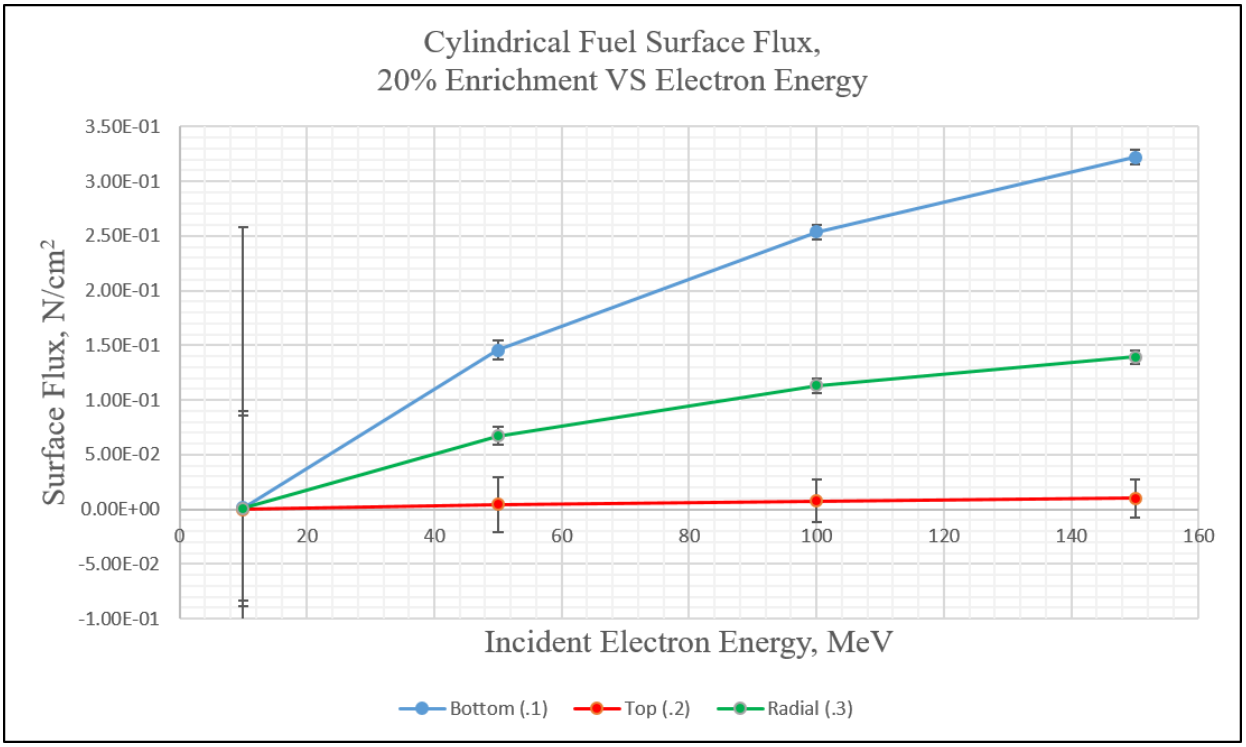

Figure 14: Neutron flux about surfaces of 20% enriched fuel

Figure 14 depicts the neutron flux about the three surfaces of the fuel as a function of the incident energy of a single electron for 20% fuel enrichment. The largest of these fluxes is the bottom flux, the surface with which the incident electron makes contact with. Unfortunately the use of the term "flux" in nuclear physics is a bit of a misnomer as it holds no implication towards the directional movement of the particles through a given area but rather refers to the total movement of particles within a given area. The additional complications of the inability to run an F1 tally for more than a single particle left no definitive method to determine neutron direction through such results, but an interpretation of a significant backscatter would be consistent with the

results of the RACE experiment which empirically uncovered the backscattering phenomenon for electron beams interfaced with a flat target (see Historical Use of EADS).

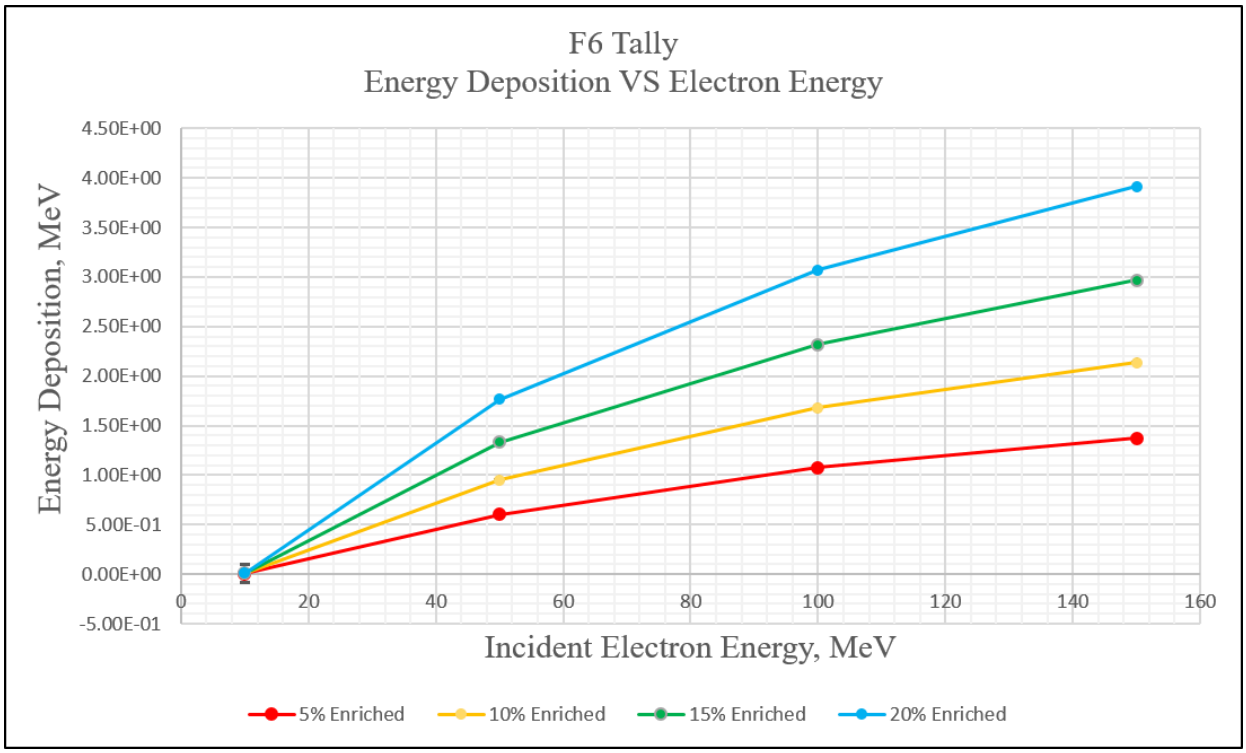

Figure 15: Energy deposition for varying enrichments

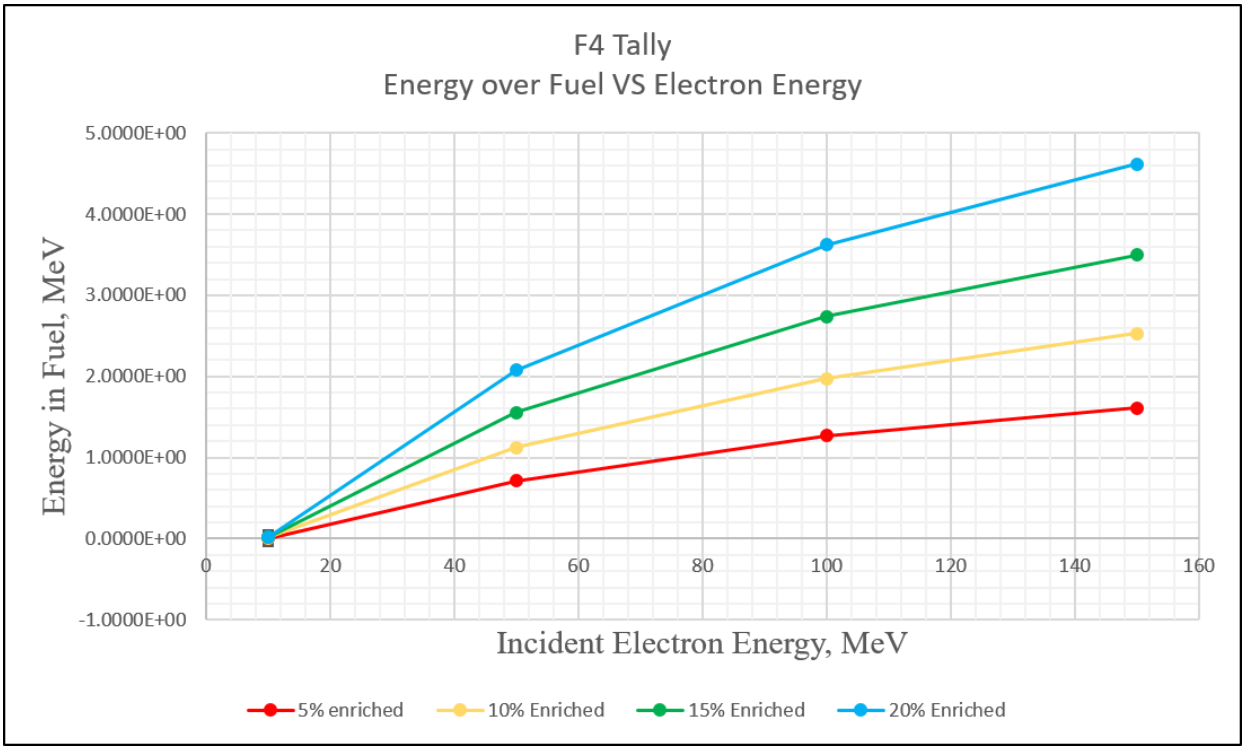

Figure 16: Energy calculated by MCNP FM on F4 Tally, as function of enrichment.

Upon examination of the F6 and F4 tallies respectively displayed in Figures 15 and 16**,** one will note despite the consistency in magnitudes of values reported by both tallies, there exists some percent difference that between the values that ranges from 1.5E-3% at lower ranges of incident electron energy up to ~15% at electron energy of 150MeV. Across all sets of data, the F6 energy deposition tally consistently reported an average of .433 less MeV compared to the MeV results obtained through the F4+tally multiplier results. An investigation into this difference found that when just considering neutrons (as the F6 tally in this research did) MCNP tends to report the energy released per fission as less than 200MeV and that a true energy deposition value using an F6 tally must be obtained as the sum of an F6 tally specifically scored to neutrons and an F6 tally specifically scored to photons[28]. Due to the F4 tally using a user defined tally multiplier of an assumed 200MeV per fission, this value then incorporated the energy not effectively captured by the F6 tally sampling energy deposition due to neutrons and fission products; for this reason the

results of the F4 tally were used in further analysis.

It cannot go unnoticed that in all 3 tallies used (F2, F4 & F6), the magnitude of values obtained with an incident electron energy of 10MeV had values that where are seemingly represented at zero in Figures 14-16. In actuality these values were just orders of magnitude lower, in the E-2 range for tallies F4 and F6 and ranges as low as E-6 for the F2 tally. It was speculated that this is a result of the primary mechanism for nuclei excitation, the giant dipole resonance, not being activated at the 10MeV energy range. As reported in Section 3.1, the giant dipole resonance for a U235 atom has been empirically seen to begin around 30MeV. To confirm the photonuclear physics utilized in this research are functionally consistent with previously obtained results, a separate analysis of incident electron energies ranging from 20-40MeV was conducted with a F4 tally (coupled with a tally multiplier) on a 20% enriched core.

The results of this analysis are displayed in Figure 17 and display a large jump in scored values around an incident electron energy of 32.5MeV. Uncertainties in Figure 17 are roughly 2 orders of magnitude greater than those in Figures 11-16, as a consequence of only a single set of seed and stride values input into the randomnumber generator as opposed to the 3 different sets of input values used in the initial parameterization.

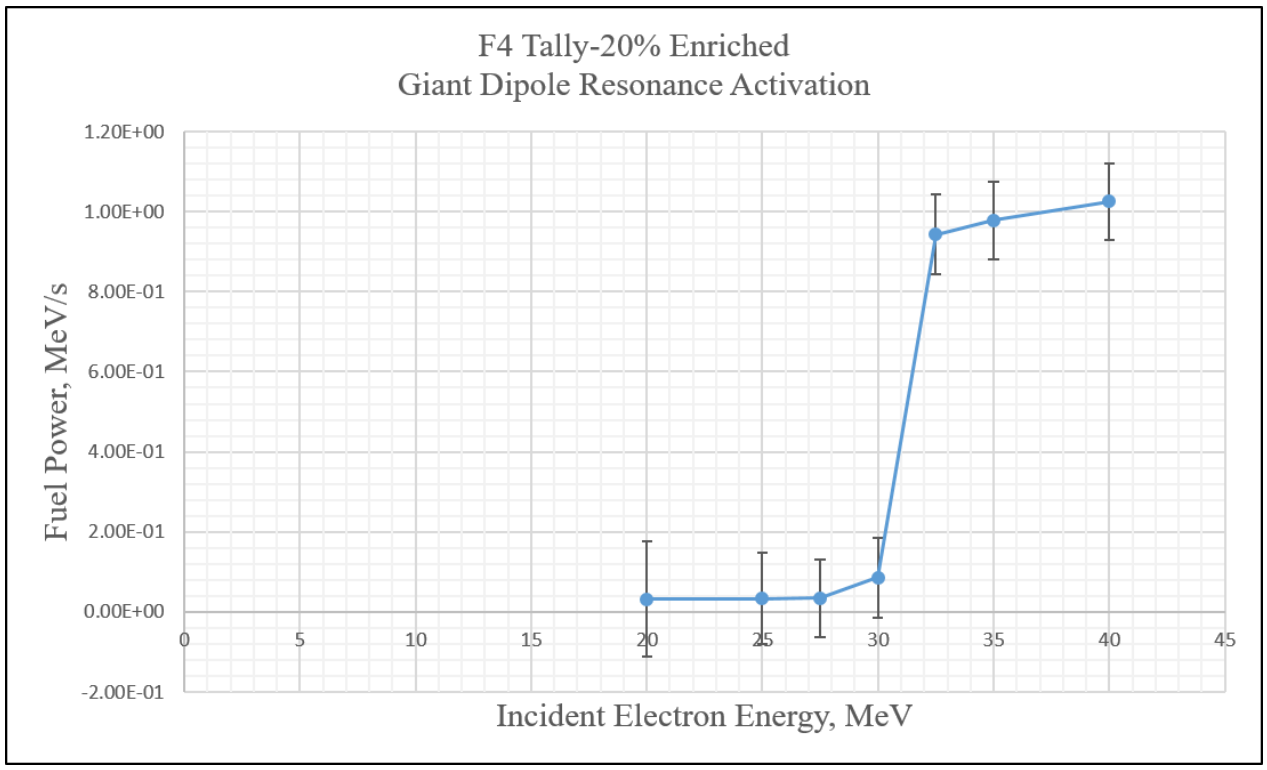

Figure 17: Capture of Giant Dipole Resonance at 32.5 MeV

Having confirmed the functionality of the photonuclear physics in MCNP and finding a near consistency between the F4 and F6 tally results, this research proceeded to determine the electron beam parameters required to drive the LEU KRUSTY core at normal operational power for the HEU KRUSTY of 5kW. Utilizing the values obtain through the coupled F4 and tally multiplier, for each scenario an electron intensity (e-/s) was deduced by first converting the MeV (reported per electron per second) results to joules then dividing 5000 watts by that power in joules. The viability of an electron beam's implementation is then evaluated by the power such a beam would consume as the EADS system will have to produce enough power to feed the driving beam whilst netting a 5kW gain. The power of an accelerator is given by Equation 2:

EQ2: $$P_{beam} = \delta \cdot E \cdot A$$

Where δ is the duty factor, a value relating to the ratio of operational time to nonoperational of a physical accelerator, a value neglected in this paper as such a parameter is usually operator defined

and has no means of representation in an MCNP simulation (consistently around 4% for electron linacs). E is the incident electron energy in eV and A is the current or amperage a value corresponding to coulombs per second. From the found electron intensity (e-/s) one can divide bythe number of electrons in a single coulomb, 6.241E18, to yield the effective amperage of an electron current driving the system at 5kW. Taking the product of the incident electron energy in joules and the amperage then yields the beam's operational power. The results of this arithmetic for all parameterized scenarios is given in Table 1, displays the required current as being typically on the order of milliamps. The resulting power consumed by an electron beam to drive a 5kW system is reported in the final column of Table 1 and was found to be of on the order of the megawatt range, values far exceeding that of the 5kW system. This implies that additional scaling must be taken into account for the system to operate at a power large enough to have the desired net gain. Within the context of the variables in Table 1, the new accelerator power in watts can be calculated by Equation 3:

EQ3: $$P_{beam\_Final} = \left(\left(\frac{(P_{beam} E^{-6} + 5E^{-3})}{Fuel\ Power_{watt}} \right) \left(\frac{1}{6.24E^{18}} \right) \right) (Electron\ Energy_{eV})$$

A more direct relationship can be deduced for an accelerator's relationship to enrichment for the KRUSTY design as depicted in Figure 18.

Table 1: Results of parametric MCNP trial and accelerator power

Enrichment	Electron Energy	Fuel Power		Scale for 5kWth		Accelerator Power
Weight Percent	**MeV**	**MeV/S**	**Joules/S**	**Intensity** e^-/s	**Amperes** c/s	**No Gain MW**
5%	10	4.9203E-03	7.8833E-16	6.3426E+18	1.0164E+00	1.0164E+01
	50	7.1174E-01	1.1403E-13	4.3846E+16	7.0266E-03	3.5133E-01
	100	1.2663E+00	2.0288E-13	2.4645E+16	3.9495E-03	3.9495E-01
	150	1.6078E+00	2.5760E-13	1.9410E+16	3.1105E-03	4.6658E-01
10%	10	8.1825E-03	1.3110E-15	3.8139E+18	6.1120E-01	6.1120E+00
	50	1.1199E+00	1.7944E-13	2.7865E+16	4.4656E-03	2.2328E-01
	100	1.9752E+00	3.1647E-13	1.5799E+16	2.5320E-03	2.5320E-01
	150	2.5264E+00	4.0477E-13	1.2353E+16	1.9796E-03	2.9694E-01
15%	10	1.3629E-02	2.1836E-15	2.2898E+18	3.6695E-01	3.6695E+00
	50	1.5523E+00	2.4871E-13	2.0104E+16	3.2217E-03	1.6109E-01
	100	2.7351E+00	4.3822E-13	1.1410E+16	1.8285E-03	1.8285E-01
	150	3.4970E+00	5.6029E-13	8.9239E+15	1.4301E-03	2.1452E-01
20%	10	1.5208E-02	2.4366E-15	2.0521E+18	3.2886E-01	3.2886E+00
	50	2.0798E+00	3.3322E-13	1.5005E+16	2.4047E-03	1.2023E-01
	100	3.6208E+00	5.8013E-13	8.6188E+15	1.3812E-03	1.3812E-01
	150	4.6159E+00	7.3955E-13	6.7608E+15	1.0835E-03	1.6252E-01

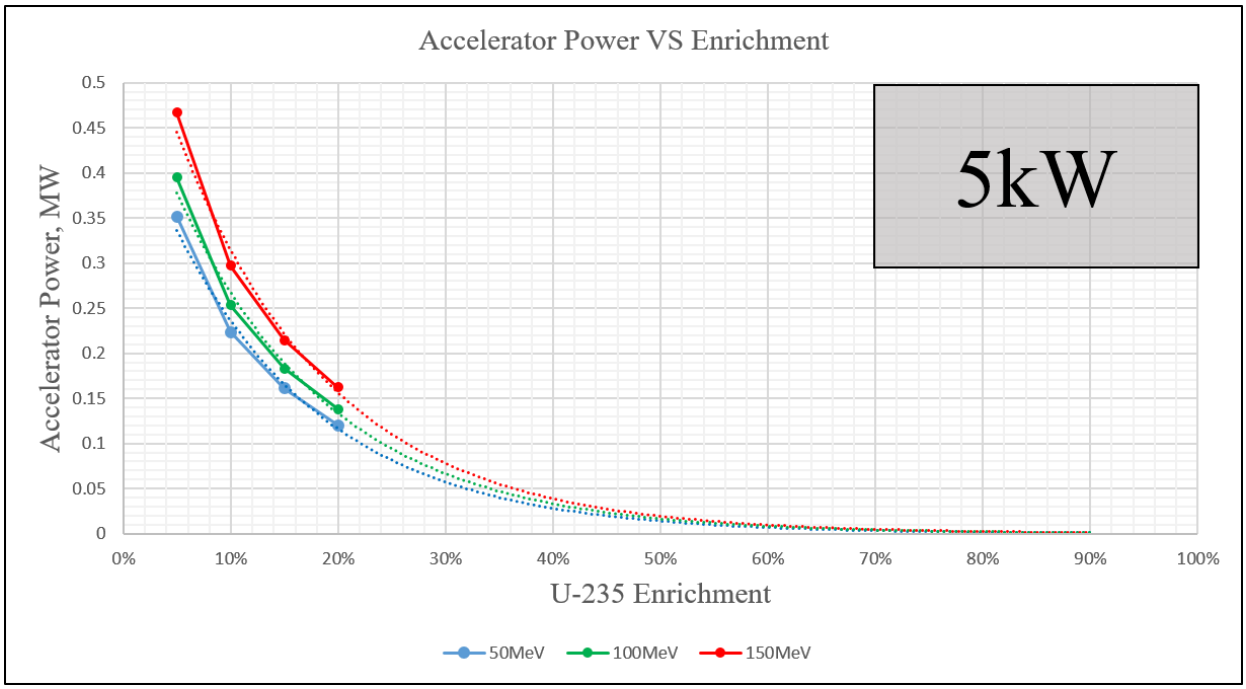

Figure 18: Shows optimal enrichments for electron beam use

Use of Fmeshes for Visual Behavior Analysis:

In MCNP an Fmesh is a tool used to apply a mesh of tallies over a geometry, ultimately allowing for a visual analysis of particle presence to be localized to a given region of that geometry. Limitations of the MCNP6.2 software permit the use of Fmeshes exclusively for F4 tallies[29] thus limiting the visual representation of an Fmesh to that which pertains to a volume flux. Using Fmesh tool, the fuel core was divided up into 500 subsections (25 sub-disks axially, 5 rings radially, and 4 sectors azithumally) in which the fluxes for electrons, bremsstrahlung photons and neutrons were sampled to explore the core's performance as a function of its geometry. Fmesh depictions of the core were collected for both a 10MeV and 150MeV electron incident upon 5 and 20% enriched fuel cores, allowing for the spatial behaviors of the particles produced to be analyzed as a function of incident electron energy and enrichment. Figures 19-43 of Appendix B depict these results. Figures 19, 20, 25 and 26 depict electron behavior as a function of enrichment and indicate that enrichment plays a nonexistent role in the single incident electron's ability to interact with the fuel's deeper atoms via photoatomic interactions. Radial scattering and capture likely dominate at this energy preventing the initial electron from axially distributing its energy into the fuel and thus from effectively axially driving the fuel. This phenomenon's dependence is clearly related to the incident electron energy as shown when comparing Figures 31, 32, 37 and 38 which indicate the incident electron's momentum experiences less axial and radial attenuation at higher energy levels. As a result, while a low energy incident electron is able to produce a nearly uniform photon distribution (Figures 21, 22, 27 and 28), it does not produce photons with high enough energy levels to allow that distribution to dictate that of the photonuclear generated neutrons (Figures 23, 24, 29 and 30). The neutron profile generated in response to a high energy incident electron is then only likely to mimic that of the natural resonance profile for the given geometry (in the case of a

cylinder, the Bessel function) if the system's ability to multiply neutrons is sufficient enough as seen when comparing Figures 35, 36, 41 and 42.

Chapter 5: Analytical Validation

Method of Eigenfunction Expansions:

This section intends to provide a conceptual prediction to the behavior of KRUSTY when driven by a source which for this exercise will be treated as a finite cylinder. Though previous analyses of the core axially and radially reflected particles with BeO, a separate, unreflected model has been created. The goal of this solution is to help understand the flux profile results obtained through MCNP simulations. The flux profile of an un-reflected reactor can be deduced analytically through use of the 1 speed, steady state, diffusion equation modified for a multiplying media driven by an external source, which in this case is intended to be an electron accelerator, Equation 4.

EQ4: $$\nabla^2\phi + B^2\phi = -\frac{S}{D}$$

Where B^2 is material buckling given by Equation 5, and explored in Appendix C:

EQ5: $$B^2 = \frac{\upsilon\cdot\Sigma_f - \Sigma_a}{D}$$

S refers to the # of neutrons per unit volume per unit time contributed to the system by the accelerator's influence and D refers to the diffusion coefficient. It is assumed that in both the axial and radial dimensions of the cylinder, the flux vanishes at some extrapolated distance away from the geometry's confinement. Due to the presence of a source distribution and flux that vanish at extrapolated boundaries, the flux profile is ideally solved via the *method of eigenfunctions*. The goal of this method is to obtain a solution to the diffusion equation in terms of solutions to another differential equation limited by similar boundary conditions but not in the presence of a source distribution. Consider:

EQ6: $$\nabla^2\psi + {B_n}^2\psi = 0$$

Where the solution to Equation 6 is derived based on the cylindrical geometry of the core (when origin is at base of cylinder), See Appendix D which yields Equation 7:

EQ7:

$$\psi_n(z,r) = Sin\left(\frac{n\cdot\pi}{\widetilde{H}}z\right)\cdot J_o\left(\frac{\upsilon_n}{\widetilde{R}}r\right)$$

Where nontrivial solutions are avoided by the eigenfunctions' respective eigenvalue's ability to satisfy the extrapolated boundary conditions for both degrees of freedom; thus n=even integers for the sine function. From orthogonality properties (in that the product of two different eigenfunctions integrated over the same domain are nonzero), the functions of the original, desired flux and the source distribution can be expanded out in a series of eigenfunctions (Equations 8 and 9) since a function that is said to be orthogonal in a basis can be expressed by the expansion of any function within that same basis. In this case, the homogenous function (z, r), is treated as the orthogonal function for which the nonhomogenous, $\phi(r,z)$

EQ 8:

$$\phi(z,r) = \sum_n A_n\psi_n(z,r)$$

EQ 9:

$$S(z,r) = \sum_n S_n\psi_n(z,r)$$

To define our source distribution further consider the implications of orthogonality. If one multiplies both sides of the source eigenfunction expansion by another eigenfunction, say $\psi_m(z,r)$ and integrates over the domain, the resultant will be that for all n≠m, the integrated expansion will fall to 0 only able to yield a nontrivial solution when the two eigenfucntions have equal eigenvalues n=m. Thus the left hand side of the integrated source eigenfunction expansion, will be equal to the product of the source term Sn and the nontrivial, orthogonal solution, in this the case of this problem is$\frac{H}{2}$. This allows one to then solve for Sn in terms of a predefined source distribution, as

seen in Equation 10:

EQ10:

$$S_n = \frac{2}{H}\iint_{0,0}^{H,R} S(z,r)\cdot\psi_n(z,r)r\,dr\,dz$$

Returning to address the eigenfunction expansion of the function (z, r), one can then insert the eigenfunction expansion into the nonhomogenous diffusion equation, yielding Equation 11 which expands into Equation 12:

EQ11:

$$\nabla^2\left(\sum_n A_n\psi_n(z,r)\right)+\frac{\upsilon*\Sigma_f-\Sigma_a}{D}\left(\sum_n A_n\psi_n(z,r)\right)=-\frac{1}{D}\left(\sum_n S_n\psi_n(z,r)\right)$$

EQ12:

$$\sum_n A_n\left(\frac{1}{r}*\frac{\partial}{\partial r}\left(r*\frac{\partial\psi_n(z,r)}{\partial r}\right)+\frac{\partial^2\psi_n(z,r)}{\partial z^2}+\frac{\upsilon*\Sigma_f-\Sigma_a}{D}*\psi_n(z,r)\right)=-\frac{1}{D}\left(\sum_n S_n\psi_n(z,r)\right)$$

Recall that $\psi_n(z,\ r)$ satisfies the homogenous diffusion eigenfunction (which has its own eigenvalue, B_n, which allows the avoidance of a trivial solution) that can be reworked to show Equation 13:

EQ13:

$$\frac{1}{r}*\frac{\partial}{\partial r}\left(r*\frac{\partial\psi_n(z,r)}{\partial r}\right)+\frac{\partial^2\psi_n(z,r)}{\partial z^2}\ =\ -{B_n}^2\psi_n(z,r)$$

Where ${B_n}^2=\left(\frac{\upsilon_n}{\tilde{R}}\right)^2+\left(\frac{n*\pi}{\tilde{H}}\right)^2$

Substituting back into the expanded nonhomogeneous equation:

EQ14:

$$\sum_n A_n\left(-\left(\frac{\upsilon_n}{\tilde{R}}\right)^2-\left(\frac{n*\pi}{\tilde{H}}\right)^2+\frac{\upsilon*\Sigma_f-\Sigma_a}{D}\right)*\psi_n(z,r)=-\frac{1}{D}\left(\sum_n S_n\psi_n(z,r)\right)$$

Noting the presence of the $\psi_n(z,\ r)$ on each side of the equality, one can reorganize for An in terms of Sn, Equation 15:

EQ15:

$$A_n = -\left(\frac{S_n}{D}\right) * \frac{1}{-\left(\frac{\upsilon_n}{\tilde{R}}\right)^2 - \left(\frac{n * \pi}{\tilde{H}}\right)^2 + \left(\frac{\upsilon * \Sigma_f - \Sigma_a}{D}\right)}$$

Plugging back into the Equation 8 results in a solution to the initial flux being Equation 16:

EQ16:

$$\phi(z,r) = \sum \left(\left(\frac{S_n}{D}\right) * \frac{1}{\left(\frac{\upsilon_n}{\tilde{R}}\right)^2 + \left(\frac{n * \pi}{\tilde{H}}\right)^2 - \left(\frac{\upsilon * \Sigma_f - \Sigma_a}{D}\right)} \right) \psi_n(z,r)$$

Recall the Equation 10 term:

$$Sn = \frac{2}{H} \int_{0,0}^{H,R} S(z,r) * \psi_n(z,r)\, r\, dr\, dz$$

Where (r, z) is the source distribution driving the multiplying media. This source distribution was visually produced in MCNP through the Fmesh tool in a simulation where fissions were turned off, allowing the produced neutron flux graph to be the sole result of photoneutrons, Figure 44. It was determined that the source must be symmetric and anisotropically biased towards the positive z-direction; thus a line source that attenuates as a function of the reactor height has been chosen for an approximation, Equation 17:

EQ17:

$$S(r,z) = H - z$$

After normalization of the source distribution (see Appendix E), the source term, Sn is then found by:

EQ18:

$$Sn = \frac{2}{H} \iiint_{0,0,0}^{H,2\pi,R} \left(\frac{\mathbf{S}(\mathrm{H} - \mathrm{z})}{\pi r H^2} * \left(Sin\left(\frac{n * \pi}{\tilde{H}} z\right) * J_o\left(\frac{\upsilon_n}{\tilde{R}} r\right) \right) \right) * r * dr\, d\Theta\, dz$$

Where S is the total source strength. Solving Equation 18 yields Equation 19 (from Mathematica):

EQ19:

$$Sn = \frac{4 * \widetilde{H} * \widetilde{R} * R * \mathbf{S}}{H^3 * n^2 * \pi^2 * \upsilon_n}\left((H * n * \pi) - Sin^2\left(\frac{n * \pi * \widetilde{H}}{4}H\right)\right)J_1\left(\frac{\upsilon_n}{\widetilde{R}}R\right)$$

Plugging back into the Equation 16:

EQ20:

$$\phi(z,r) = \sum\left(\left(\frac{\frac{4 * \widetilde{H} * \widetilde{R} * R * \mathbf{S}}{H^3 * n^2 * \pi^2 * \upsilon_n}\left((H * n * \pi) - Sin^2\left(\frac{n * \pi * \widetilde{H}}{4}H\right)\right)J_1\left(\frac{\upsilon_n}{\widetilde{R}}R\right)}{D}\right) * \frac{1}{\left(\frac{\upsilon_n}{\widetilde{R}}\right)^2 + \left(\frac{n * \pi}{\widetilde{H}}\right)^2 - \frac{\upsilon * \Sigma_f - \Sigma_a}{D}}\right)\psi_n(z,r)$$

Where $\psi_n(z, r)$ satisfies Equation 6

$$\nabla^2\psi_n(z,r) + {B_n}^2\psi_n(z,r) = 0$$

Producing the following expression for the nonhomogenus flux term, Equation 21:

EQ21:

$$\phi(z,r) = \sum\left(\left(\frac{\frac{4 * \widetilde{H} * \widetilde{R} * R * \mathbf{S}}{H^3 * n^2 * \pi^2 * \upsilon_n}\left((H * n * \pi) - Sin^2\left(\frac{n * \pi * \widetilde{H}}{4}H\right)\right)J_1\left(\frac{\upsilon_n}{\widetilde{R}}R\right)}{D}\right) * \frac{1}{\left(\frac{\upsilon_n}{\widetilde{R}}\right)^2 + \left(\frac{n * \pi}{\widetilde{H}}\right)^2 - \left(\frac{\upsilon * \Sigma_f - \Sigma_a}{D}\right)}\right)\left(sin\left(\frac{n * \pi}{\widetilde{H}}z\right) * J_o\left(\frac{\upsilon_n}{\widetilde{R}}r\right)\right)$$

Where the source term contributes only as a modifying perturbation to the flux as the z and r dependence is entirely contained in the eigenfunction. Acknowledging that the attenuated line

source distribution was elected for both its relative accuracy and simplicity of normalization, its approximation with a sine function requires a decent set of terms (30+) to produce an accurate representation. Adhering to the ideology, the following distribution was produced (Figures 44 and 45) using Mathematica:

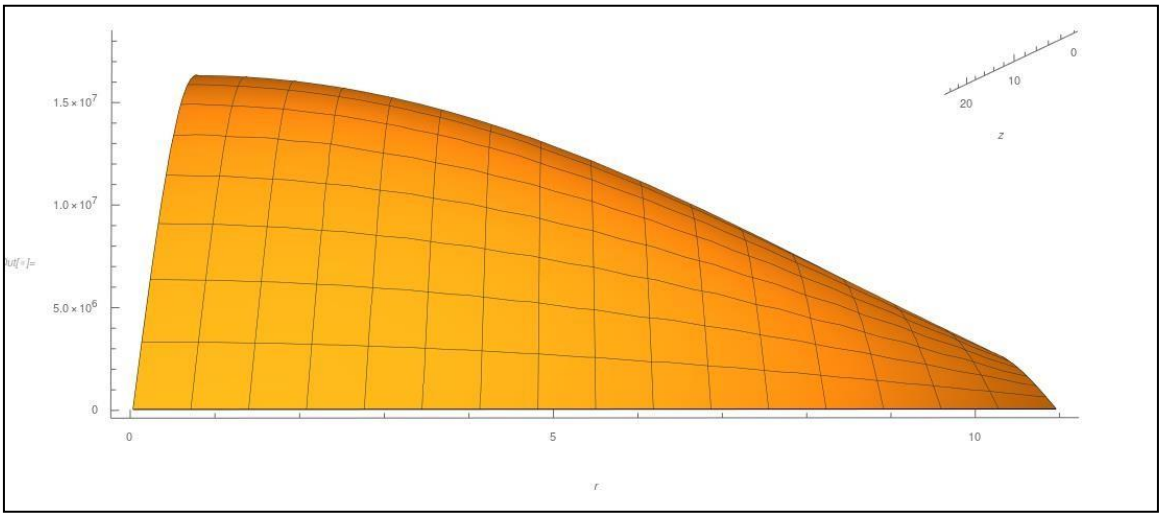

Figure 44: Flux profile as function of radius

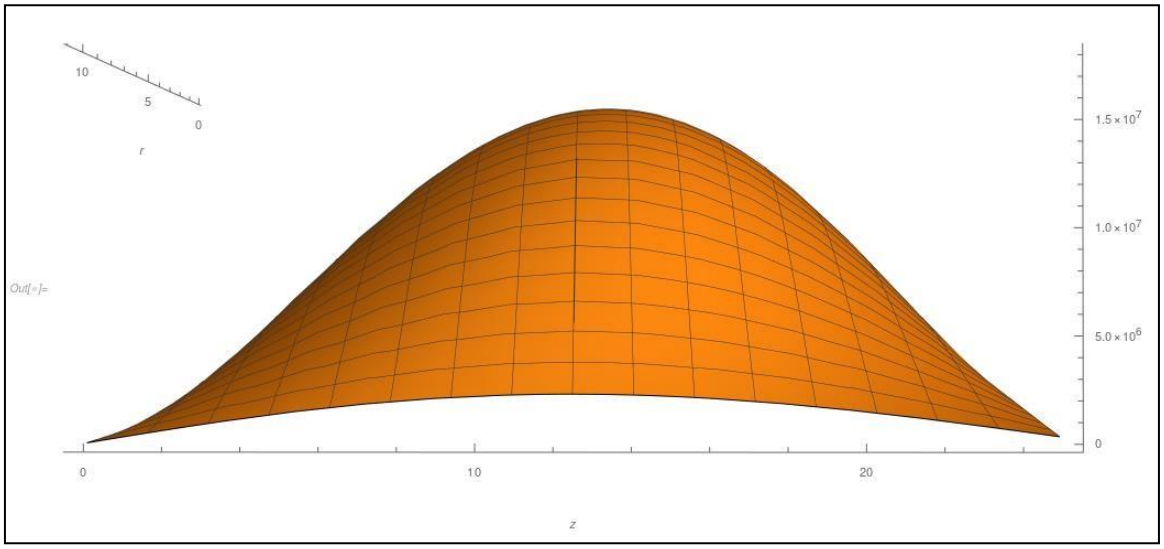

Figure 45: Flux profile as function of height

To elaborate on Figures 44, one can see the expected behavior of the radial component, a function that vanishes as r→R, the same cannot be said about Figure 45**.** What is depicted is solely behavior of the sine function; while it can be confirmed that the method of eigenfunctions does in

theory allow for the accurate depiction of a source driven flux, it must be reiterated that the notion of orthogonality is only valid if within the function's full range, which for sine is within -1→1. Recall that the attenuated line source's behavior should cause the flux profile to die out as a function of z, which would be accurately described by half the range of the sine function. Thus, given that orthogonality was imposed, regardless of the number of terms added, a convergence to the line source is not possible. This inconsistency between the source term and the desired use of only half the range of the sine function then affects both the source term eigenfunction and the flux term eigenfunction.

Expansion coefficients are responsible for perturbing the flux of a non-source driven system to towards that of the desired source driven system. Analysis into the respective An and Sn expansion coefficients as a function of their eigenvalue terms provides rationale into the behaviorsexhibited in Figures 44 and 45**.** Displayed in Table 2 one can see the An coefficient gradually converges, allowing the flux profile to be reflective of the proposed eigenfucntion. Alternatively, the Sn coefficient does not seem to converge, preventing the source from effectively influencing the flux profile but rather rendering the offset sine profile along the Z-axis, Figure 45. The 5^{th} and6^{th} terms of Table 2 are seen to maintain positive values for both An and Sn which is explained by An's dependence on Sn and this being the term set where Sn diverges.

Table 2: Expansion coefficient terms

N	An	Sn
1	1.81751E7	4777027
2	-468.886	-66483.4
3	46791.2	16213.7
4	-8410.3	-5386.34
5	980.325	1003.46
6	382.262	571.85
7	-533.397	-1097.5
8	492.278	1333.27
9	-339.327	-1170.14
10	251.574	1076.14

Chapter 6: Depletion and Longevity Analysis

ORIGEN Conceptual Functionality:

In the context of a simulated system, the determination of the EADS KRUSTY's performance as a function of time is best described by its constantly updated material composition. An isotope's decay response to a specific type of radiation is yet another statistically inferred probability, one commonly defined in cross sectional libraries. While software like MCNP also make use of such libraries, this use is limited to the normalized instance of the problem as MCNP does not continue to update the isotopic changes that occur due to irradiation unless one is additionally using another tool, the KCODE that is functionally incompatible with other useful tallies[31]. ORIGEN is a software developed as part of the Oak Ridge National Laboratory's SCALE package capable of interfacing with MCNP output and functioning as a tracker for produced and depleted isotopes. The software is in principle simulating all possible isotopes as they decay and transmute according to interactions referenced in a cross sectional library. As the referenced interactions are energy dependent, ORIGEN requires knowledge regarding the energy spectra of a flux produced in a given simulation such that it can sample isotope depletion (and associated creation) within the proper statistical range. One yields this spectra data from MCNP through the use of the Tally Energy tool which collects the energy spectra of a given tally for a given particle into several prespecified energy bins, where the binning is done over the same energy ranges covered in the to-be-referenced cross sectional library. The bridge gap between MCNP and ORIGEN is then interfaced using COUPLE, another software specifically used to format the energy spectra of a simulated flux into one that is consistent in format with the cross sectional library ORGIEN intends to read from. Referencing the reformatted energy spectra, ORGIEN then applies it to its referenced cross sectional library, effectively irradiating it and yielding a new material composition.

Considering the dependent nature a scenario's material composition has on its ability to produce a given flux, and how it is the intensity of said flux that drives the depletion, it reasons that iterative, small time steps must take place to properly capture the effects material transmutation has on the flux and ensure library irradiation is being updated as a result. Between these time steps, a user would ideally update their initial MCNP input with the irradiated material composition produced by ORIGEN to produce new flux spectra which would then be routed into the cycle process of COUPLE→ORGIEN→MCNP→COUPLE etc. As a consequence of the use of MCNP's Tally Energy tool, the simulation must be re-ran for each energy bin, and given ORIGEN uses 252 energy group cross sectional libraries (again, for which the bins in MCNP have to be consistent with) this process can be a lengthy computational endeavor. Ultimately, such computation is still more ideal than an analytical tracking of all depleted and produced isotopes as the two coupled resulting in a solution containing 19+ linearly coupled differential equations. Use of ORIGEN in the presence of a photonuclear source has been verified but the user must specify all nuclides that may undergo photonuclear interactions rather than just nuclides likely to undergo fission[31].

Proposed ORIGEN Investigation:

To elaborate on the RACE target optimization study mentioned in Section 3.3, an electron beam incident upon a flat target saw its energy deposition into the fuel was quickly attenuated within the first ~5% of the target's axial length and first ~43% of its radial length as a result of bremsstrahlung process and ionization of electrons. Further investigation revealed significant backscattering was additionally contributing to the rapid fall off energy deposition in the fuel. As a remedy to this, a target geometry was proposed in the form of a conical void in the base of the target with the optimal functionality being that the incident beam would have its electron distribution applied largely onto the conical gradient Figure 46, spreading the axial power distribution. Given that such an improvement to the target geometry would increase its operational power with no modification to the beam power, and considering that such an improvement could not be effectively simulated using a single incident electron (as this electron would merely fall incident into the conical void's vertex), a simulation of a beam source scaled to the appropriate intensities listed in Table 1**,** could prove useful in reducing beam power for a 5kW assembly. The depletion effects of more fuel use at lower power levels in contrast to less fuel use at higher power levels would need to be evaluated via an additional simulated problem of a scaled beam source incident upon a flat target. Flux spectra obtained in both scenarios (Figure 47) would then be introduced to ORIGEN yielding two respective sets of new material composition for a given time step from which new operational powers could be deduced.

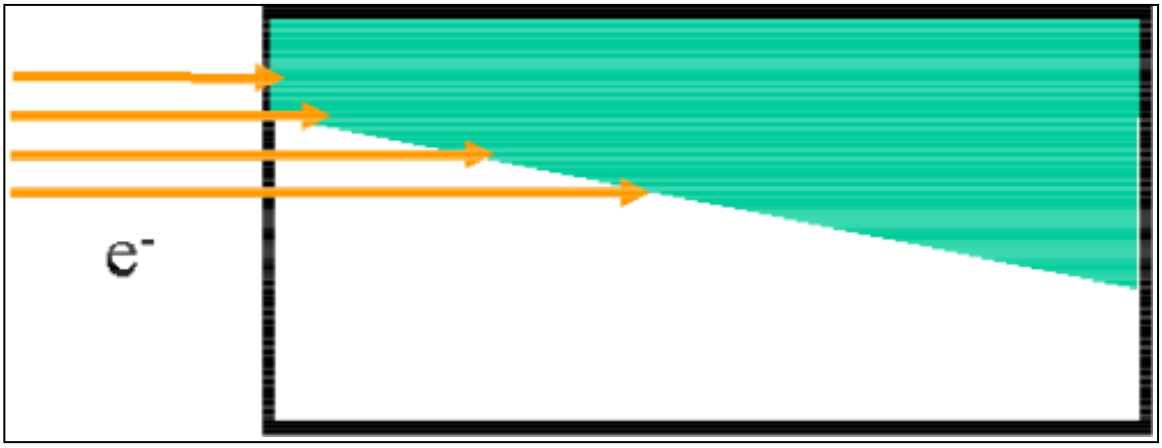

Figure 46: Depiction from RACE Spiral II-Geometry Improvement

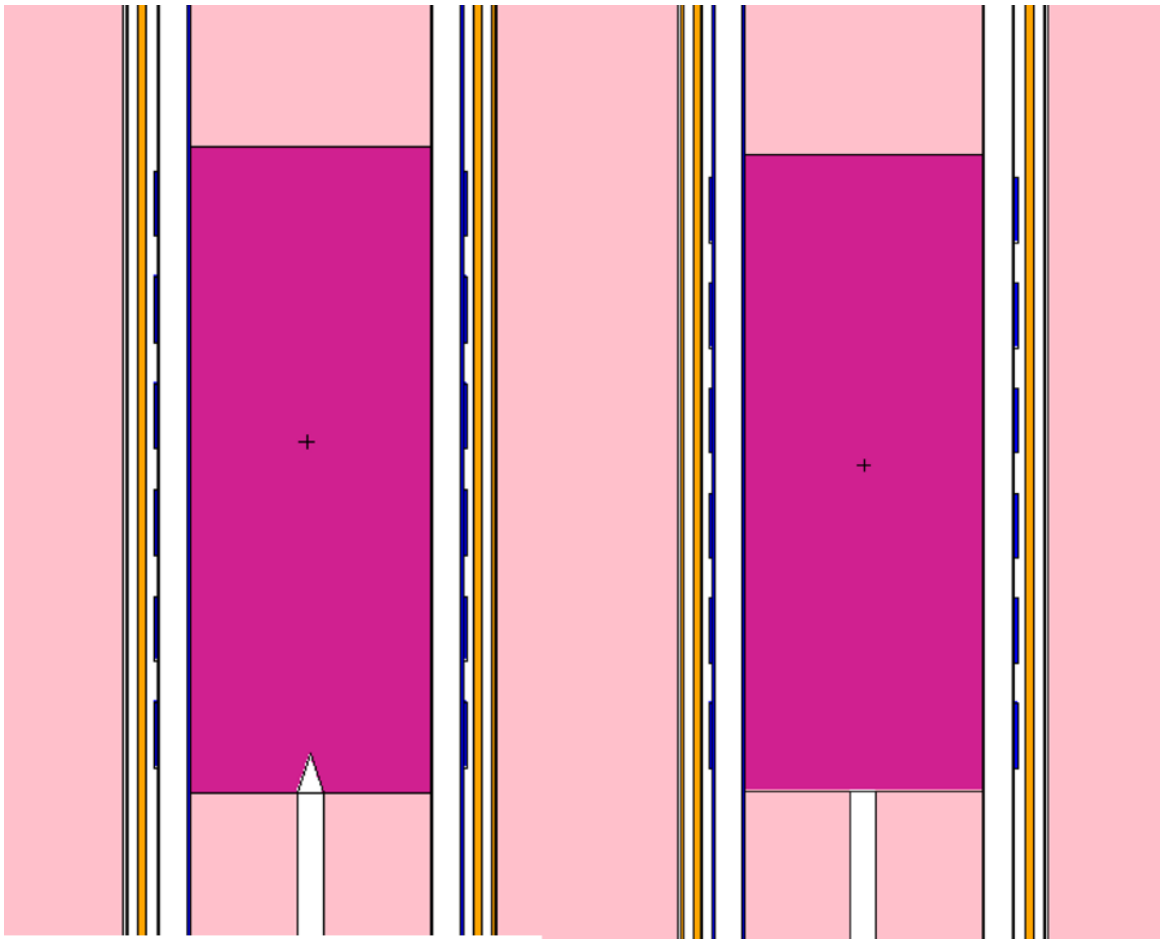

Figure 47: Displays the two KRUSTY cores for which a beam source depletion is proposed

Preliminary Considerations for an EADS KRUSTY:

Reactor operation is officially compromised when the desired energy level can no longer be achieved as result of excessive isotope depletion that negatively affects reactivity and thus the neutron population. For KRUSTY, this would be when power falls below 5kW, or for an ADS system, the instance when reactor power equals that of the driving accelerator. Understanding that core power is a function of neutron population, particles produced through the depletion/transmutation of the uranium isotopes, it follows that while one may be able to run their reactor at a higher power, doing so directly increases the rate of burn up. Suppose the use of KRUSTY at the necessary power insulated at in Table 1 for a 5kW net gain, the depletion rate can be approximated by Equation 22 as a function of the rate of fission[32]:

EQ22: $$Depletion\ Rate = \left(\frac{Power{*}Time}{Energy_{per\ fission}}\right)\left(\frac{Atomic\ Mass}{Avogadro's\ \#}\right)$$

Which for a MW power level reactor with burn steps approximated daily by gram, leaves:

$$Depletion\ Rate\frac{Grams}{Day} = 0.895 * \left(\frac{Power_{MW} * Atomic\ Mass}{Energy_{per\ fission\ MeV}}\right)$$

$$0.895 * \left(\frac{1E^{-1} * 235}{200}\right) = .105\frac{Grams}{Day}$$

A general implication of this relation is the requirement of ~1 gram of U235 consumed per 1MW day of usage. Since KRUSTY is only 28kilograms of uranium, (5.6kg U235 in a LEU configuration), this implies that at 15 years of operation, the system will have experienced ~10% burnup, 100x more than its HEU, non-EDAS configuration. So if longevity is infringed on when reactor power = accelerator power, the question becomes “how long at 1MW until 5kW worth of

U235 is depleted?” Such a question cannot accurately evaluated until fuel material composition-flux relationship behavior for a photonuclear system is analyzed.

Simulations and Resulting Effects of Depletion on Power:

Using electron intensity data from Table 1, a beam source was defined in MCNP consistent with 50MeV electrons and 20% enriched fuel at 5kW. The nature of this beam was scripted such that ithad two major axes (a cylindrical beam limited in shape by the 1" beam port leading to the fuel interface as seen in the bases of Figure 47) and maintained 63% of the total electrons within 1 standard deviation of its center, Figure 48. In respective simulations, this beam source was then driven incident against the base of flat and conically indented KRUSTY. Core power yields were then reexamined to investigate potential performance enhancement from the use of the conically indented target. Figures 49 and 50 respectively display the neutron flux profiles and yielded power levels obtained from these target geometries when operating at the proposed scaled intensity. The 1.5cm deep cone target allowed for more axial and radial propagation of energy into the core, resulting in conical core power being ~1.06x greater than that of the flat core's.

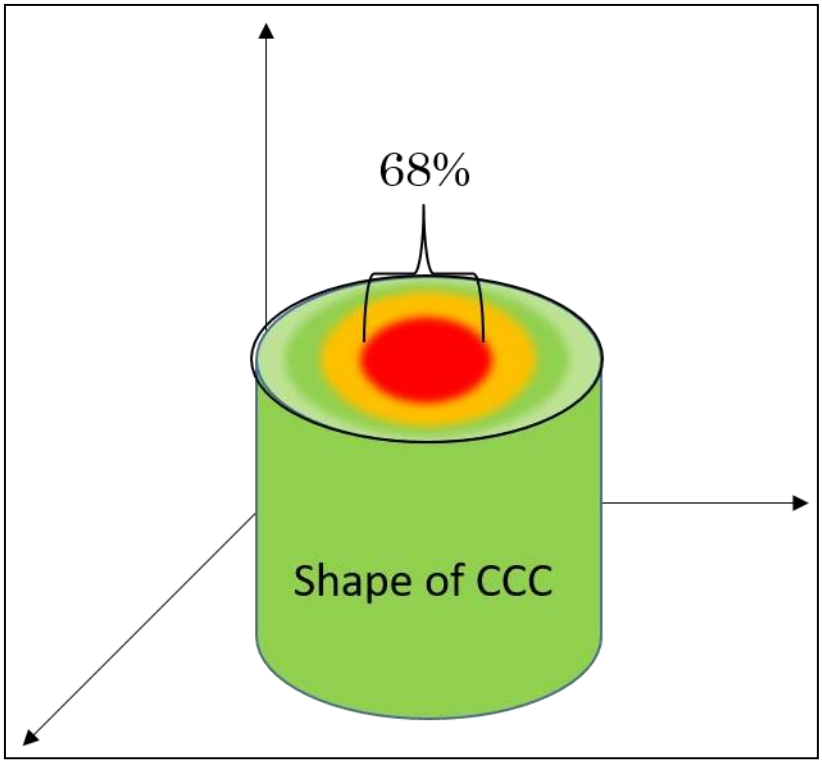

Figure 48: MCNP beam geometry

With enhanced performance in mind, the electron intensity was rescaled to the desired power and the beam source simulation was re-run for the conical target, this time using the MCNP tally tool, the E Card, to capture the energy spectrum of the produced neutrons in desired energy bins. The yielded neutron energy spectra was then input into a COUPLE-ORIGEN input script, Appendix G, and a single burn step of 30 days was performed. From the fuel's initial UMo content, ORIGEN produced a list of 252 different isotopes (some metastable variants) which were then carefully integrated back into the rescaled, conical target MCNP input deck. Considering that neither the ENDF8 nor TENDL-2019 particle cross sectional libraries contained photonuclear data on all of the isotopes yielded from ORIGEN, the use of the MCNP's MX card was employed. The MX card allows the substitution of the photonuclear cross section for an unknown nuclide for that of a known; this was done in attempt to remain consistent with isotope stability (usually substituting for the next closest, known isotope of that element). Running MCNP once more on the fuel's new material composition (normalized from the gram values yielded from ORIGEN), the effects of a 30 day operation were investigated. Figures 51 and 52 respectively display the effects of burnup on the neutron flux profile and effects on the operational power which was reduced from desired power levels by ~97%.

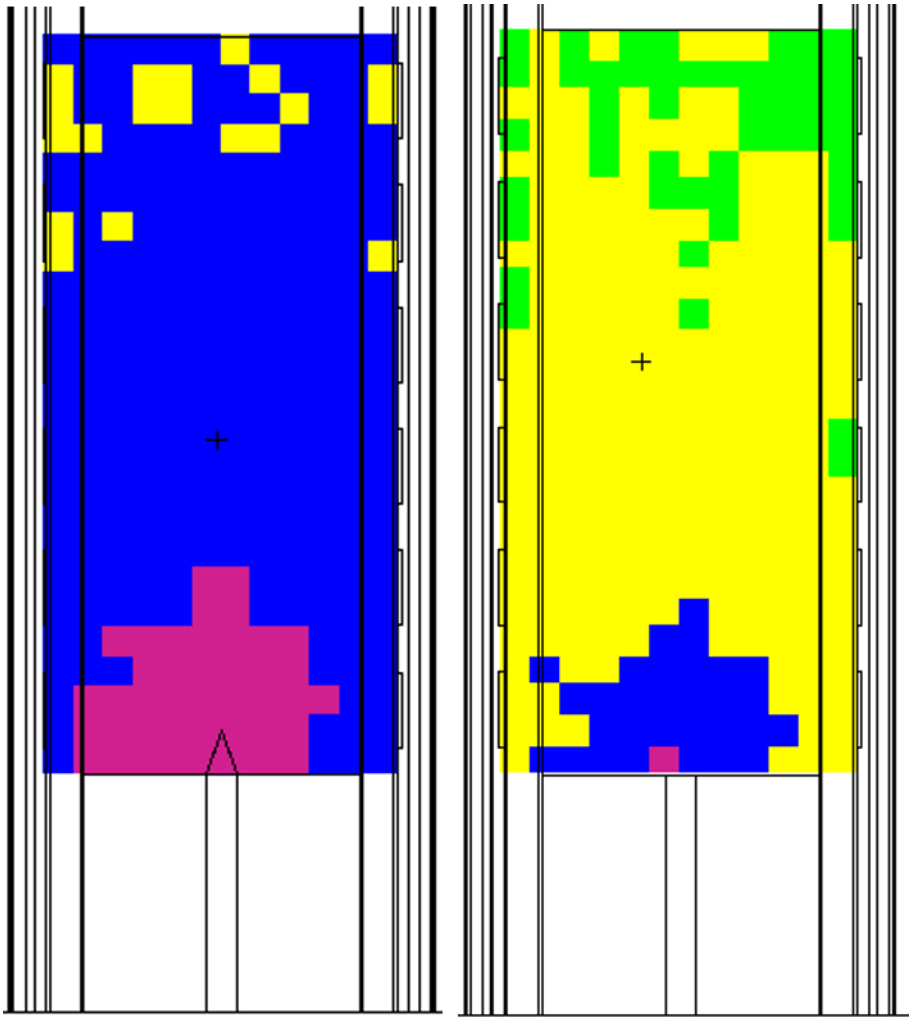

Figure 49: Neutron Flux VS Target Geometry, Cone (left), Flat (Right)

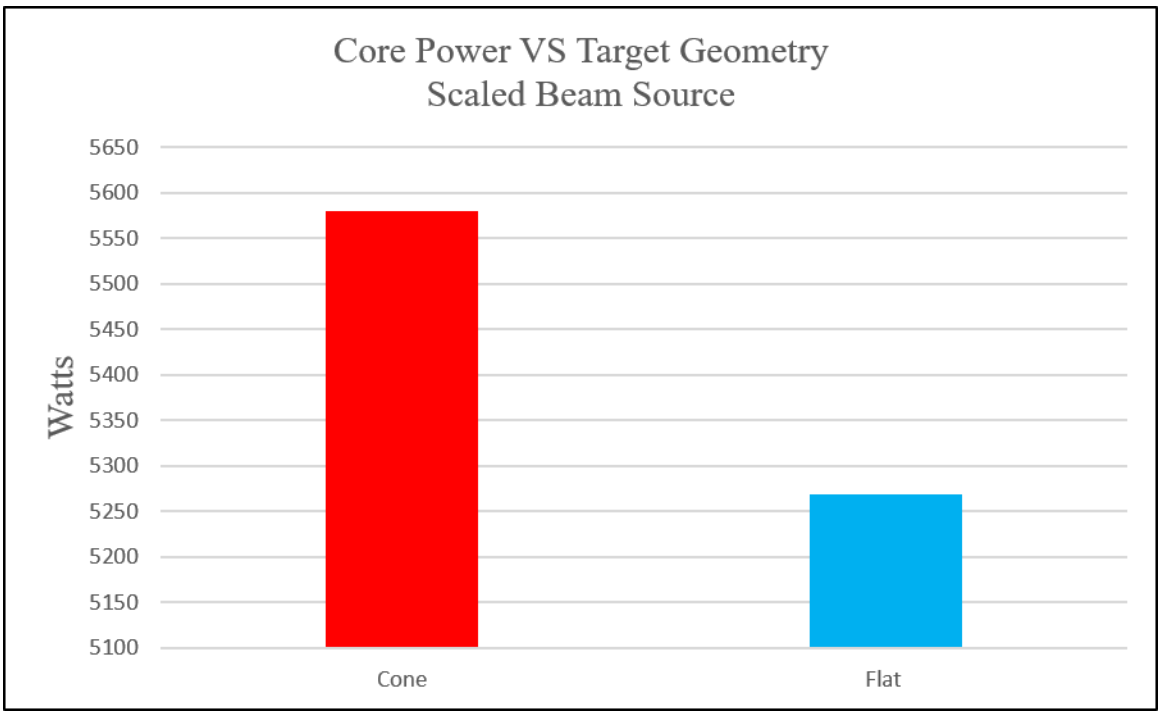

Figure 50: Core Power VS Geometry

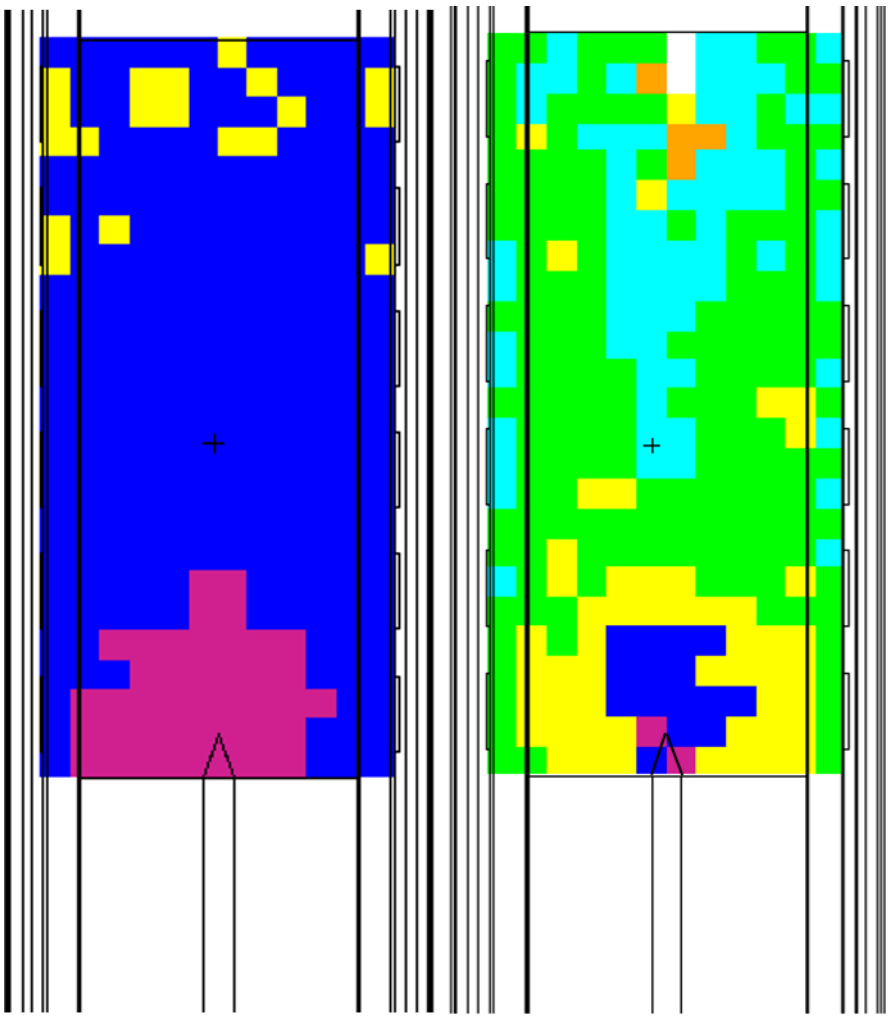

Figure 51: Neutron Flux VS BURN, Fresh (left), BURN (right)

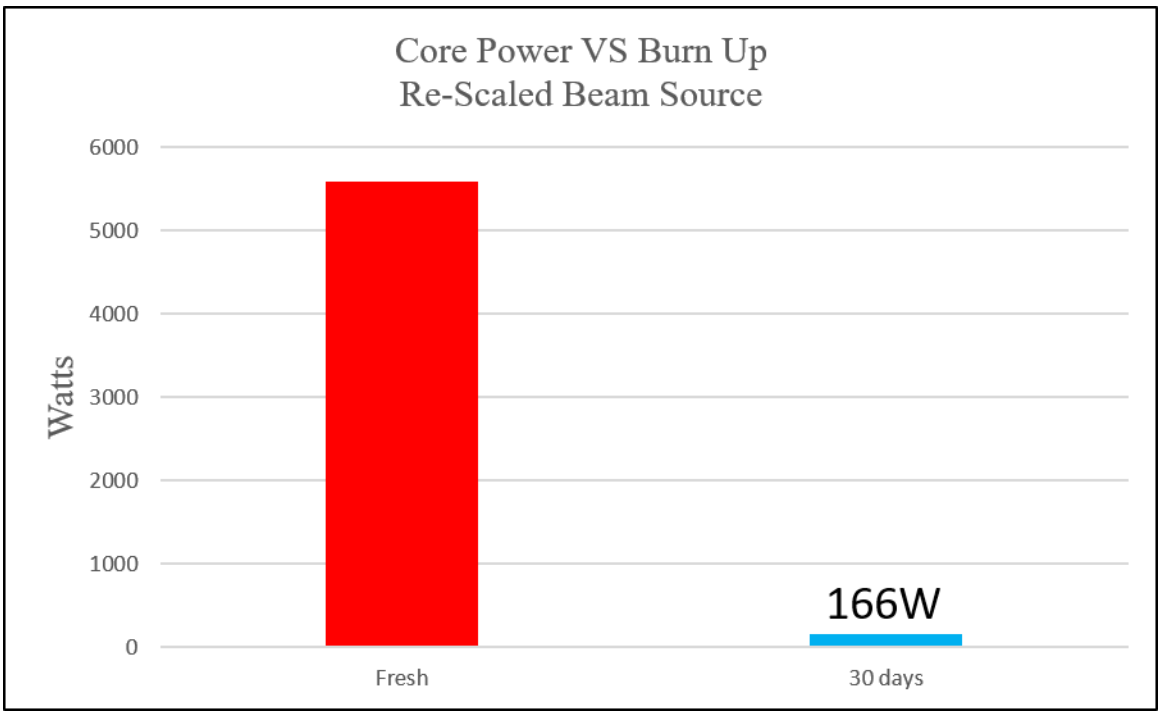

Figure 52: Core Power VS BURN

Chapter 7: Conclusion

The KRUSTY core has been recreated in MCNP such to capture all geometric and material properties of its traditional HEU design. The photonuclear effect's primary mechanism for excitation was validated to be in effect within the energy levels covered in this research. Electron stimulation of an LEU version of the core, found that KRUSTY's low multiplication required the majority of the desired neutron population to be sourced from photoneutrons rather than fission. Visual representation of the various particle fluxes suggest that energy deposition into the core was largely captured within the bottom 20-50% of the core likely biasing tally results as they were normalized by the fuel's volume. The suggested use of a 100kW beam is consistent with the historical usage of EDAS and given that such a beam power is roughly 20x larger than that of the desired operational power of the reactor, it would be difficult to justify the reduction of the core'sU235 weight percentage to LEU levels. That said, values extrapolated from this research's parameterization does indicate that for a near 20% bump in power from 5.1 to 6kWth, the KRUSTY design could be assembled with enrichments as low as 70%, 23% less than its current configuration. Potential cost savings from such a reduction in enrichment are negated by the well-known enrichment threshold costs which indicate savings would likely be negligible as the majority of the seperative work is localized in the 1st 20% of enrichment and IAEA regulatory policies still apply at all enrichments above 20%. Proposed depletion analyses using the ORIGEN software are presently underway to determine the role of geometric optimization in both efficiency and fuel utilization as a function of time. Approximated looks into the fuel's depletion in response to operating at a higher power ($5_{kW} + Power_{beam}$), suggest the use of EADS increases the 15 year burn up of KRUSTY to roughly 100x that of to that of its original configuration.

References:

1. Poston, D., Gibson, M., McClure, P., Godfroy, T., "*KRUSTY Reactor Design*," Los Alamos National Lab; National Aeronautics and Space Administration, Jun 2020.

2. Poston, D., *"KRUSTY: The first nuclear-powered test of a new US fission reactor concept in over 40 years*," University of Tennessee at Knoxville, Department of Nuclear Engineering Colloquium, Feb, 3, 2021

3. Johnson, S., Center for Space Nuclear Research, Prelude to Project Presentations, Aug, 10, 2021.

4. Poston, D., Gibson, M., McClure, P., *"Kilopower Reactors for Potential Space Exploration Missions*," Nuclear and Emerging Technologies for Space, American Nuclear Society Topical Meeting, Feb 2019.

5. Poston, D., McClure, P., "*Use of LEU for Space Reactor*," LA-17-27226, Aug, 11, 2017.

6. Gibson, M., Poston, D., McClure, P., Sanzi, L., Godfroy, T., "*Heat Transport and Power Conversion of the Kilopower Reactor Test,*" Nuclear Technology Journal, Volume 206, Oct, 14, 2019.

7. Marc, G. "*Demonstration Proves Nuclear Fission System can Provide Space Exploration Power,*" Nasa.gov, Press Release, May, 2, 2018.

8. Nasa.gov, "*Fission Surface Power, Space Technology Mission Directorate*," Press Release, May, 7, 2021.

9. Baldwin, G., Klaiber, G., "*Photo-Fission on Heavy Element*," Physical Review, Vol 71, Jan, 1, 1947.

10. Clayton, D., "*Principles of Stellar Evolution and Nucleosynthesis*," University of Chicago Press, 1984.

11. Thorton, S., Rex, A., "*Modern Physics for Scientists and Engineers*," 4th Edition, Chapter 12. 2013.

12. Steinberg, E., "*Nuclear Fission, Induced Fission*" Encyclopedia Britannica, Apr, 10, 2020.

13. Clarke, S., Wieger, B., Enqvist, A., "*Measurement of the Energy and Multiplicity Distribution of Neutrons from the Photofission of U235*," Lawrence Livermore National Laboratory, DOC 732408, June, 4, 2017.

14. Feynman, R., "*The Feynman Lectures on Physics, Vol II*," Published by Addison-Wesley, 1964.

15. L'Annuizata, M., "*Radioactivity: Introduction and History, from the Quantum to Quarks, 2nd Edition*," Published by Elsevier B.V, 2016.

16. Raskinyte, I., Dupont, E., Ridikas, D., "*Photonuclear Evaluation of 235-U*," JEFF Meeting: DOC-1117, Nov, 28, 2005.

17. Ridikas, D., Safa, H., Maubornge, M., "*Conceptual Study of Neutron Irradiator Driven by Electron Accelerator*," Nov, 2002.

18. Vretenar, M., "*Differences Between Electron and Ion Linacs*," CERN, 2006.

19. Mishin, A., "*Advances in X-Band and S-Band Linear Accelerators for Security, NDT and Other Applications*," American Science & Engineering INC., Proceedings of 2005 Particle Accelerator Conference.

20. Guillen, D., Seviour, R., "*RF Cavity design for a Low Cost 1 MeV Proton Source*," University of Huddersfield, IPA Proceedings, 2017.

21. Beller, D., "*Overview of the AFCI Reactor-Accelerator Coupling Experiments (RACE) Project,*" Idaho Accelerator Center, Idaho State University.

22. Krakowiak, C., Safa, H., Bergeron, A., "*Preliminary Study of the RACE Target*," French Alternative Energies and Atomic Energy Commission, Jun, 21, 2005.

23. Gohar, Y., Bolshinsky, I., Karnaukov, I., "*KIPT Accelerator-Driven System Design and Performance*," Nuclear Energy Agency, 2015.

24. Mamtimin, M., Diemer, J., Grimm, T., Odeh, F., "*High Power Liquid Lead-Bismuth Targetry for Intense Fast Neutron Sources Using a Superconducting Electron Linac*," High Power Targetry Workshop, June, 2018.

25. Poston, D., Gibson, M., Godfroy, T., McClure, P., "*Design of the KRUSTY Reactor*," Nuclear and Emerging Technologies for Space Conference, Feb, 26, 2018.

26. Poston, D., "*KRUSTY Design and Modeling*," LA-UR-16-2877, Nov, 1, 2016.

27. Talanov, V., "*Calculate Manually Reaction rate in MCNP with F4 Tally*," Paul Scherrer Institute, Apr, 13, 2016.

28. Bergeron, A., Talamo, A., Subhasish, M., "*Monte Carlo Calculation of the Energy Deposition in the Transformational Challenge Reactor*," ANL, ORNL, DOC: 1760101, 2020.

29. Los Alamos National Laboratory, "*MCNP6.2 User's Manual, Section 3.3.5.25, Superimposed Mesh Tally*" LA-UR 17-29981, Oct, 27, 2017.

30. Los Alamos National Laboratory, "*MCNP6.2 User's Manual, Section 3.3.4.13, BURN*" LA-UR-17-29981, Oct, 27, 2017

31. General Atomics, "*Mo-99 Target Assembly Nuclear Design for Once-Though Operation*," Reactor-Based Molybdenium-99 Supply System Project, NRC DOC: ML1713A244, Jan, 19, 2017

32. Lamarsh, "*Nuclear Reactor Analysis, Section 3.6*,"Addison-Wesley Publishing, 1966.

Appendix A

Surface Flux VS Enrichment 5-15%

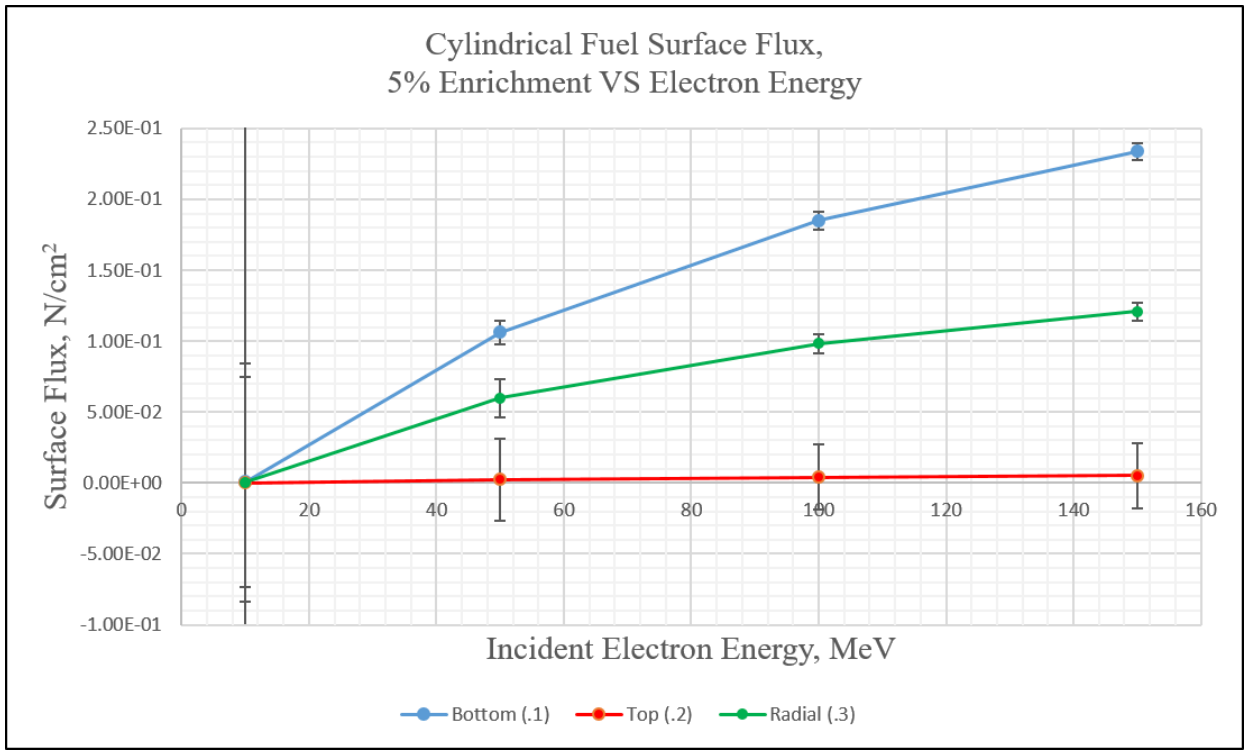

Figure 11: Surface Fuel Flux 5% Enriched

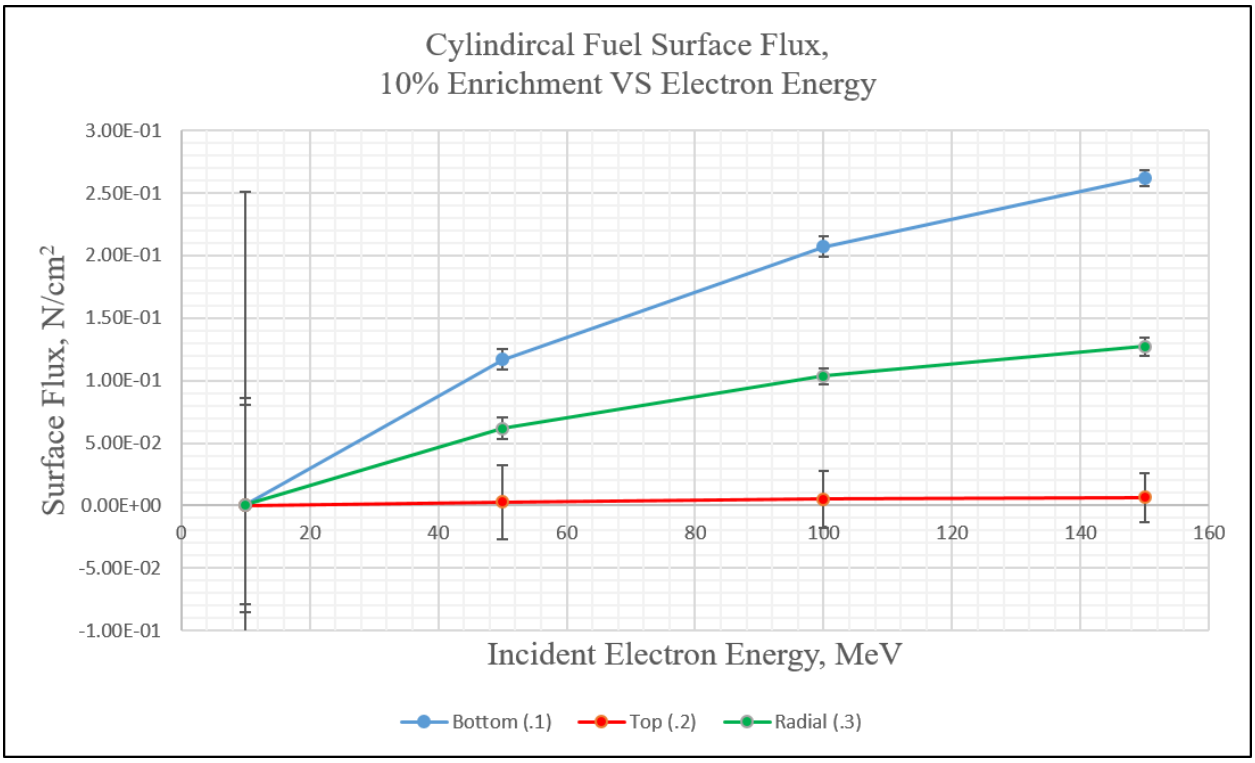

Figure 12: Surface Flux, 10% Enriched

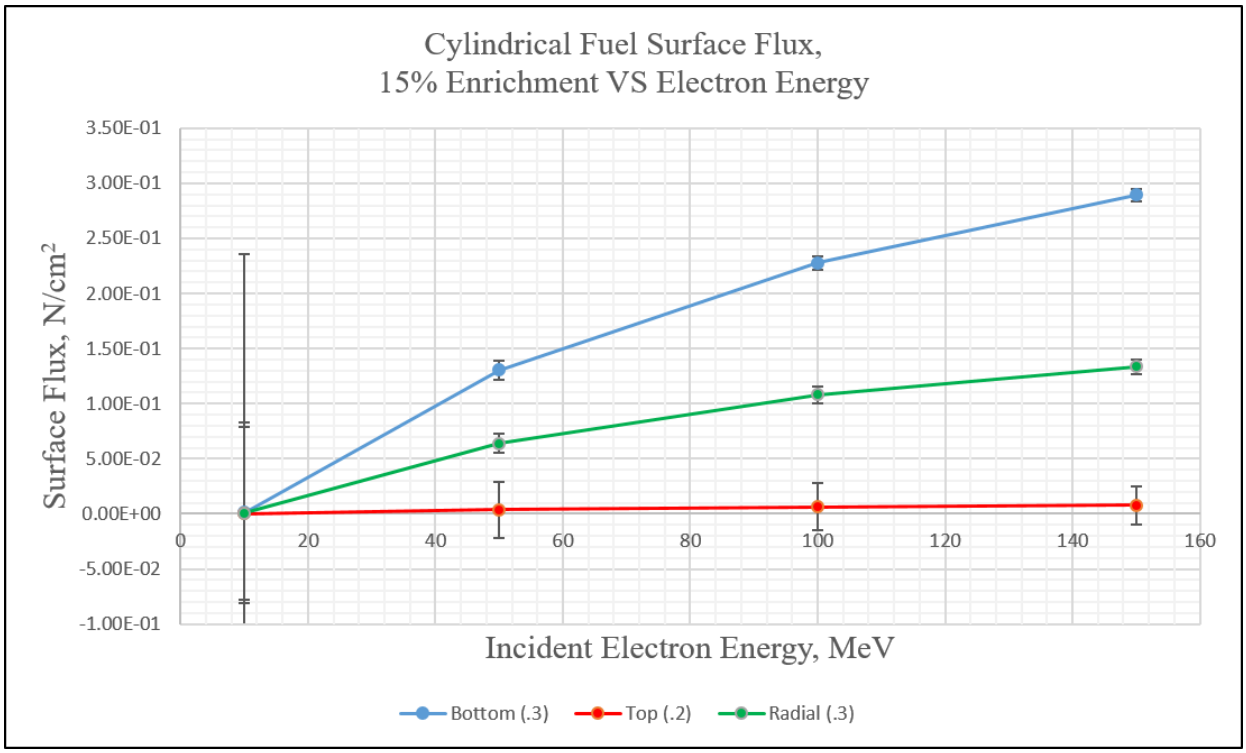

Figure 13: Surface Flux 15% Enriched

Appendix B

Fmesh Profiles

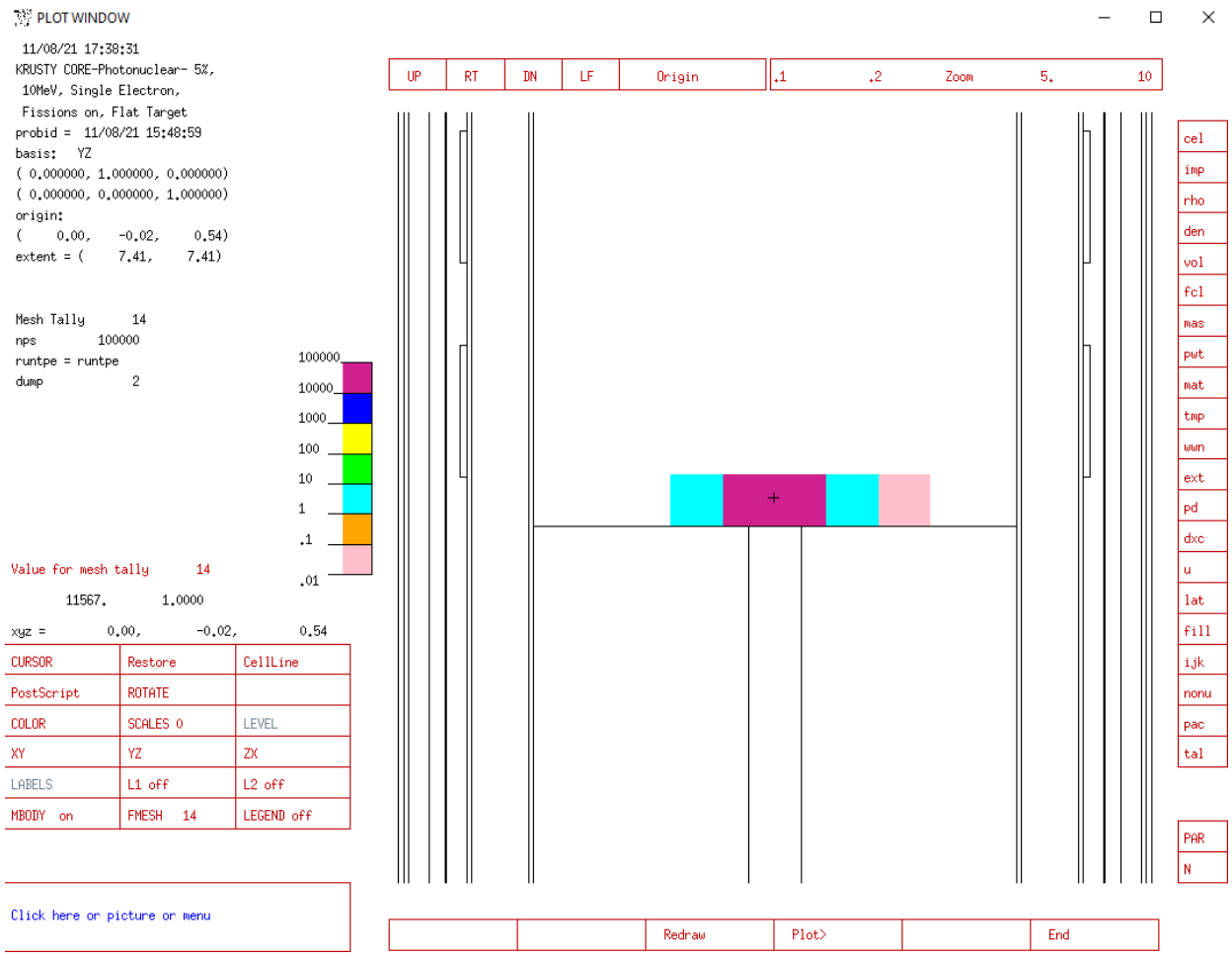

Figure 19: Electron flux, 5% Enrichment, 10meV side view.

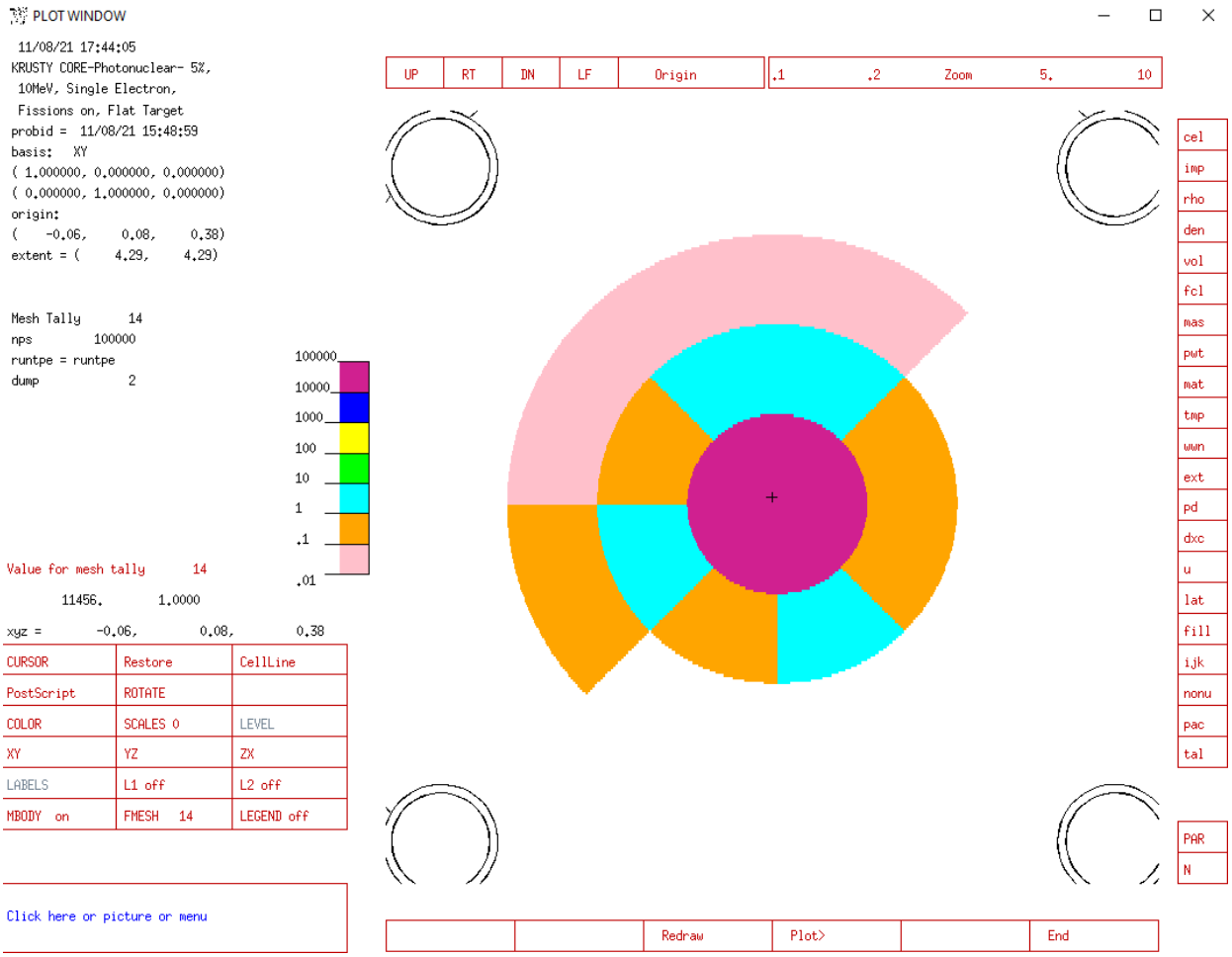

Figure 20: Electron Flux, 5% Enriched, 10MeV, top view

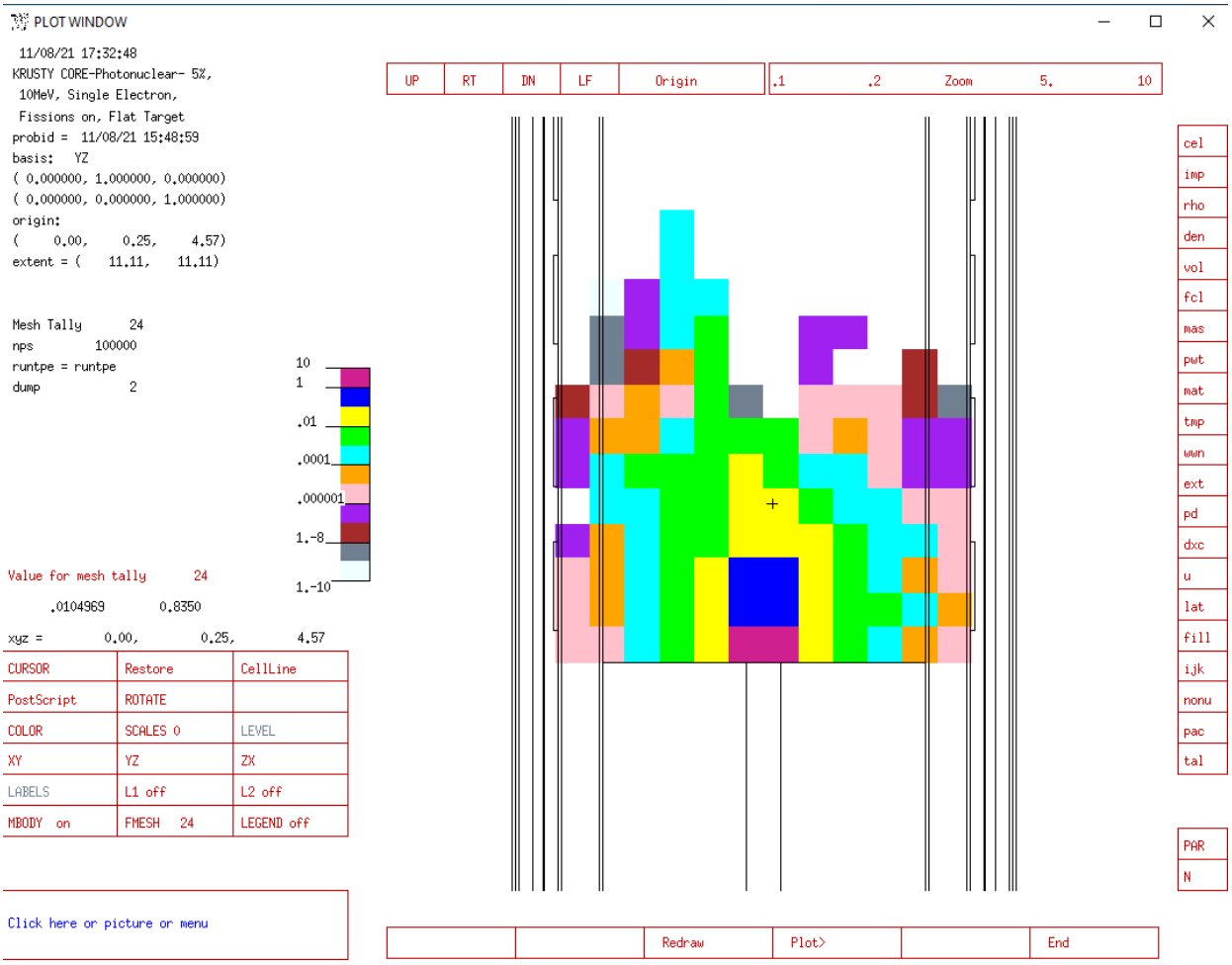

Figure 21: Photon Flux, 5% enriched, 10MeV, side view

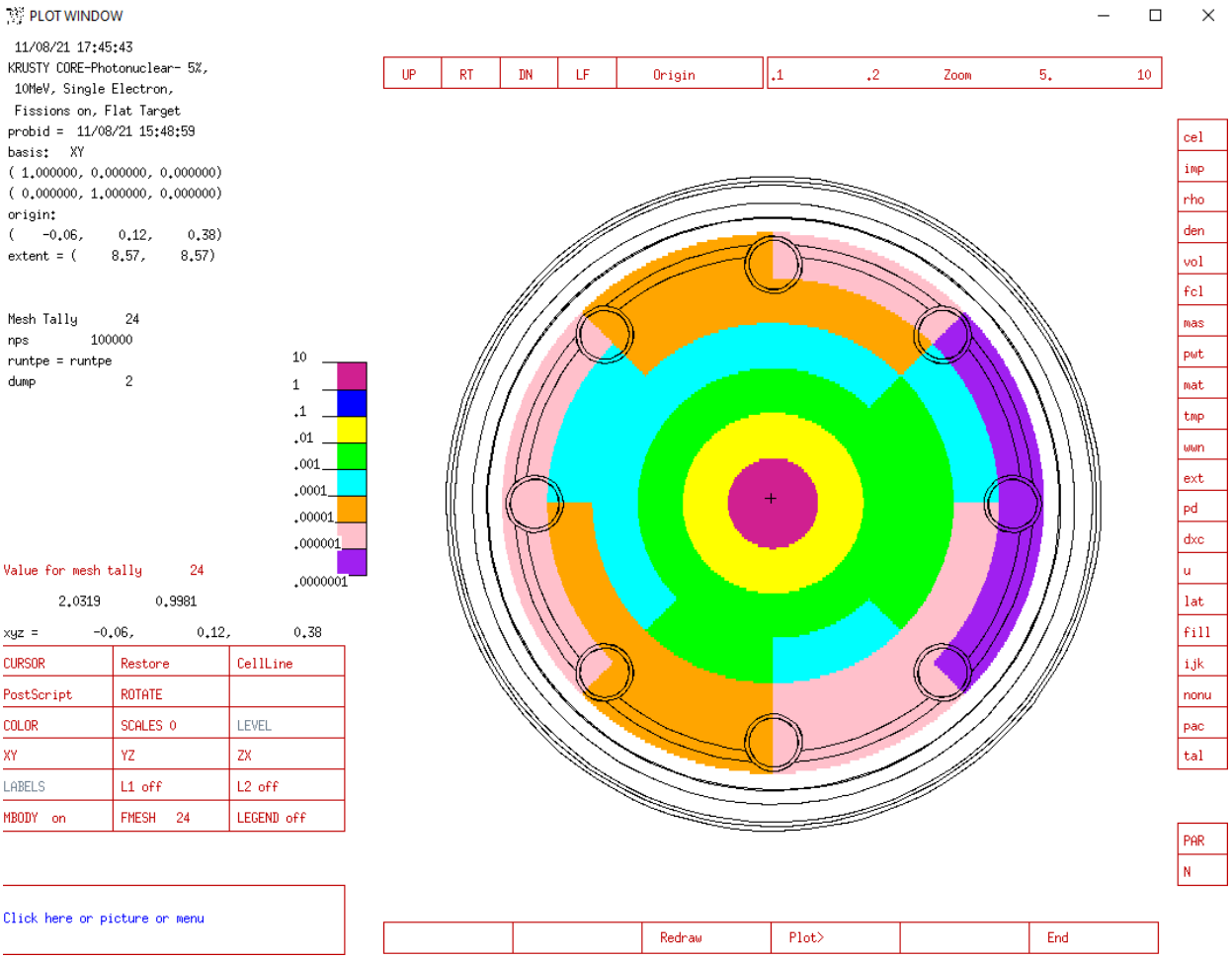

Figure 22: Photon flux, 5% enriched, 10MeV, top view

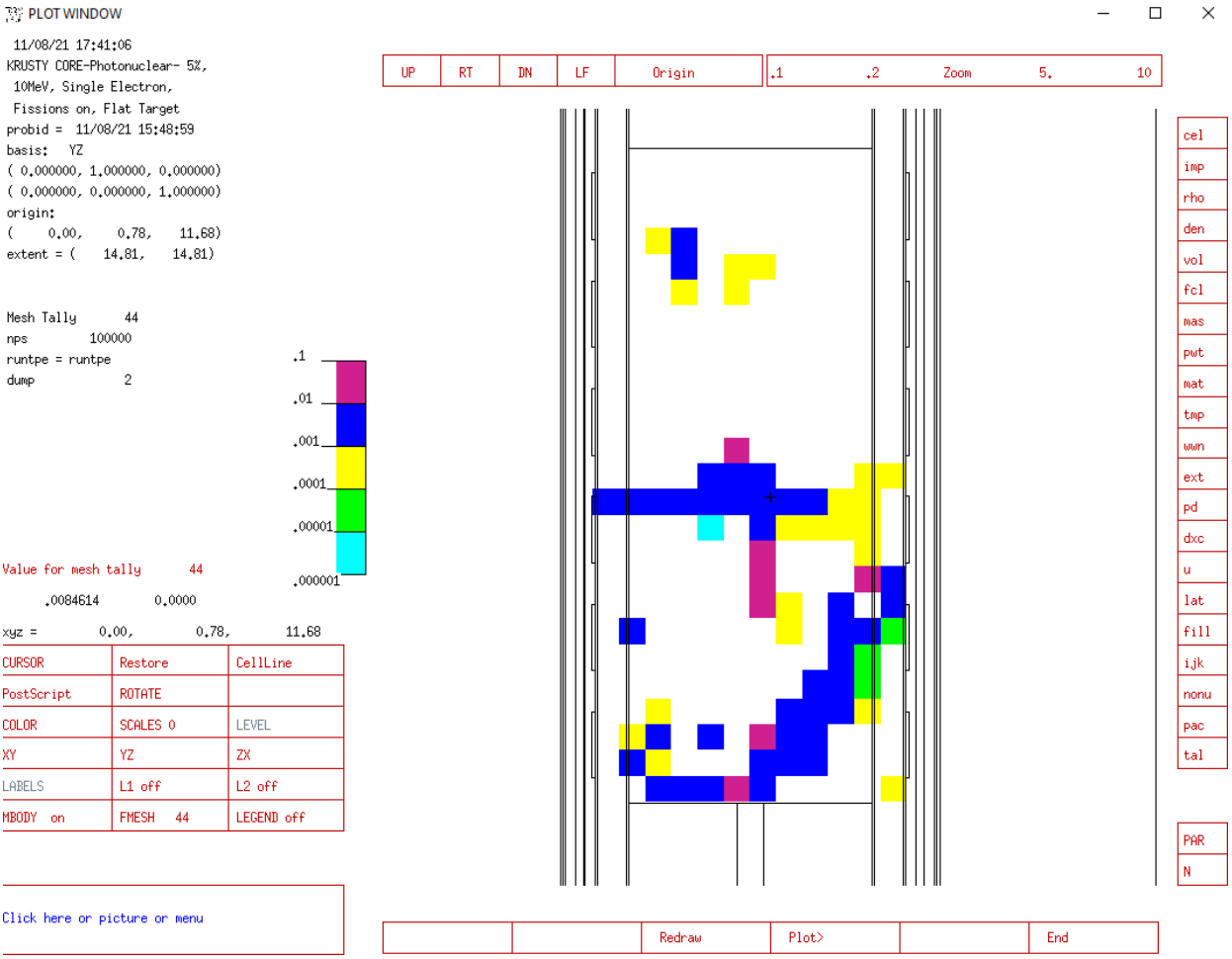

Figure 23: Neutron flux, 5% enriched, 10MeV, side view

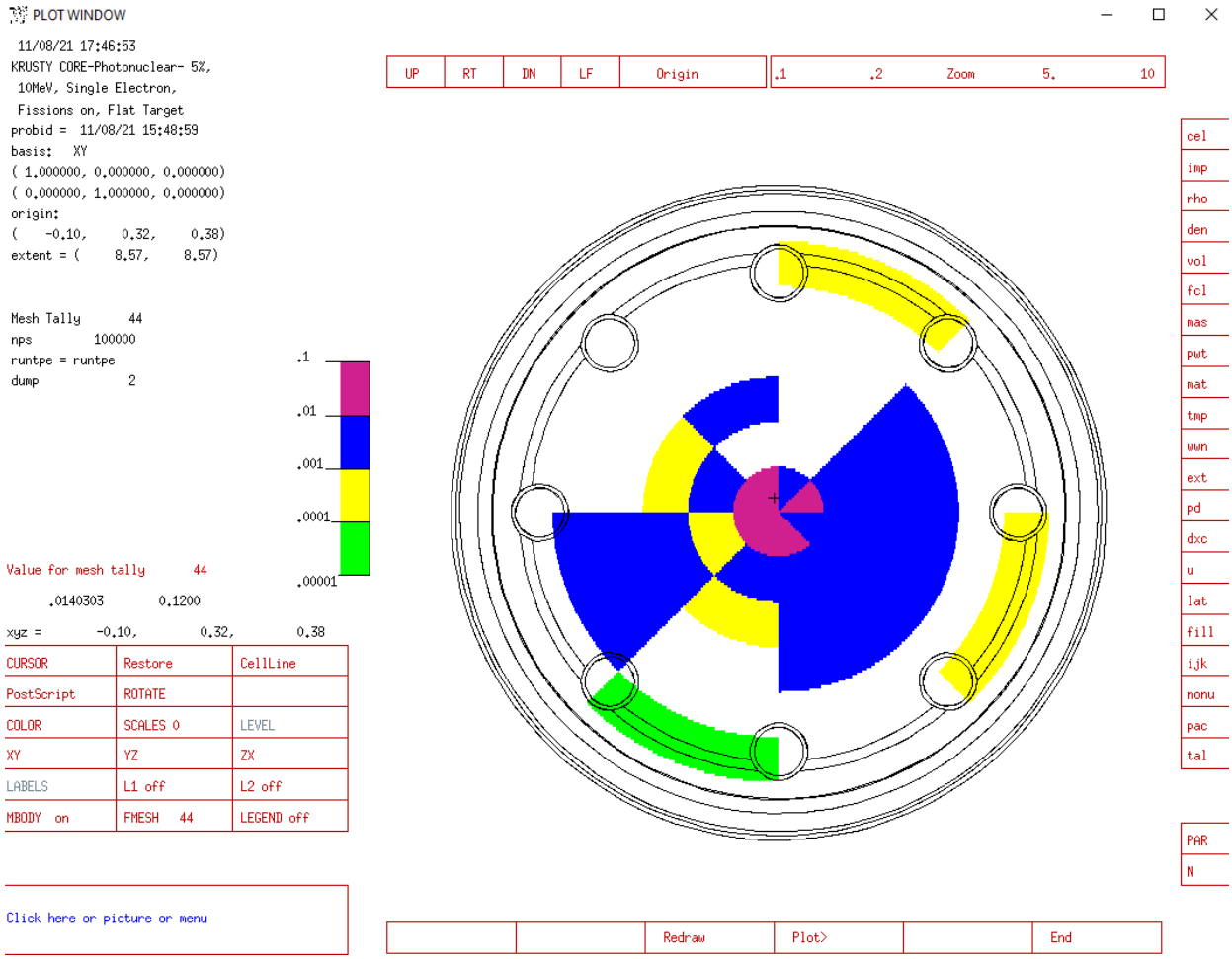

Figure 24: Neutron flux, 5% enriched, 10MeV, top view

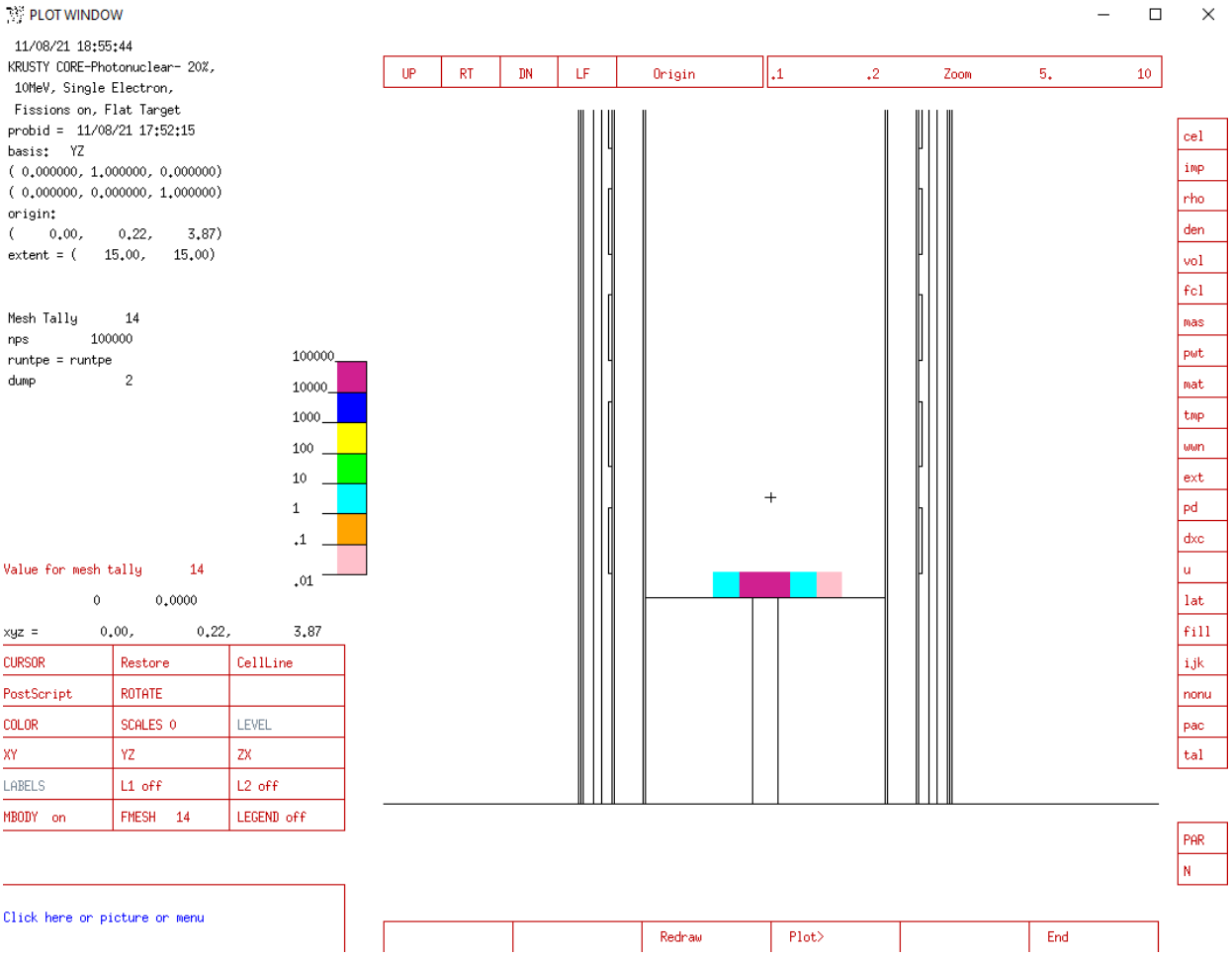

Figure 25: Electron flux, 20% enriched, 10MeV, side view

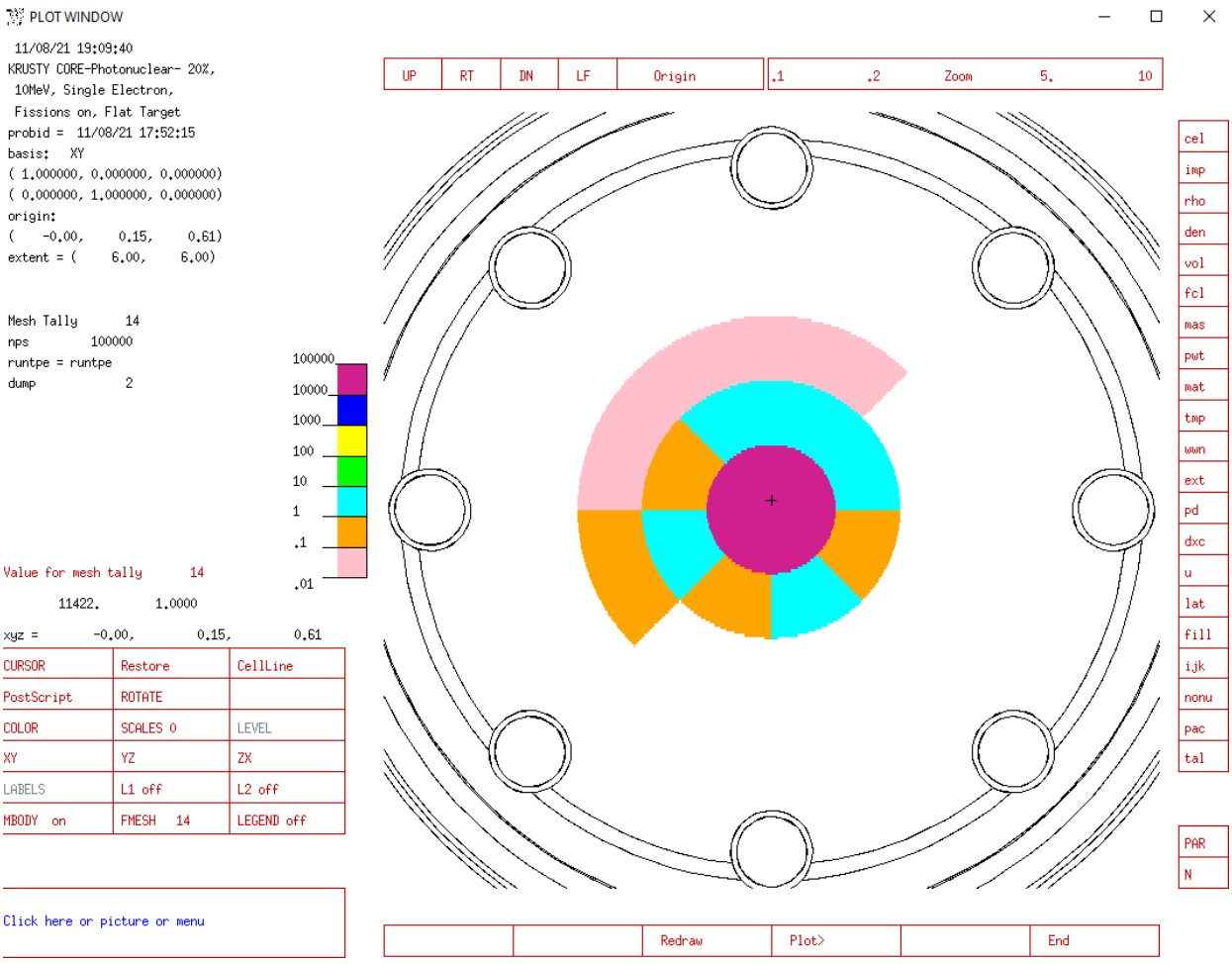

Figure 26: Electron flux, 20% enriched, 10MeV, side view

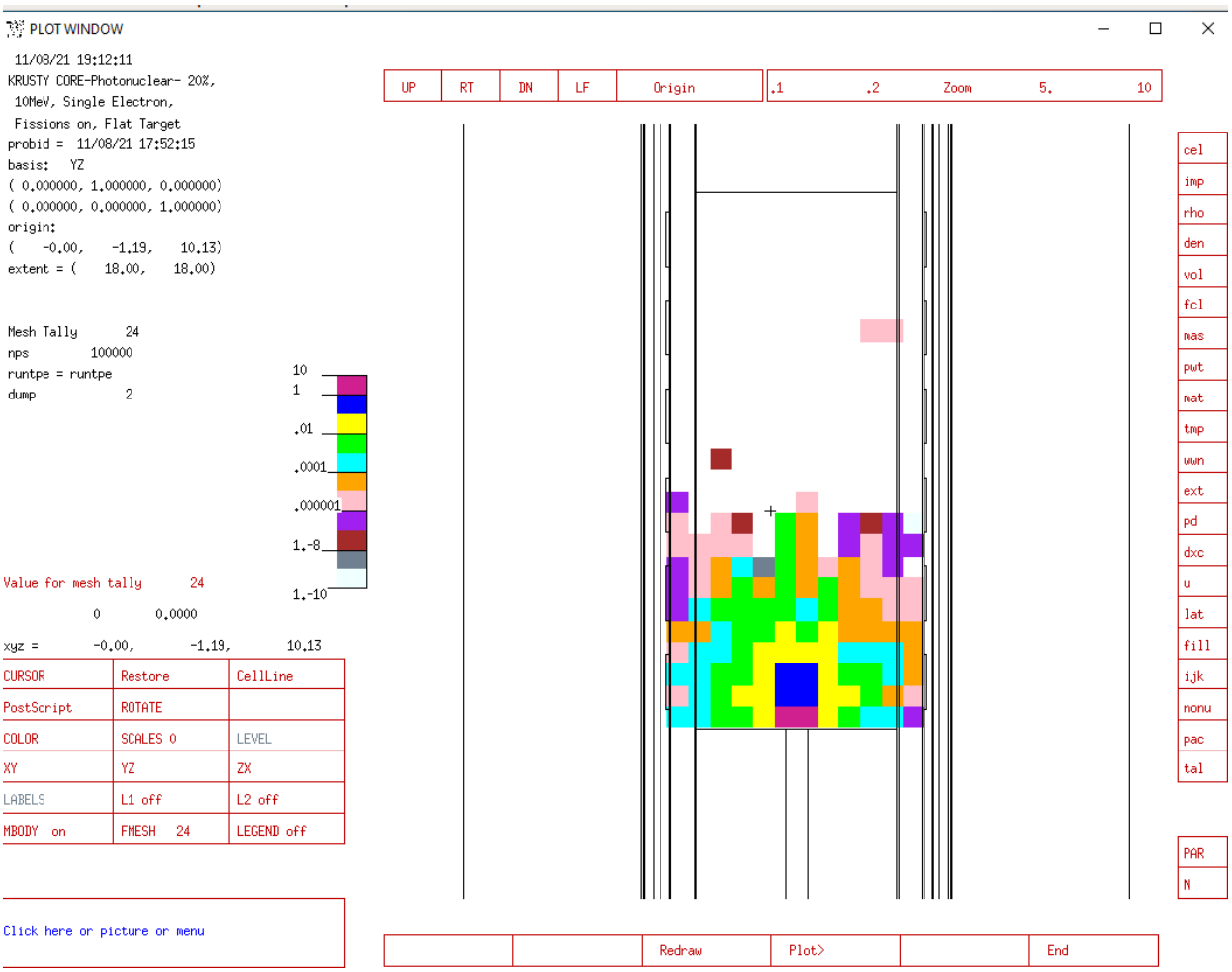

Figure 27: Photon flux, 20% enriched, 10MeV, side view

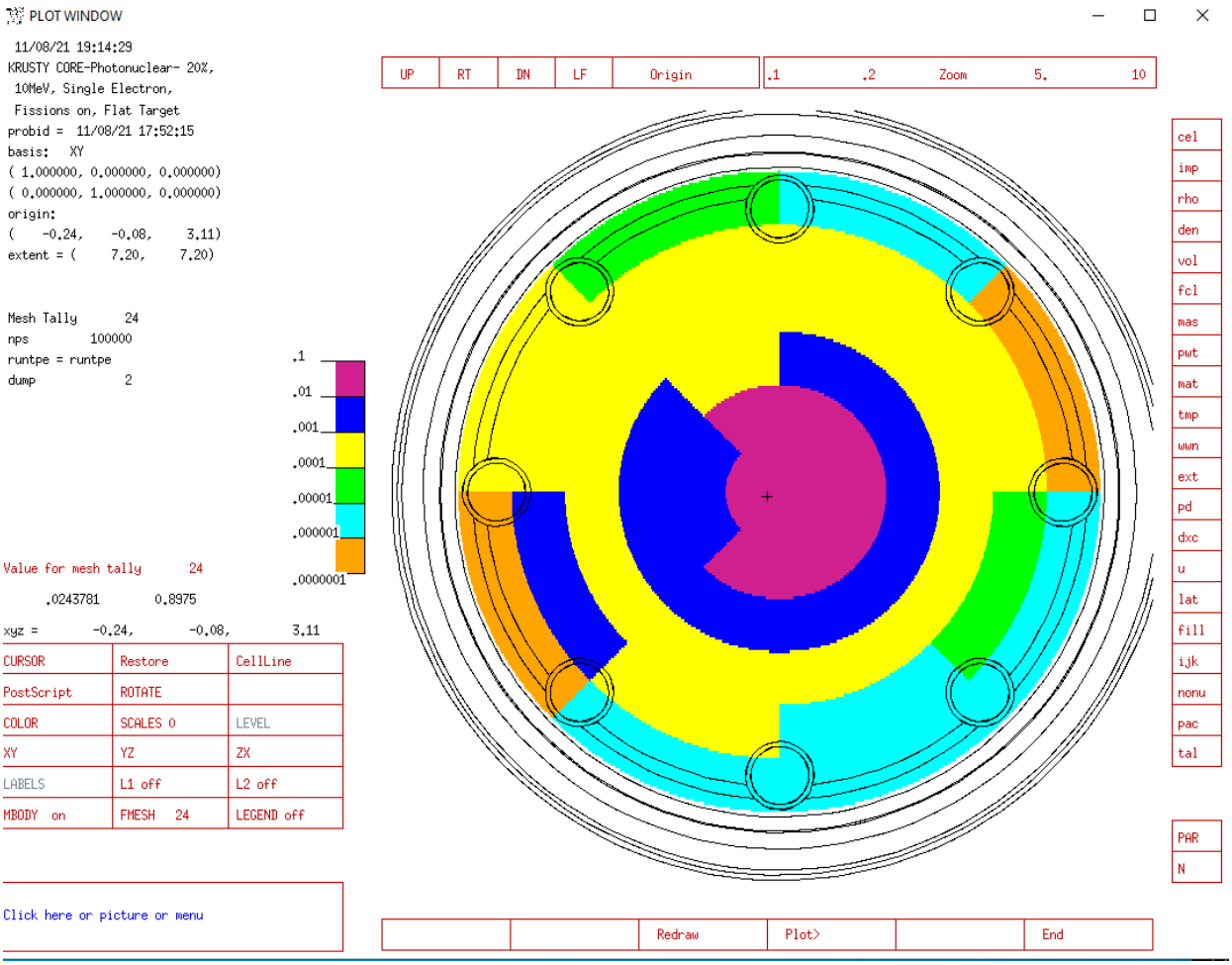

Figure 28: Photon flux, 20% enriched, 10MeV, top view

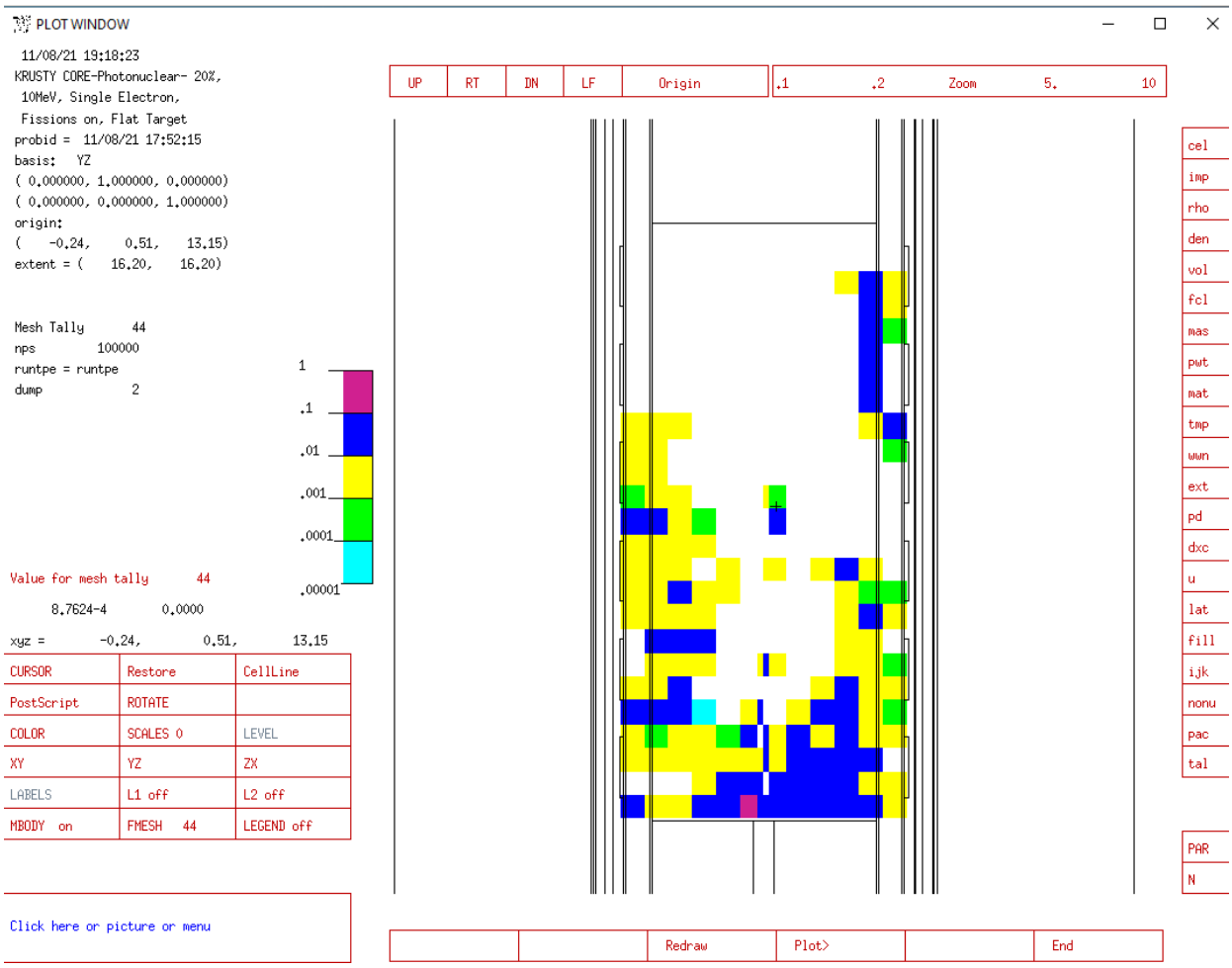

Figure 29: Neutron flux, 20% enriched, 10MeV, side view

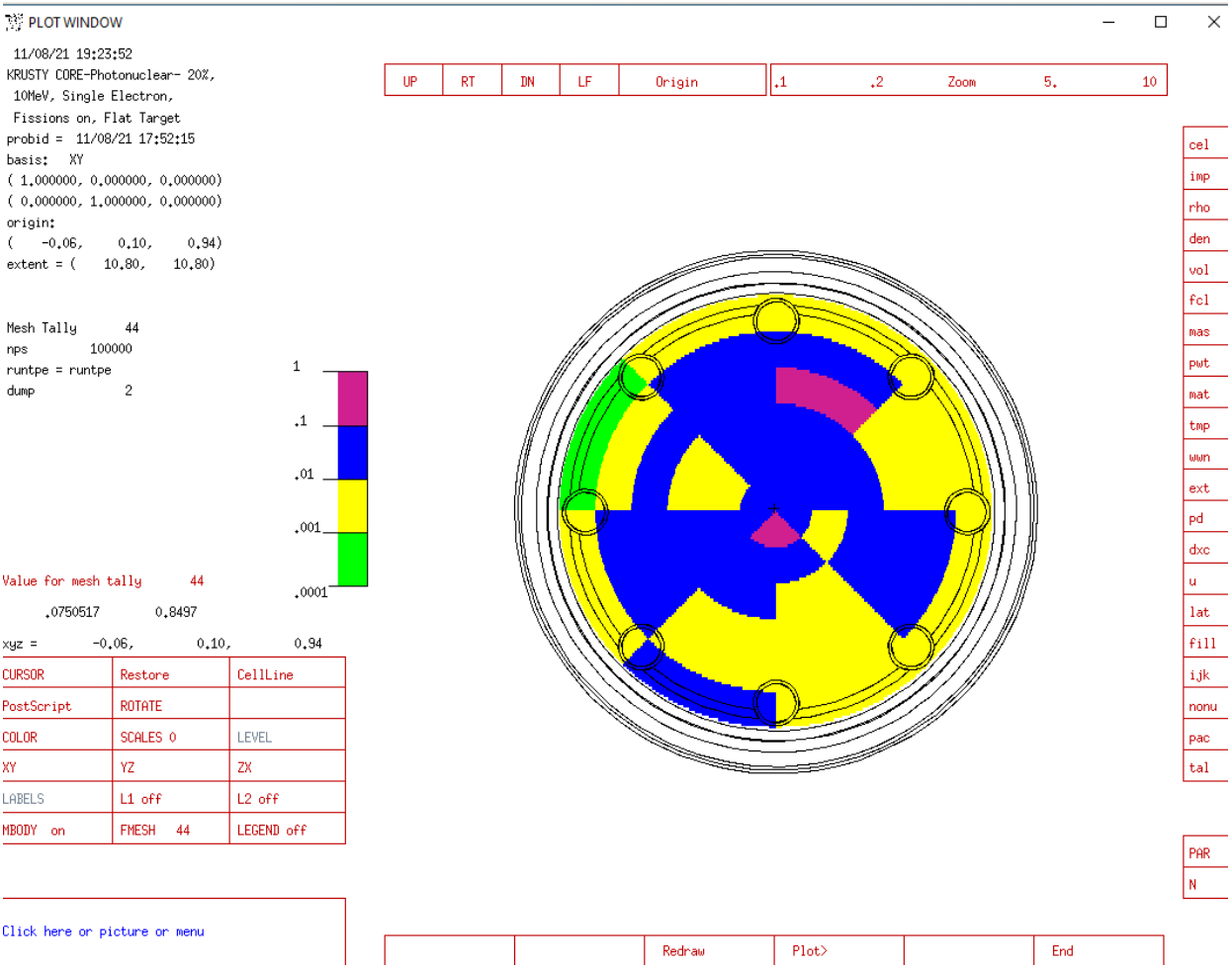

Figure 30: Neutron flux, 20% enriched, 10MeV, top view

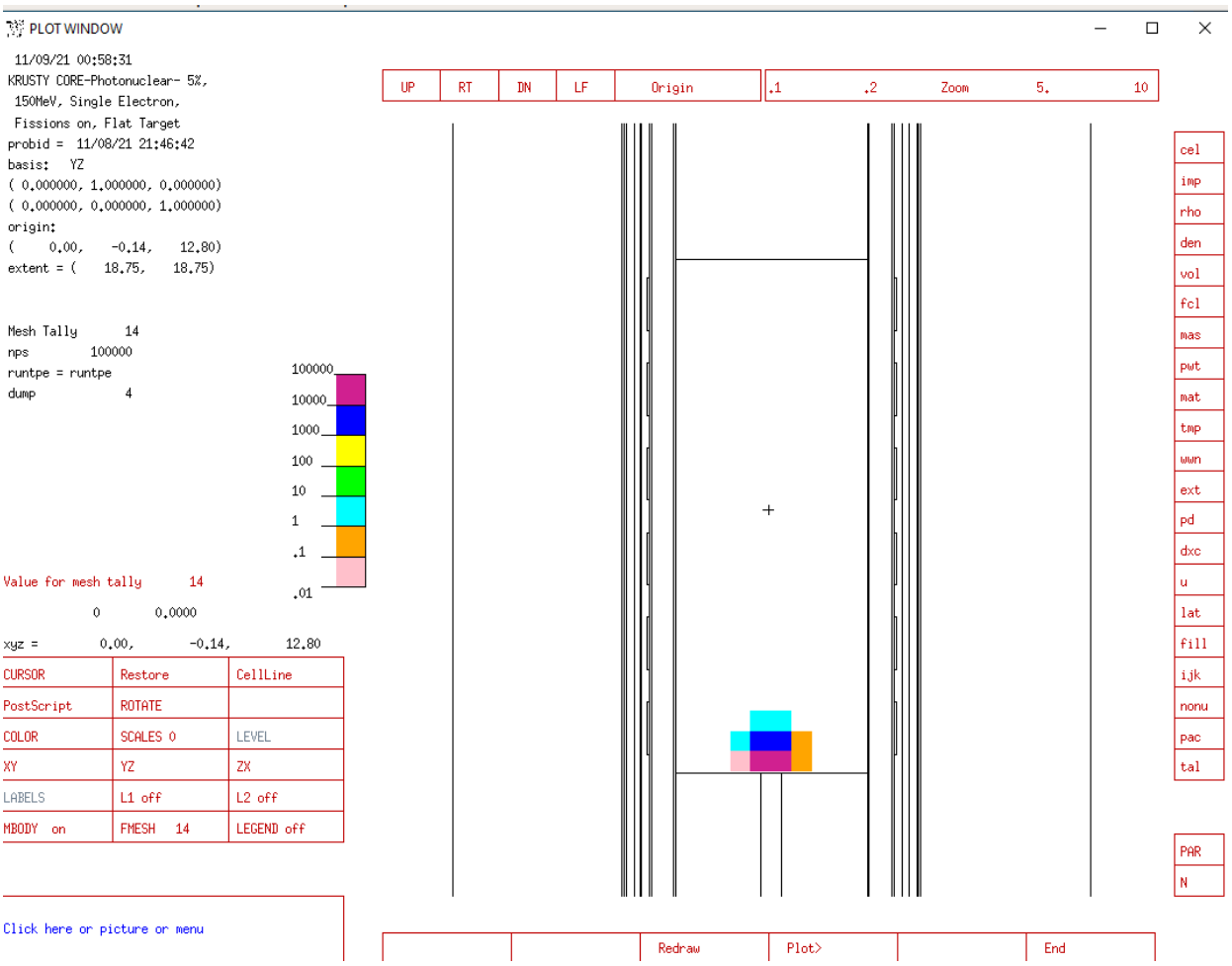

Figure 31: Electron flux, 5% Enriched, 150MeV, side view

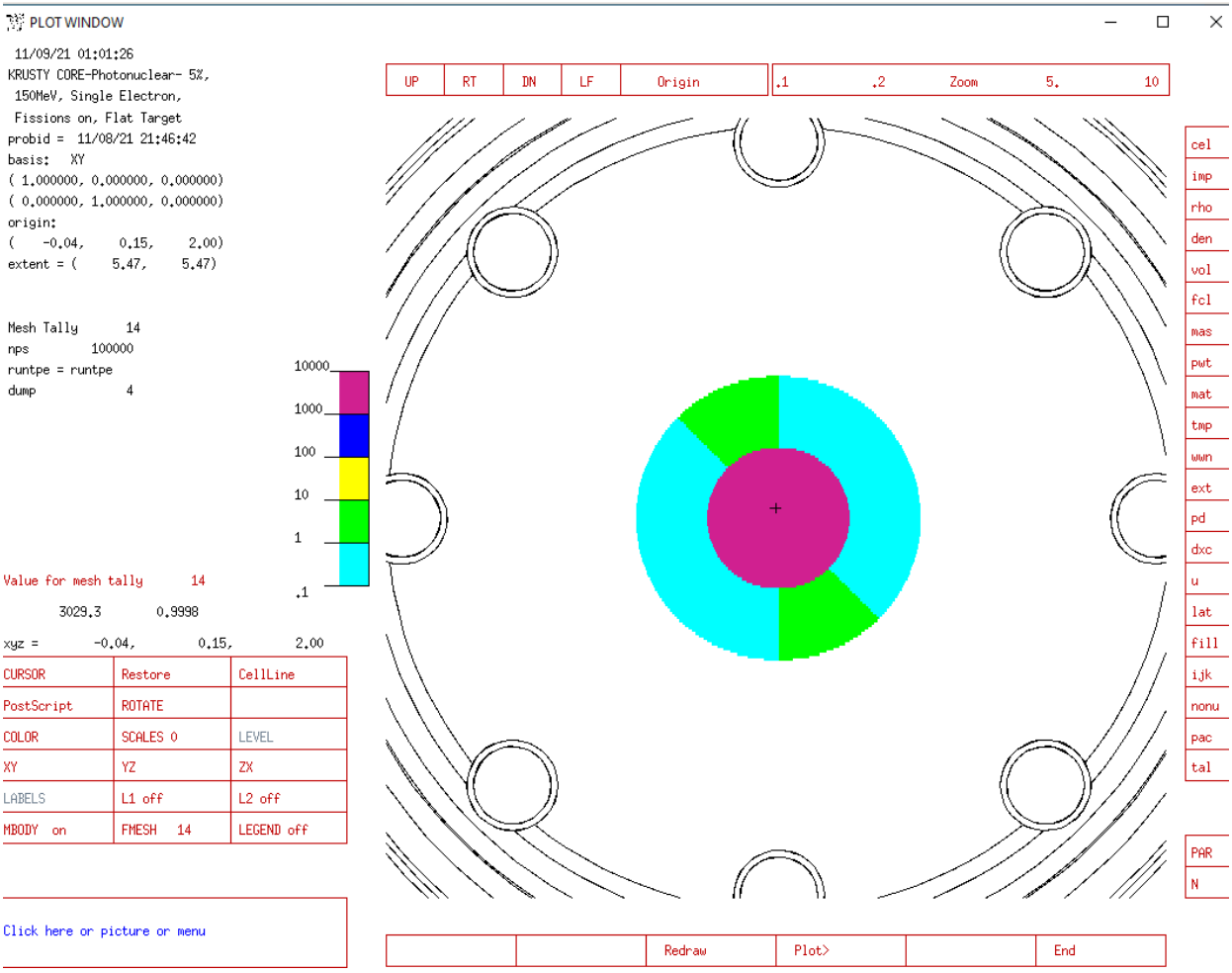

Figure 32: Electron flux, 5% enriched, 150MeV, top view

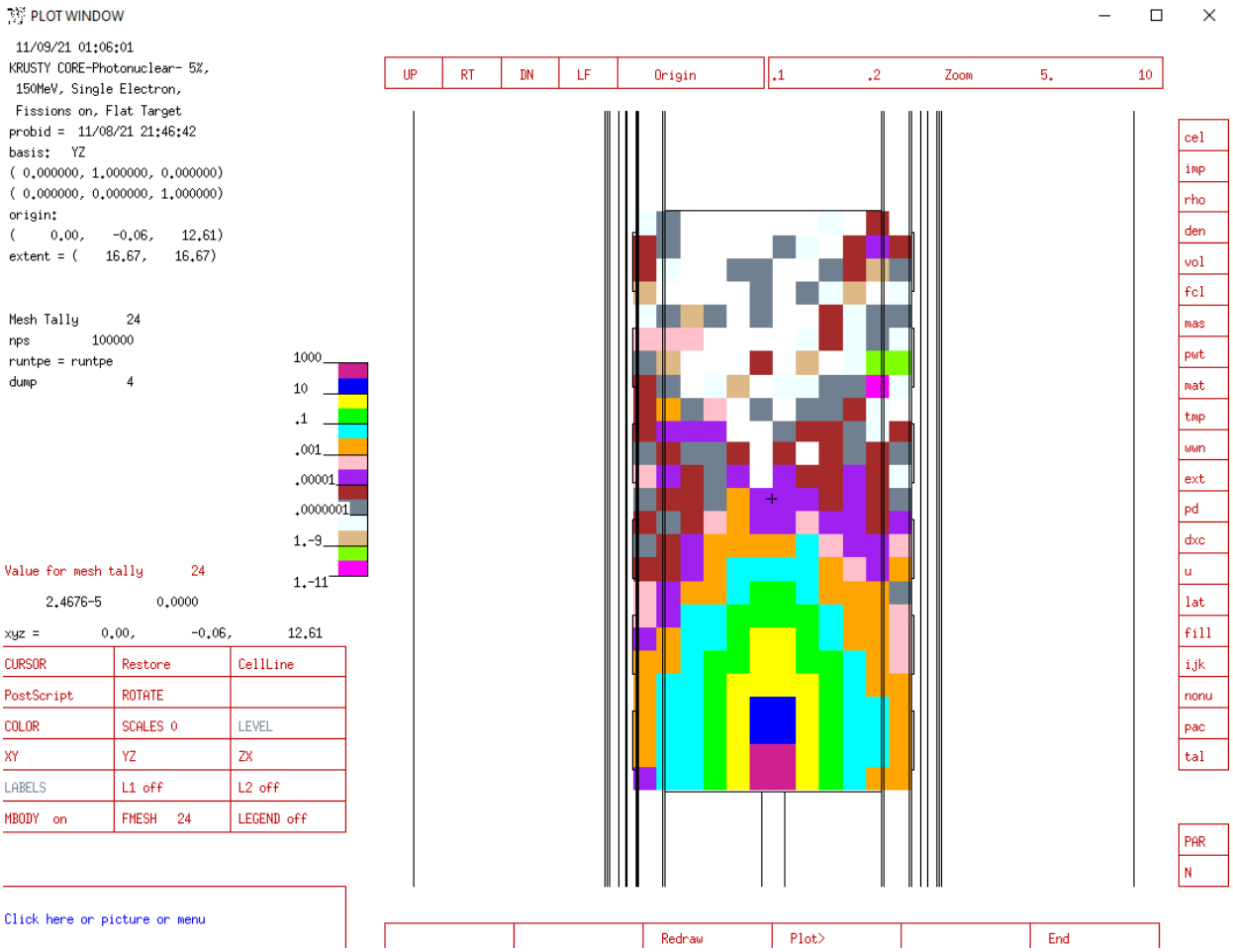

Figure 33: Photon flux, 5% enriched, 150MeV, side view

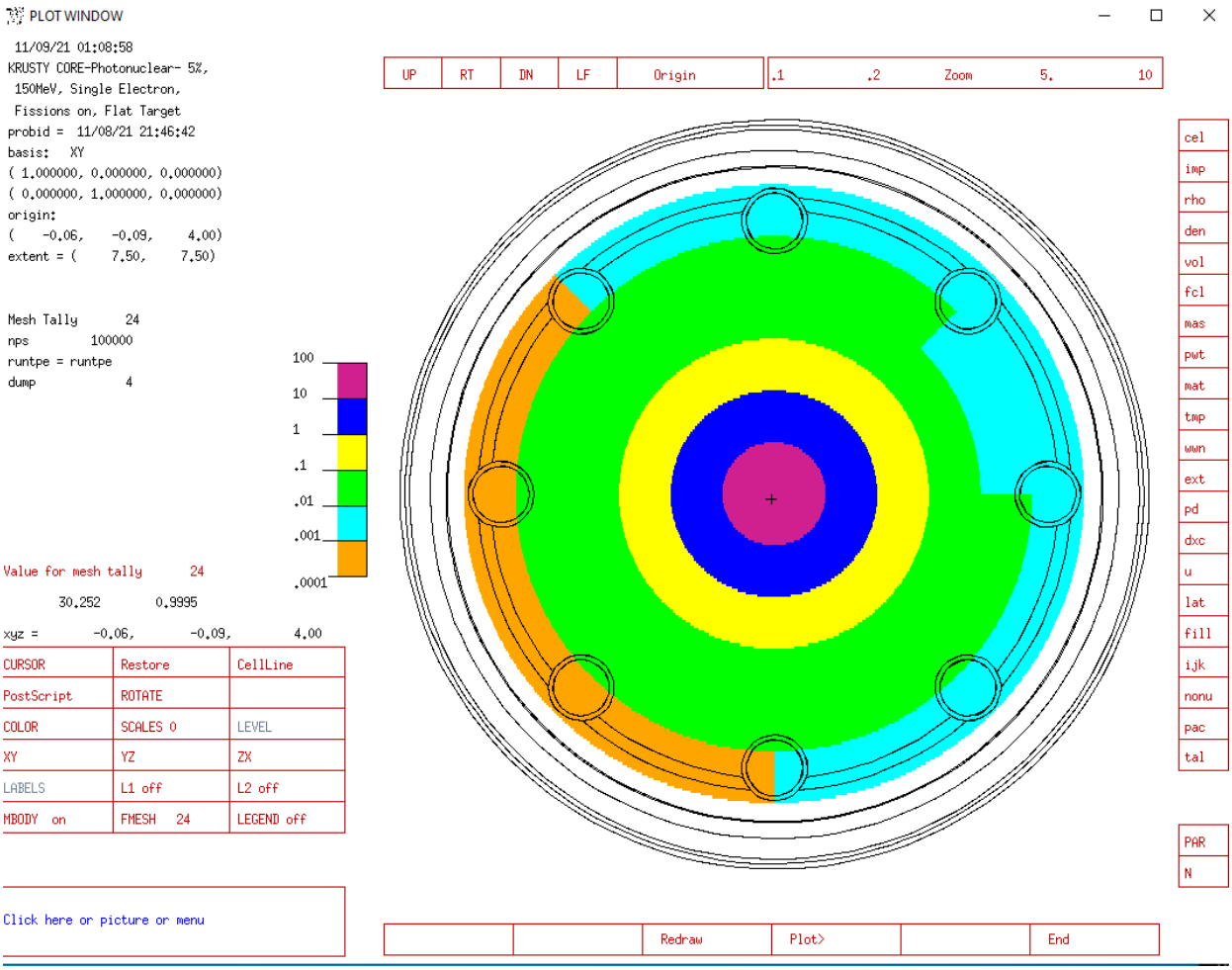

Figure 34: Photon flux, 5% enriched, 150MeV, top view

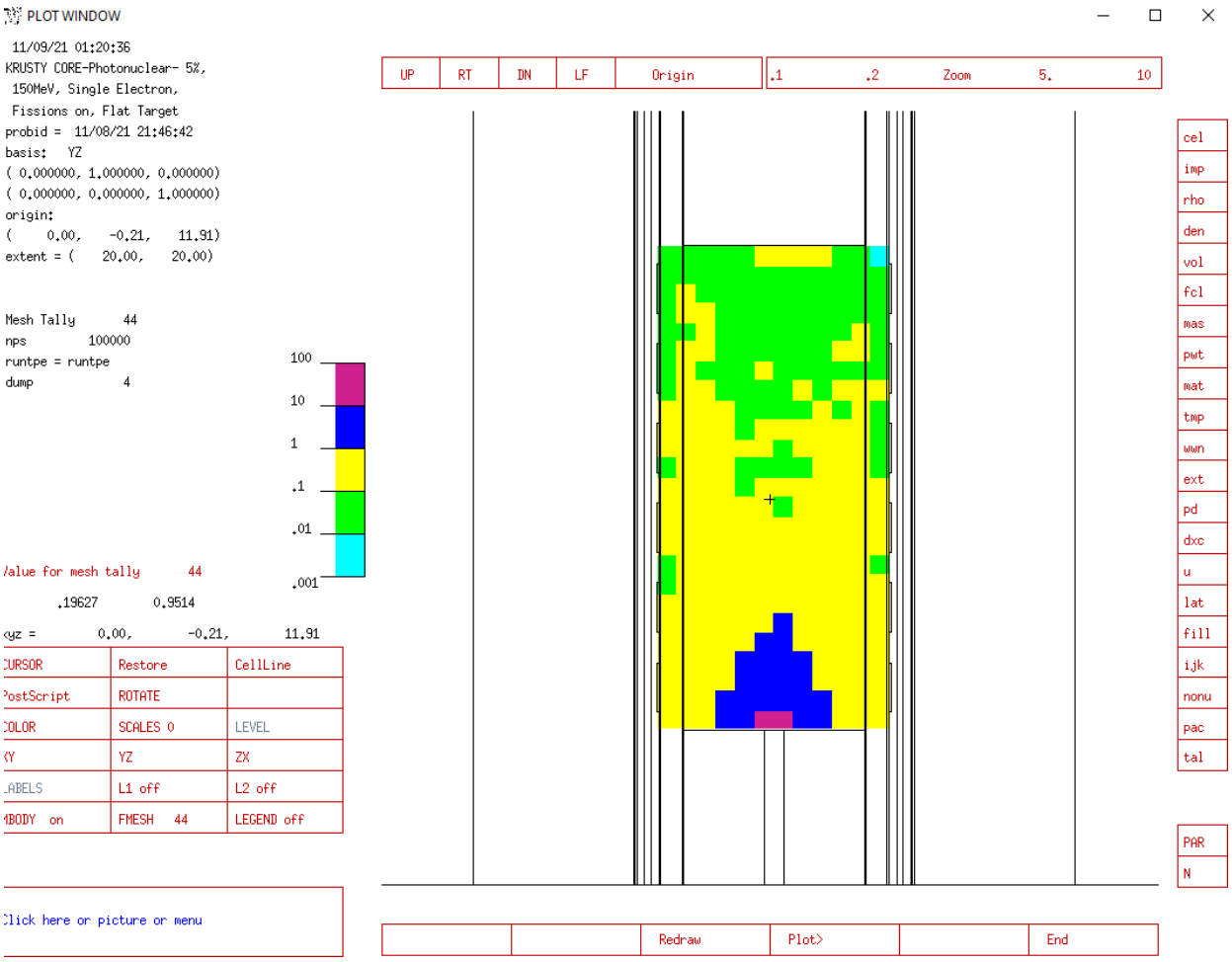

Figure 35: Neutron flux, 5% enrichment, 150MeV, side view

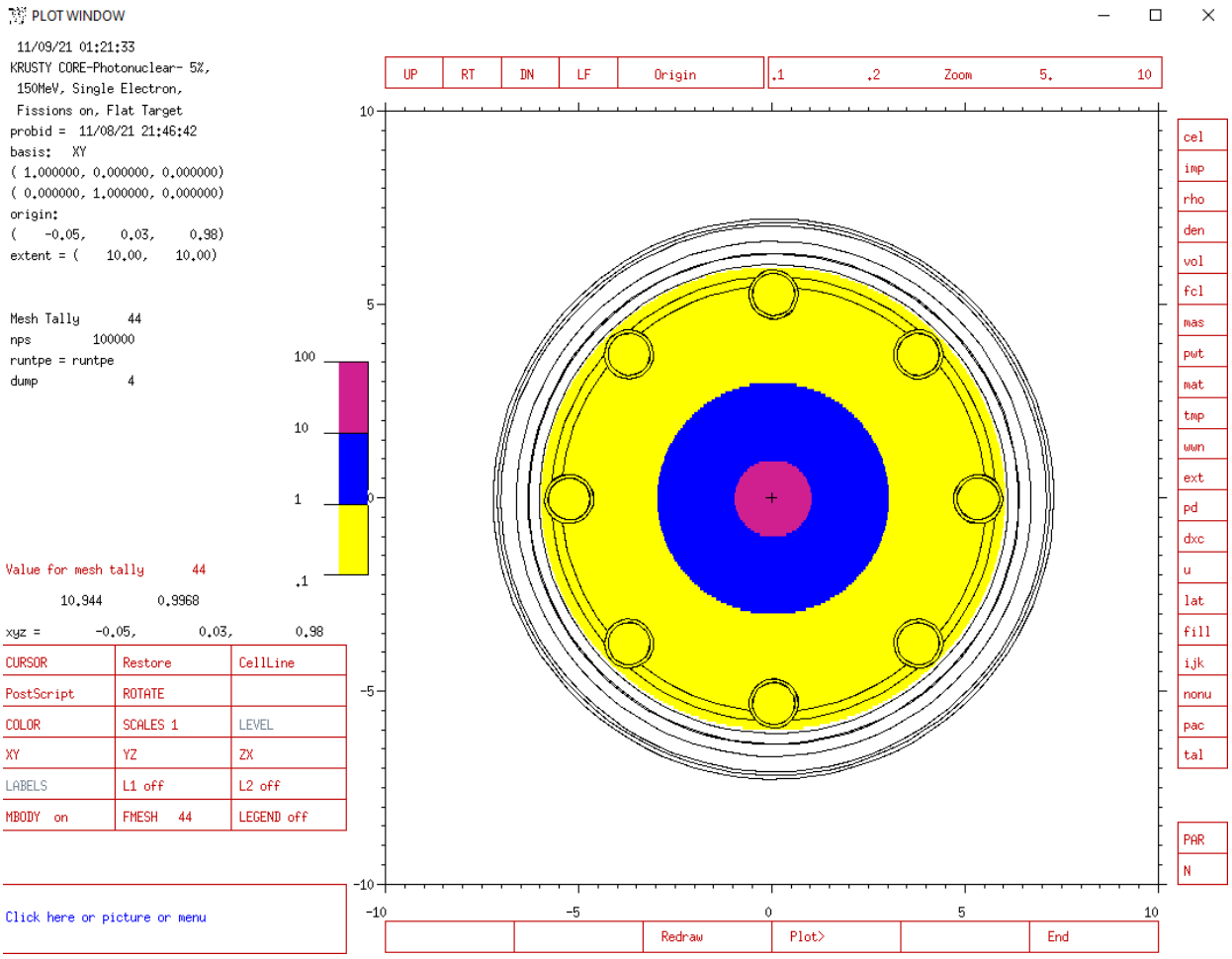

Figure 36: Neutron flux, 5% enrichment, 150MeV, top view

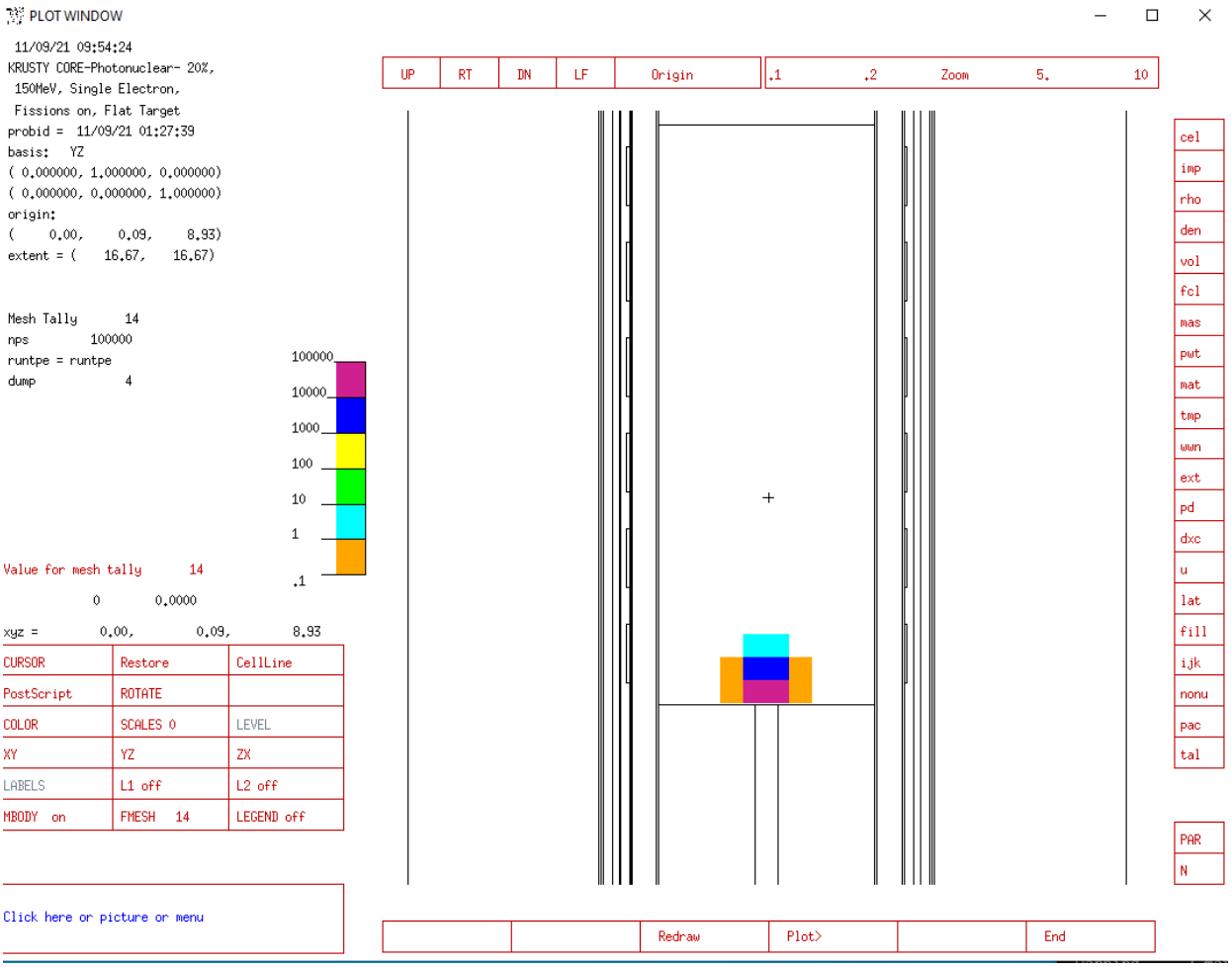

Figure 37: Electron flux, 20% enriched, 150MeV, side view

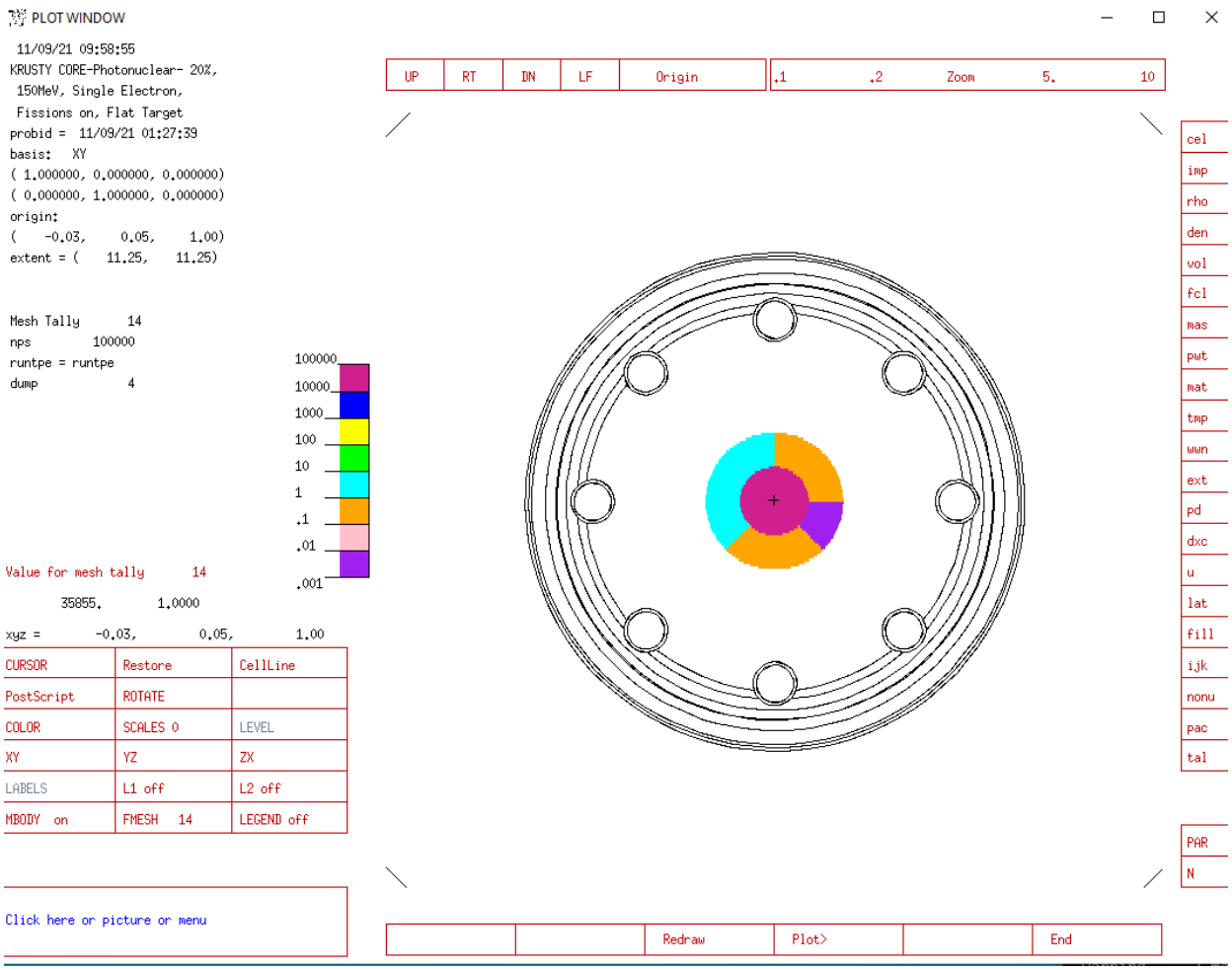

Figure 38: Electron flux, 20% enriched, 150MeV, top view

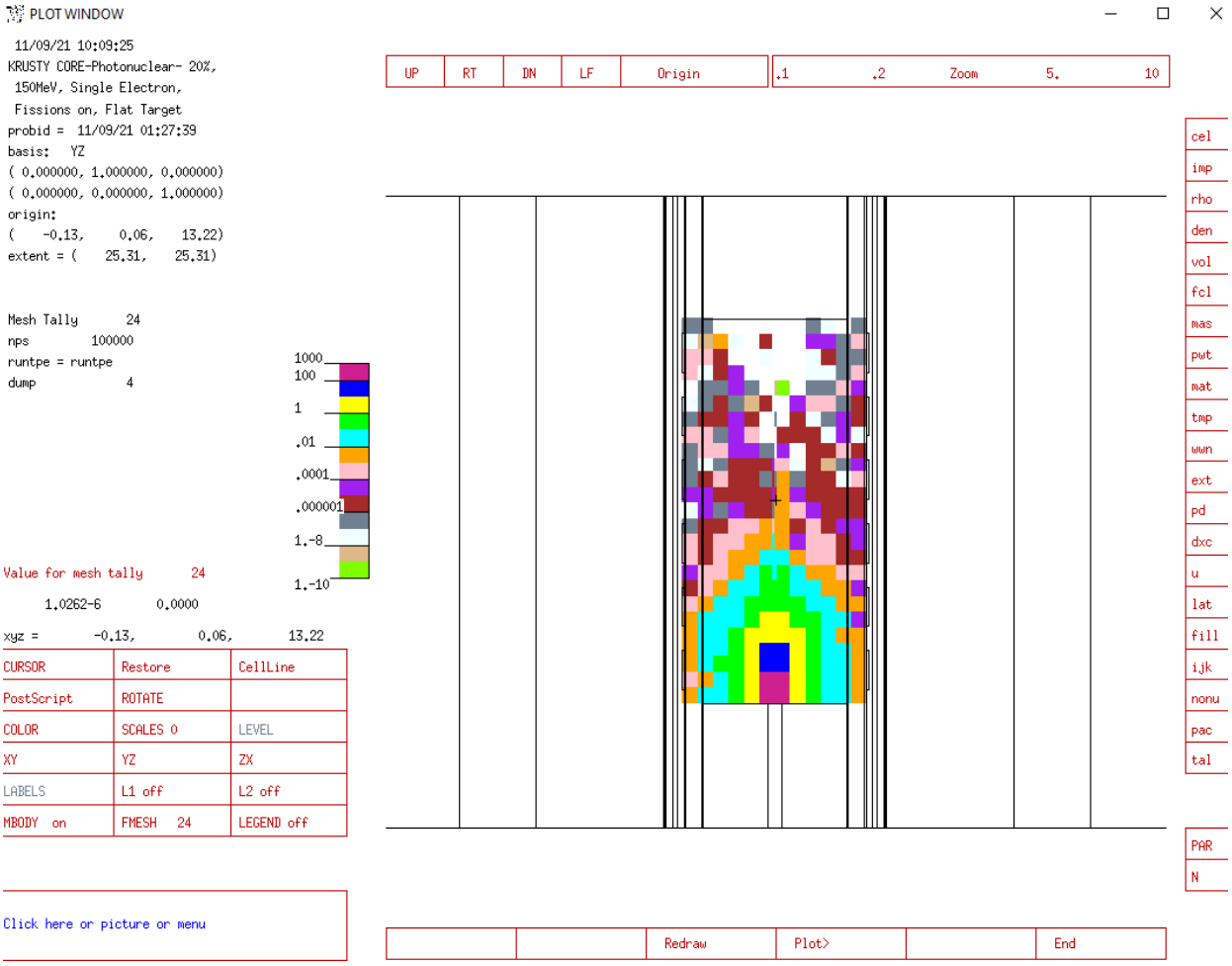

Figure 39: Photon flux, 20% enriched, 150MeV

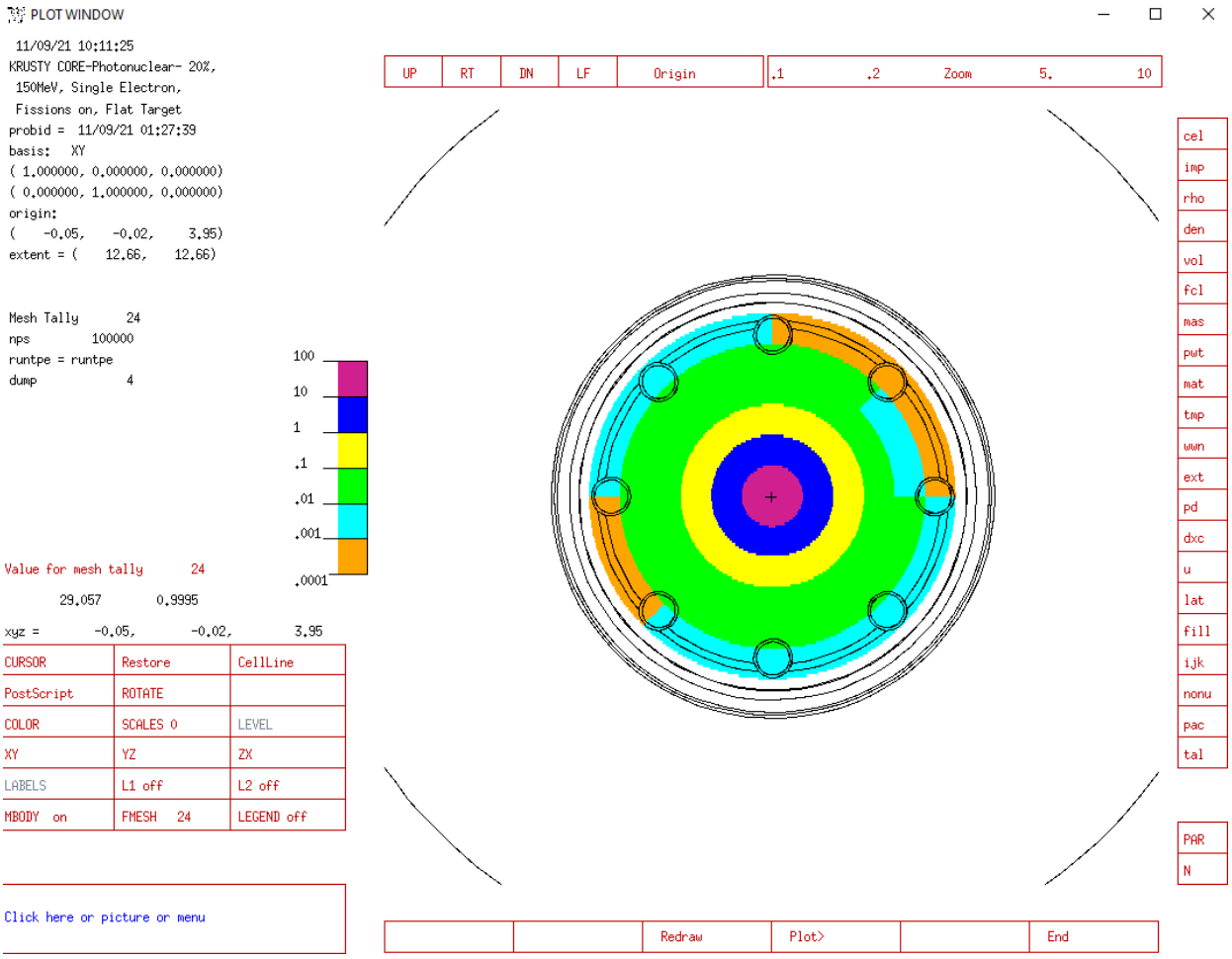

Figure 40: Photon flux, 20% enriched, 150MeV, top view

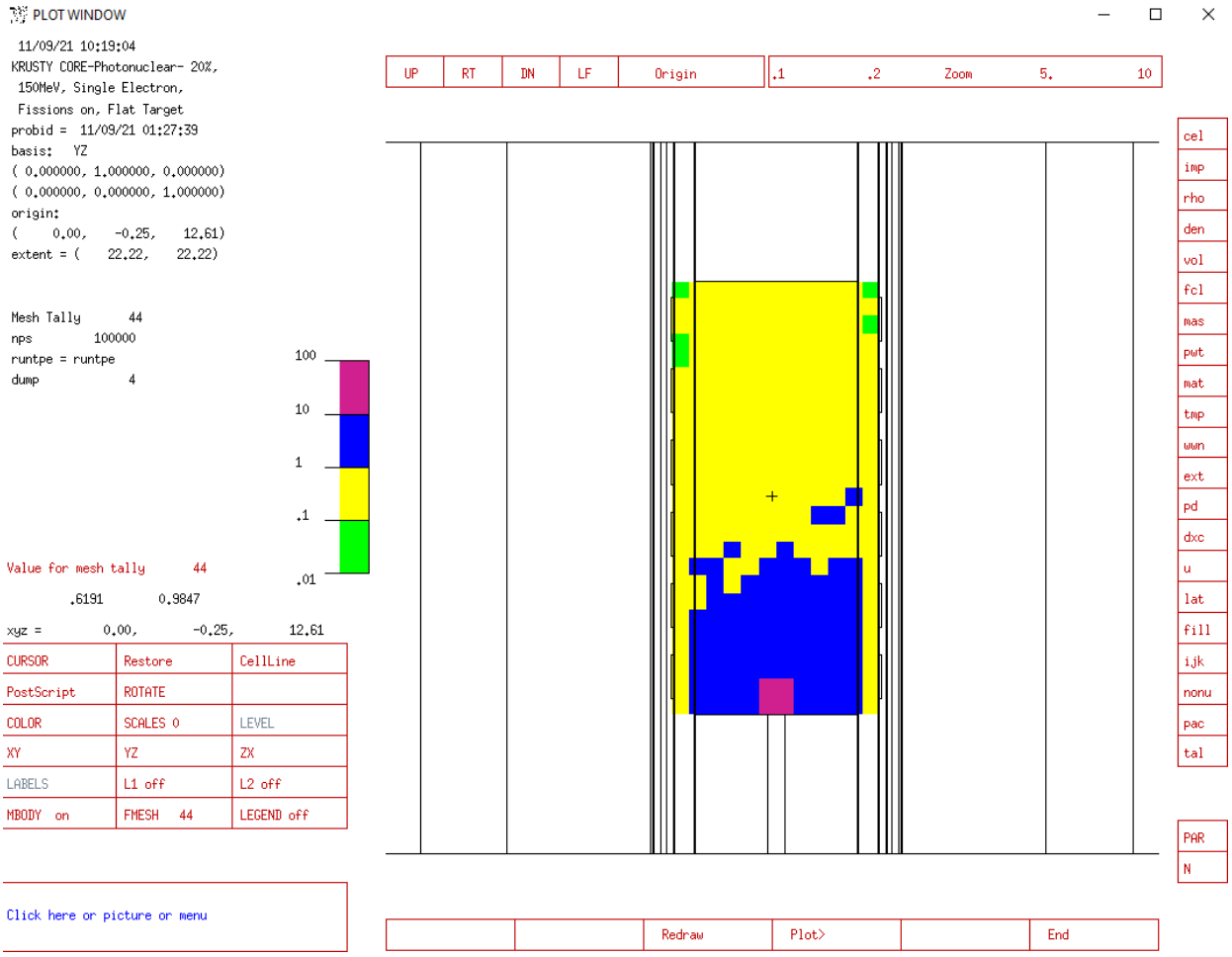

Figure 41: Neutron flux, 20% enriched, 150MeV, side view

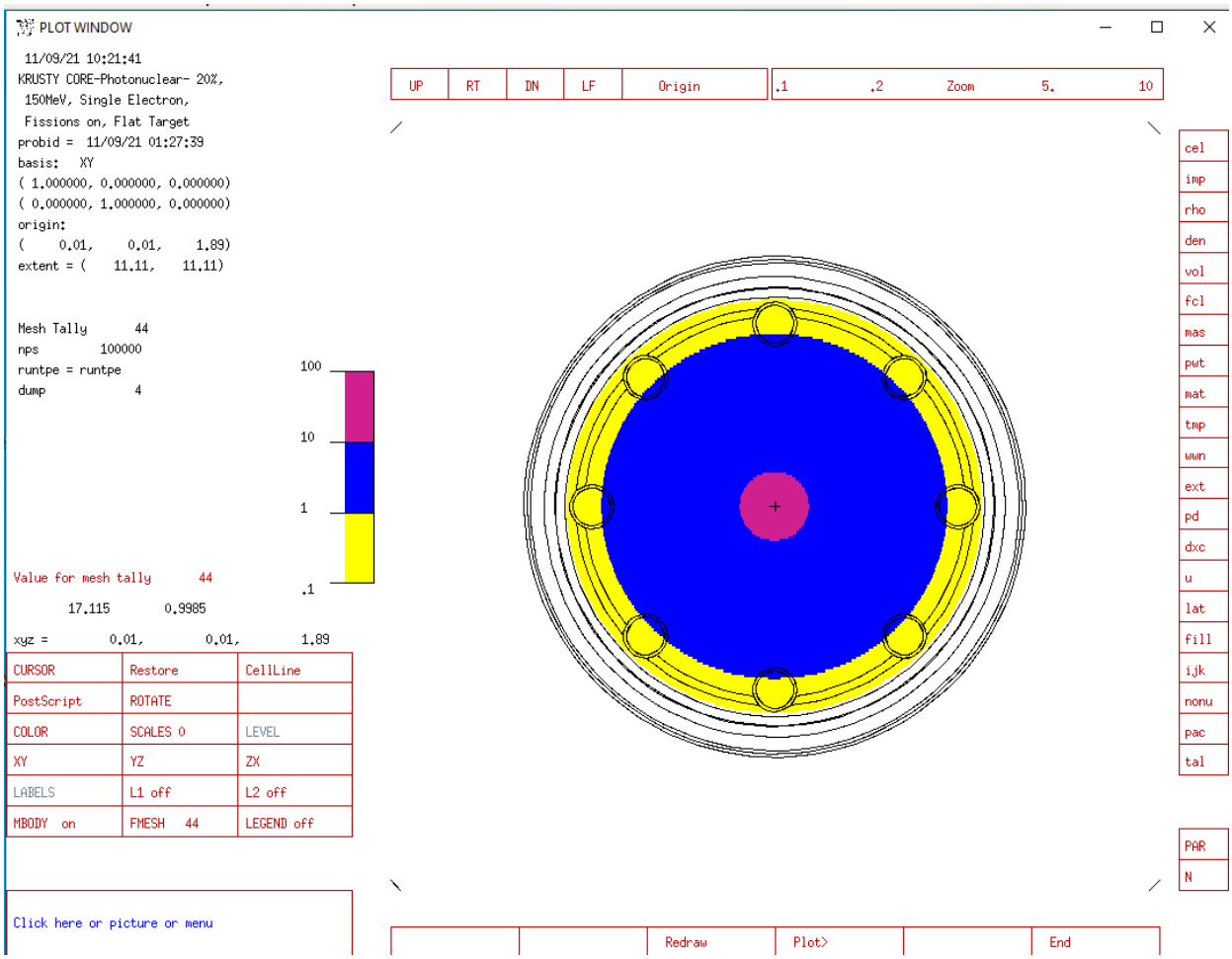

Figure 42: Neutron flux, 20% enriched, 150MeV, top view

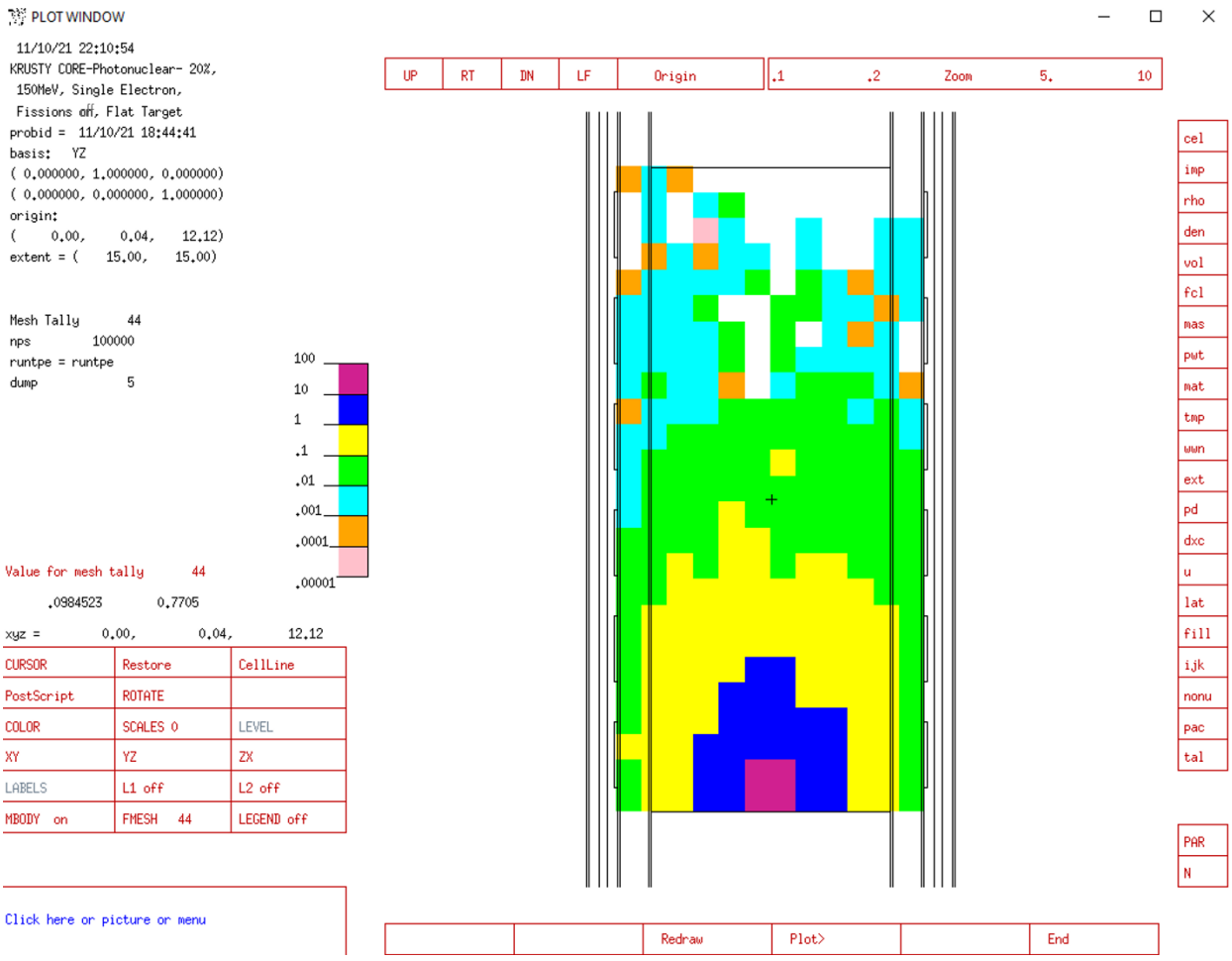

Figure 43: Neutron Flux, 20% Enriched, 150MeV, No Fissions

Appendix C

KRUSTY's Multiplication Factor

Maintaining consistency with the parametrized MCNP scenarios, the fuel's density shall remain a constant despite changes in enrichment: 17.34g/cm3. The fuel's Mo content is 7.65 weight percent.

5% Enriched:

- Atom density for U235:
  First find density for Uranium from density of UMo by product of U wt% and UMo density:

$$\left(.9235\frac{gU}{gUMo}\right)\left(17.34\frac{gUMo}{cm^3}\right)=16.0135\frac{gU}{cm^3}$$

  Find density of U235 by product of U235 wt% and U density:

$$\left(.05\frac{gU235}{gU}\right)\left(16.0135\frac{gU}{cm^3}\right)=0.800675\frac{gU235}{cm^3}$$

  Proceed with atom density calculation:

$$\frac{\left(\left(0.800675\frac{gU235}{cm^3}\right)\left(.6022141\frac{Atoms}{mol}\frac{cm^2}{b}\right)\right)}{235.0439\frac{gU235}{mol}}=2.051E-3\frac{Atom}{b\ cm}$$

- Atom density for U238:

  Find density of U238 by product of U238 wt% and U density:

$$\left(.95\frac{gU235}{gU}\right)\left(16.0135\frac{gU}{cm^3}\right)=15.2128\frac{gU238}{cm^3}$$

  Proceed with atom density calculation:

$$\frac{\left(\left(15.2128\frac{gU238}{cm^3}\right)\left(.6022141\frac{Atoms}{mol}\frac{cm^2}{b}\right)\right)}{238.0507\frac{gU235}{mol}}=3.8485E-2\frac{Atom}{b\ cm}$$

- Atom density for elemental Mo:

  Find density of Mo by product of Mo wt% and UMo density:

$$\left(.0765\frac{gU}{gUMo}\right)\left(17.34\frac{gUMo}{cm^3}\right)=1.32651\frac{gMo}{cm^3}$$

  Proceed with atom density calculation:

$$\frac{\left(\left(1.32651\frac{gMo}{cm^3}\right)\left(.6022141\frac{Atoms}{mol}\frac{cm^2}{b}\right)\right)}{95.94\frac{gU235}{mol}}=8.326E-3\frac{Atom}{b\ cm}$$

Continuing with this method, one finds the remaining atom densities as a function of enrichment to be:

Table 3: Uranium Atom Densities VS Enrichment

Enrichment	**U235**	**U238**
5%	2.051E-3 $\frac{Atom}{b\ cm}$	3.8485E-2 $\frac{Atom}{b\ cm}$
20%	8.206E-3 $\frac{Atom}{b\ cm}$	3.2408E-2 $\frac{Atom}{b\ cm}$
93%	3.8157E-2 $\frac{Atom}{b\ cm}$	2.836E-3 $\frac{Atom}{b\ cm}$

From here one can consider:

$$K=\frac{\left(\upsilon*\Sigma_f^{Fuel}\right)}{DB^2+\Sigma_a^{Fuel}}$$

Where B^2 is the geometric buckling given by: $\left(\frac{\pi}{\tilde{H}}\right)^2+\left(\frac{2.405}{\tilde{R}}\right)^2$
And D is the diffusion coefficient.

The numerator represents the number of neutrons born in fission while the denominator represents neutron loss by the sum of the leakage and absorption.

This equation is derived from steady state time independent conditions which are applicable despite a multiplying medium because the proposed source is a consistent beam of electrons with static intensity.

Using this fundamental equation as is requires the identification of some constants:

Table 4: Fuel Material Constants

Material	**Density g/cm^3**	υ**-fission**	σ_f	σ_a	σ_s
Sources: Lamarsh Table 6.1 & NNDC					
U235	.955	2.6n	1.4	1.65	4
U238	18.145	2.6n	0.95	.255	5.16
Mo	10.2	-	-	-	6.37

Where the macroscopic cross sections of absorption and fission in the fuel can be approximated by just the uranium content:

Table 5: Fuel Macroscopic Cross Sections VS Enrichment

Enrichment	Σ_f^{Fuel}	Σ_a^{Fuel}
5%	6.499E-3 cm^{-1}	1.3121E-2 cm^{-1}
20%	1.456E-2 cm^{-1}	2.1804E-2 cm^{-1}
93%	5.368E-2 cm^{-1}	6.3682E-2 cm^{-1}

Considering that MCNP models have shown that the fluxes produced through each surface of the fuel are not equal when multiplied by their respective surface areas, it reasons that the source is anisotropic, and thus the diffusion coefficient must be calculated by:

$$D = \frac{1}{\left(3\Sigma_s^{Fuel}\right)(1-\bar{\mu})}$$

Where $\bar{\mu}$ is the product of 2/3 and 1 over the molar mass of the fuel.

Table 6: U Molar Mass VS Enrichment

Enrichment	$\mathbf{M_U}$
5%	237.899 g/mol
20%	237.443 g/mol
93%	235.252 g/mol

Allowing:

Table 7: UMo Molar Mass VS Enrichment

Enrichment	$\mathbf{M_{UMo}}$
5%	213.708 g/mol
20%	213.368 g/mol
93%	211.732 g/mol

Now finding Σ_s^{Fuel}:

Table 8: Fuel Macroscopic Cross Section of Scatter VS Enrichment

Enrichment	Σ_s^{Fuel}
5%	2.5827E-1 cm^{-1}
20%	2.5308E-1 cm^{-1}
93%	2.0581E-1 cm^{-1}

The diffusion coefficient is then:

Table 9: Diffusion Coefficient VS Enrichment

Enrichment	D
5%	1.29468
20%	1.32132
93%	1.62473

The geometric buckling is not independent of enrichment as it is found using the extrapolated height and radius of the fuel. The extrapolation distance is found by 2.13*D, resulting in:

Table 10: Extrapolated Dimensions VS Enrichment

Enrichment	He	Re
5%	27.7577	13.7577
20%	27.8142	13.8142
93%	28.4607	14.4607

Allowing B^2 to be found:

Table 11: Geometric Buckling VS Enrichment

Enrichment	B^2
5%	4.336E-2
20%	4.306E-2
93%	3.984E-2

Finally allowing for the K calculation:

Table 12: Multiplication VS Enrichment

Enrichment	K
5%	0.228024
20%	0.449587
93%	1.01582

Appendix D
Finite Cylinder Diffusion Solution

Starting with the reactor equation:

$$\nabla^2\phi + B^2\phi = 0$$

Where:

$$B^2 = \frac{\upsilon\Sigma_f - \Sigma_a}{D}$$

Applying the Laplacian in cylindrical geometry:

$$\frac{1}{r} * \frac{\partial}{\partial r}\left(r * \frac{\partial\phi}{\partial r}\right) + \frac{\partial^2\phi}{\partial z^2} + B^2\phi = 0$$

Evaluate through separation of variables:

$$\phi = R(r)H(z)$$

$$\frac{1}{r} * \frac{\partial}{\partial r}\left(r * \frac{\partial}{\partial r}R(r)H(z)\right) + \frac{\partial^2}{\partial z^2}R(r)H(z) + B^2R(r)H(z) = 0$$

$$\left(\frac{1}{r} * \frac{\partial R}{\partial r} + \frac{\partial^2 R}{\partial r^2}\right)H(z) + \frac{\partial^2 H}{\partial z^2}R(r) + B^2R(r)H(z) = 0$$

Divide out the flux variables:

$$\left(\frac{1}{r} * \frac{\partial R}{\partial r} + \frac{\partial^2 R}{\partial r^2}\right)\frac{1}{R(r)} + \frac{\partial^2 H}{\partial z^2}\frac{1}{H(z)} + B^2 = 0$$

To permit solutions for the z and r axes respectively, consider:

$$B^2 = \alpha^2 + \beta^2$$

Allowing:

$$\left(\frac{1}{r} * \frac{\partial R}{\partial r} + \frac{\partial^2 R}{\partial r^2}\right)\frac{1}{R(r)} = -\alpha^2$$

$$\frac{\partial^2 H}{\partial z^2}\frac{1}{H(z)} = -\beta^2$$

Considering the radial part 1st:

Reorganize to homogenous 2nd ODE:

$$\frac{\partial^2 R}{\partial r^2} + \left(\frac{1}{r} * \frac{\partial R}{\partial r}\right) + \alpha^2 R(r) = 0$$

It is known that ordinary Bessel functions appropriately represent 2nd ODEs of the form:

$$y'' + \frac{1}{x}y' + \alpha^2 y = 0$$

Thus:

$$R(r) = C_1 J_o(\alpha\, r) + C_2 Y_o(\alpha\, r)$$

For a finite cylinder, flux must be finite, and since at the origin Yo $= -\infty$, C_2 must be zero.

$$R(r) = C_1 J_o(\alpha\, r)$$

Considering how the finite flux must still apply, apply the extrapolated boundary condition:

$$R(\tilde{R}) = C_1 J_o(\alpha\, \tilde{R}) = 0$$

Avoiding a trivial solution, consider the roots of the Jo Bessel function as υ_n:

$$R(r) = C_1 J_o\left(r * \frac{\upsilon_n}{\tilde{R}}\right)$$

Now proceeding with the axial term reorganize as homogenous 2nd ODE:

$$\frac{\partial^2 H}{\partial z^2} + \beta^2 H(z) = 0$$

By inspection deduce:

$$H(z) = C_3 \cos(\beta z) + C_4 Sin(\beta z)$$

Consider that the flux is required to be finite at its center and thus must have some maximum, limiting value. A maximum point in a function occurs when the derivative equals 0.

$$H'(H/2) = -C_3 \beta \sin(H/2) + C_4 \beta cos(H/2) = 0$$

Assuming a periodic fluctuation, one can think if H/2 as π/2 implying C_3 must be 0 to permit H'=0 since Sin(π/2)=1

$$H(z) = C_4 \mathrm{Sin}(\beta z)$$

Considering a cylinder centered on its base, the flux at the extrapolated height, $\tilde{H}$=0

$$H(\tilde{H}) = C_4 \sin(\beta \tilde{H}) = 0$$

So if sin(n*π) = 0 then $\beta = \frac{n\pi}{\tilde{H}}$, where n=1,2,3…

Leaving:

$$H(z) = C_4 \sin\left(\frac{n\pi}{\tilde{H}} z\right)$$

Finally by separation of variables definition:

$$\phi(z, r) = C * \sin\left(\frac{n\pi}{\tilde{H}} z\right) J_o\left(r \frac{\upsilon_n}{\tilde{R}}\right)$$

Appendix E
Normalization of Source Distribution

Reasoning:
A source distribution, S(r), must be defined such that when integrated over a volume, one obtains the total source strength, **S**. This is of particular importance for distributions like the paraboloid as it allows for the additional representation of neutrons within the distribution rather than just those that compose the surface. Thus:

$$\int q(\underline{r}) \cdot d^3r = \mathbf{S}$$

Where this volume integral operates on q(r), the number of neutrons per cm^3 per second, to yield **S**, the total number of neutrons per second. Where mathematically q(r) can be represented by the product of dirac-delta functions for all influential degrees of freedom and the initial source distribution.

- **Line source along z-axis**:

Expanding the number of neutrons per cm^3 per second, being a line source one only wants the source to be present at r=0; thus a dirac in this degree of freedom is used:

$$q(\underline{r}) = f(\underline{r})\delta(\mathrm{r})(\mathrm{H}-\mathrm{z})$$

Applying the volume integral of the pertaining cylindrical geometry:

$$\iiint_{0,0,0}^{R,H,2\pi} f(\underline{r})\delta(\mathrm{r})(\mathrm{H}-\mathrm{z})\mathrm{rdrdzd}\Theta = \mathbf{S}$$

For a line source, there is no dependence on Θ, and there is no change in r. Thus after normalizing, we find that:

$$q(\underline{r}) = \frac{\mathbf{S}(\mathrm{H}-\mathrm{z})}{\pi H^2}$$

Appendix F
MCNP Input Deck- 150MeV, 20% Enriched

```
KRUSTY CORE-Photonuclear- 20%, 150MeV, Single Electron, Fissions on, Flat
Target
c Start cells
c Fuel
2 2 -17.34 -2 3 4 5 6 7 8 9 10 19 20
      21 22 23 24 25 26 VOL=2248.19 IMP:N,E,P=1
c heat pipe 0degrees
3 0 -27 IMP:N,E,P=1 $ void for coolant
4 6 -8.9 -19 27 IMP:N,E,P=1 $ Ni Wick
5 3 -8.91 -11 19 IMP:N,E,P=1 $ Haynes 230
6 5 -8.96 -3 11 IMP:N,E,P=1 $ Cu Foil
c heat pipe 45degrees
7 0 -28 IMP:N,E,P=1 $ void for coolant
8 6 -8.9 -20 28 IMP:N,E,P=1 $ Ni Wick
9 3 -8.91 -12 20 IMP:N,E,P=1 $ Haynes 230
10 5 -8.96 -4 12 IMP:N,E,P=1 $ Cu Foil
c heat pipe 90degrees
11 0 -29 IMP:N,E,P=1 $ void for coolant
12 6 -8.9 -21 29 IMP:N,E,P=1 $ Ni Wick
13 3 -8.91 -13 21 IMP:N,E,P=1 $ Haynes 230
14 5 -8.96 -5 13 IMP:N,E,P=1 $ Cu Foil
c heat pipe 135degrees
15 0 -30 IMP:N,E,P=1 $ void for coolant
16 6 -8.9 -22 30 IMP:N,E,P=1 $ Ni Wick
17 3 -8.91 -14 22 IMP:N,E,P=1 $ Haynes 230
18 5 -8.96 -6 14 IMP:N,E,P=1 $ Cu Foil
c heat pipe 180dgrees
19 0 -31 IMP:N,E,P=1 $ void for coolant
20 6 -8.9 -23 31 IMP:N,E,P=1 $ Ni Wick
21 3 -8.91 -15 23 IMP:N,E,P=1 $ Haynes 230
22 5 -8.96 -7 15 IMP:N,E,P=1 $ Cu Foil
c heat pipe 225degrees
23 0 -32 IMP:N,E,P=1 $ void for coolant
24 6 -8.9 -24 32 IMP:N,E,P=1 $ Ni Wick
25 3 -8.91 -16 24 IMP:N,E,P=1 $ Haynes 230
26 5 -8.96 -8 16 IMP:N,E,P=1 $ Cu Foil
c heat pipes 270degrees
27 0 -33 IMP:N,E,P=1 $ void for coolant
28 6 -8.9 -25 33 IMP:N,E,P=1 $ Ni Wick
29 3 -8.91 -17 25 IMP:N,E,P=1 $ Haynes 230
30 5 -8.96 -9 17 IMP:N,E,P=1 $ Cu Foil
c heat pipe 315degrees
31 0 -34 IMP:N,E,P=1 $ void for coolant
32 6 -8.9 -26 34 IMP:N,E,P=1 $ Ni Wick
33 3 -8.91 -18 26 IMP:N,E,P=1 $ Haynes 230
34 5 -8.96 -10 18 IMP:N,E,P=1 $ Cu Foil
c Gap between clamps and fuel
35 0 -35 2 3 4 5 6 7 8 9 10 11 12 13 14 15
      16 17 18 19 20 21 22 23 24 25 26 27
```

```
      28 29 30 31 32 33 34 IMP:N,E,P=1
c Haynes 230 clamp 1st
36 3 -8.91 -36 3 4 5 6 7 8 9 10 11 12 13 14 15
      16 17 18 19 20 21 22 23 24 25 26 35 IMP:N,E,P=1
c Haynes 230 clamp 2nd
37 3 -8.91 -37 3 4 5 6 7 8 9 10 11 12 13 14 15
      16 17 18 19 20 21 22 23 24 25 26 35 IMP:N,E,P=1
c Haynes 230 clamp 3rd
38 3 -8.91 -38 3 4 5 6 7 8 9 10 11 12 13 14 15
      16 17 18 19 20 21 22 23 24 25 26 35 IMP:N,E,P=1
c Haynes 230 clamp 4th
39 3 -8.91 -39 3 4 5 6 7 8 9 10 11 12 13 14 15
      16 17 18 19 20 21 22 23 24 25 26 35 IMP:N,E,P=1
c Haynes 230 clamp 5th
40 3 -8.91 -40 3 4 5 6 7 8 9 10 11 12 13 14 15
      16 17 18 19 20 21 22 23 24 25 26 35 IMP:N,E,P=1
c Haynes 230 clamp 6th
41 3 -8.91 -41 3 4 5 6 7 8 9 10 11 12 13 14 15
      16 17 18 19 20 21 22 23 24 25 26 35 IMP:N,E,P=1
c Gap between clamp and MLI
42 0 -42 3 4 5 6 7 8 9 10 35 36 37 38 39 40
      41 49 50 IMP:N,E,P=1
c MLI
43 4 -10.28 -43 42 IMP:N,E,P=1
c SS316 vacuum can
44 7 -8 -44 43 IMP:N,E,P=1
c gap between SS can and SS sleeve
45 0 -45 44 IMP:N,E,P=1
c SS316 Sleeve
46 7 -8 -46 45 IMP:N,E,P=1
c gap in bewteen sleeve and reflector
47 0 -47 46 IMP:N,E,P=1
c radial reflector
48 8 -3.02 -48 47 IMP:N,E,P=1
c Top axial reflector
49 8 -3.02 -49 2 3 4 5 6 7 8 9 10 19
      20 21 22 23 24 25 26 IMP:N,E,P=1
c Bottom axial reflector
50 8 -3.02 -50 2 3 4 5 6 7 8 9 10 19
      20 21 22 23 24 25 26 51 IMP:N,E,P=1
c Electron beam port
51 0 -51 IMP:N,E,P=1
c gap in between radial reflector and SS304
52 0 -52 48 IMP:N,E,P=1
c SS304 Shield
53 9 -8 -53 52 IMP:N,E,P=1
c outer void
54 0 53 IMP:N,E,P=0
c End cells

c Start surfaces
c U8Mo Fuel
2 RCC 0 0 0  0 0 25  5.5
c Heat Pipe Layer 1,Cu Foil
```

```
3 RCC 5.2924 0 -8  0 0 41  0.6374 $ 0degrees
4 RCC 3.742291929 3.742291929 -8  0 0 41  0.6374 $ 45degrees
5 RCC 0 5.2924 -8  0 0 41  0.6374 $ 90degrees
6 RCC -3.742291929 3.742291929 -8  0 0 41  0.6374 $ 135degrees
7 RCC -5.2924 0 -8  0 0 41  0.6374 $ 180degrees
8 RCC -3.742291929 -3.742291929 -8  0 0 41  0.6374 $ 225degrees
9 RCC 0 -5.2924 -8  0 0 41  0.6374 $ 270degrees
10 RCC 3.742291929 -3.742291929 -8  0 0 41  0.6374 $ 315degrees
c Heat Pipe Layer 2, Haynes 230
11 RCC 5.2924 0 -8  0 0 41  0.635 $ 0degrees
12 RCC 3.742291929 3.742291929 -8  0 0 41  0.635 $ 45degrees
13 RCC 0 5.2924 -8  0 0 41  0.635 $ 90degrees
14 RCC -3.742291929 3.742291929 -8  0 0 41  0.635 $ 135degrees
15 RCC -5.2924 0 -8  0 0 41  0.635 $ 180degrees
16 RCC -3.742291929 -3.742291929 -8  0 0 41  0.635 $ 225degrees
17 RCC 0 -5.2924 -8  0 0 41  0.635 $ 270degrees
18 RCC 3.742291929 -3.742291929 -8  0 0 41  0.635 $ 315degrees
c Heat Pipe Layer 3, Ni Wick
19 RCC 5.2924 0 -8  0 0 41  0.546 $ 0degrees
20 RCC 3.742291929 3.742291929 -8  0 0 41  0.546 $ 45degrees
21 RCC 0 5.2924 -8  0 0 41  0.546 $ 90degrees
22 RCC -3.742291929 3.742291929 -8  0 0 41  0.546 $ 135degrees
23 RCC -5.2924 0 -8  0 0 41  0.546 $ 180degrees
24 RCC -3.742291929 -3.742291929 -8  0 0 41  0.546 $ 225degrees
25 RCC 0 -5.2924 -8  0 0 41  0.546 $ 270degrees
26 RCC 3.742291929 -3.742291929 -8  0 0 41  0.546 $ 315degrees
c Heat Pipe Internal Void
27 RCC 5.2924 0 -8  0 0 41  0.54155 $ 0degrees
28 RCC 3.742291929 3.742291929 -8  0 0 41  0.54155 $ 45degrees
29 RCC 0 5.2924 -8  0 0 41  0.54155 $ 90degrees
30 RCC -3.742291929 3.742291929 -8  0 0 41  0.54155 $ 135degrees
31 RCC -5.2924 0 -8  0 0 41  0.54155 $ 180degrees
32 RCC -3.742291929 -3.742291929 -8  0 0 41  0.54155 $ 225degrees
33 RCC 0 -5.2924 -8  0 0 41  0.54155 $ 270degrees
34 RCC 3.742291929 -3.742291929 -8  0 0 41  0.54155 $ 315degrees
c Gap between clamps and fuel
35 RCC 0 0 0  0 0 25  5.747
c 1st Haynes 230 Clamp
36 RCC 0 0 .9398  0 0 2.54  6.065
c 2nd Haynes 230 Clamp
37 RCC 0 0 5.05588  0 0 2.54 6.065
c 3rd Haynes 230 Clamp
38 RCC 0 0 9.17196  0 0 2.54 6.065
c 4th Haynes 230 Clamp
39 RCC 0 0 13.288  0 0 2.54 6.065
c 5th Haynes 230 Clamp
40 RCC 0 0 17.4041  0 0 2.54 6.065
c 6th Haynes 230 Clamp
41 RCC 0 0 21.5202  0 0 2.54 6.065
c Gap between clamps and MLI
42 RCC 0 0 -8  0 0 41  6.3306
c MLI Region
43 RCC 0 0 -8  0 0 41  6.356
c SS 316 Ring
```

```
44 RCC 0 0 -8  0 0 41  6.661
c Gap between SS vacuum can and SS sleeve
45 RCC 0 0 -8  0 0 41  7.061
c SS 316 sleeve
46 RCC 0 0 -8  0 0 41  7.15
c Gap between ss sleeve and BeO
47 RCC 0 0 -8  0 0 41  7.25
c Radial BeO Reflector (check if shouldn't be 38.1OD)
48 RCC 0 0 -8  0 0 41  15.5
c Top Axial BeO Reflector
49 RCC 0 0 25  0 0 8   5.5
c Bottom Axial BeO Reflector
50 RCC 0 0 -8  0 0 8   5.5
c Electron Beam Port
51 RCC 0 0 -8  0 0 8   0.5
c Gap between reflector and gamma shield
52 RCC 0 0 -8  0 0 41  20.5
c SS304 gamma shield
53 RCC 0 0 -8  0 0 41  50.95
c End surfaces

c Start Data
c
mphys on
c U(7.65)Mo Fuel
M2 92235 -0.1847
      92238 -0.738800
      42092 -0.011299
      42094 -0.007061
      42095 -0.012164
      42096 -0.01276
      42097 -0.007313
      42098 -0.018505
      42100 -0.007398
c Haynes-230//Inconel N06230
M3 28058 -0.355123
      28060 -0.136793
      28061 -0.005946
      28062 -0.018959
      28064 -0.004828
      24050 -0.009559
      24052 -0.184336
      24053 -0.020902
      24054 -0.005203
      74180 -0.000168
      74182 -0.0371
      74183 -0.020034
      74184 -0.042896
      74186 -0.039802
      42092 -0.002954
      42094 -0.001846
      42095 -0.00318
      42096 -0.003336
      42097 -0.001912
```

```
      42098 -0.004838
      42100 -0.001934
      26054 -0.001754
      26056 -0.027526
      26057 -0.006357
      26058 -0.000085
      27059 -0.05
      25055 -0.005
      14028 -0.003689
      14029 -0.000187
      14030 -0.000124
      41093 -0.005
      13027 -0.003
      22046 -0.000083
      22047 -0.000074
      22048 -0.000737
      22049 -0.000054
      22050 -0.000052
      6012  -0.000989
      6013  -0.000011
      57139 -0.0002
      5010  -0.00003
      5011  -0.00012
c Mo Foil
M4 42092 -0.1477
      42094 -0.0923
      42095 -0.159
      42096 -0.1668
      42097 -0.0956
      42098 -0.2419
      42100 -0.0967
c Cu Foil
M5 29063 -0.6915
      29065 -0.3085
c Ni Heat Pipe Wick
M6 28058 -0.680769
      28060 -0.262231
      28061 -0.011399
      28062 -0.036345
      28064 -0.009256
c Stainless Steel 316
M7 6012 -0.000406
      6013  -0.000004
      14028 -0.004676
      14029 -0.000238
      14030 -0.000157
      15031 -0.000230
      16032 -0.000142
      16033 -0.000001
      16034 -0.000006
      24050 -0.007387
      24052 -0.142441
      24053 -0.016152
      24054 -0.004021
```

```
      25055 -0.010140
      26054 -0.039103
      26056 -0.613834
      26057 -0.014176
      26058 -0.001887
      28058 -0.081692
      28060 -0.031468
      28061 -0.001368
      28062 -0.004361
      28064 -0.001111
      42092 -0.003693
      42094 -0.002308
      42095 -0.003975
      42096 -0.00417
      42097 -0.00239
      42098 -0.006048
      42100 -0.002418
c Beryllium Oxide
M8 4009 -0.360320
      8016 -0.639680
c Stainless Steel 304
M9 6012 -0.000396
      6013 -0.000004
      14028 -0.004611
      14029 -0.000234
      14030 -0.000155
      15031 -0.00023
      16032 -0.000142
      16033 -0.000001
      16034 -0.000006
      24050 -0.008256
      24052 -0.159199
      24053 -0.018052
      24054 -0.004494
      25055 -0.01
      26054 -0.041016
      26056 -0.643865
      26057 -0.01487
      26058 -0.001979
      28058 -0.062971
      28060 -0.024155
      28061 -0.001054
      28062 -0.003362
      28064 -0.000856
c Pu239-> used solely for production rate
M10 94239 1
c enable photonuclear physics, upper Energy limit for photons (default 100
MeV)
c Photons can generate electrons
c Coherent photon scattering enabled
c photonuclear particle production is analog,
c      causes a photonuclear event at each photoatomic event.
c Doppler Broadening is enabled
c Photofission from ACE libraries- set energy equal to that of e-
```

```
phys:p 150 1 0 -1 0 J 0
c enables (e,photon) physics
c emax =150Mev, change depending on incident beam energy
phys:e 150 0 0 0 0 1 1 1 1 0 0 J J 0.917
      0.001 0
MODE N P E
c 150 MeV electron beam incident 90 degrees to LEU axial face.
sdef pos=0 0 0 erg=150 vec 0 0 1 dir=1 par=e
c Depletion
c surface tally for Neutron flux over all 3 sides of target and fuel
surface.
F2:N 2.1 2.2 2.3 t $ T sums them all
SD2 1 1 1 3
c cell flux tally for fuel
F4:N 2
c Energy Deposition for fuel
F6:N 2
c TallyMuliplier/unormalizesSourceParticle/ReactionRates
c Reaction Rates
c electron flux over fuel
fmesh14:e geom=CYL origin 0. 0. 0.
          axs= 0. 0. 1. vec=1. 0. 0. $ rises in z-axis and azimuth is on
x-axis
          imesh 6  iints 6
          jmesh 25   jints 25
          kmesh 1    kints 8 $ single azimuthal rotation, 8 divisions
c Photon flux over fuel
fmesh24:p geom=CYL origin 0. 0. 0.
          axs= 0. 0. 1. vec=1. 0. 0.
          imesh 6  iints 6
          jmesh 25   jints 25
          kmesh 1    kints 8
c neutron flux, will list 2 times for such to use
c in 1 fission rate; 1 production rate
fmesh34:n geom=CYL origin 0. 0. 0.
          axs= 0. 0. 1. vec=1. 0. 0.
          imesh 6  iints 6
          jmesh 25   jints 25
          kmesh 1    kints 8
fmesh44:n geom=CYL origin 0. 0. 0.
          axs= 0. 0. 1. vec=1. 0. 0.
          imesh 6  iints 6
          jmesh 25   jints 25
          kmesh 1    kints 8
c Reaction rates
c bremstra photon production rate in fuel
c +fm14 -1 2 5 $ attentuation,material,(e,y) Wait for MCNP6.3
c photonuclear reaction rate* upper E limits
+fm24 -1 2 1 $ atomden,material,(y,n)
c Pu239 production rate
+fm34 -1 10 102 $ atomden,material,(n,y)
c Fission rate in fuel
+fm44 -1 2 -6 $ atomden,mat,total fiss
c power multipliers
```

```
FM4 -449638 2 -6 $ negative=AtomDen*ConstMult for M2 * -6=total MicroCS of
Fission.
nps 1000000
RAND GEN=1 SEED=19073486328125 STRIDE=152917
c End Data
```

Appendix G
ORIGEN Input File

```
=couple

'Reaction resource 80, library file 33
0$$ a3 80 a6 33 e
'Updated library ID 9022, 3 nuclides with fission yld, 238 grp
1$$ a11 9022 a15 3 a18 238 e t
'Nuclide IDs with fission yields
7$$ 922350 922380 942380
'Flux spectrum from MCNP, high E to low
9**
0.00000E+00
0.00000E+00
0.00000E+00
0.00000E+00
0.00000E+00
0.00000E+00
0.00000E+00
0.00000E+00
0.00000E+00
0.00000E+00
0.00000E+00
0.00000E+00
0.00000E+00
0.00000E+00
0.00000E+00
0.00000E+00
0.00000E+00
0.00000E+00
0.00000E+00
0.00000E+00
0.00000E+00
0.00000E+00
0.00000E+00
0.00000E+00
0.00000E+00
0.00000E+00
0.00000E+00
0.00000E+00
0.00000E+00
0.00000E+00
0.00000E+00
0.00000E+00
0.00000E+00
0.00000E+00
0.00000E+00
0.00000E+00
0.00000E+00
0.00000E+00
0.00000E+00
0.00000E+00
0.00000E+00
```

```
0.00000E+00
0.00000E+00
0.00000E+00
0.00000E+00
0.00000E+00
0.00000E+00
0.00000E+00
0.00000E+00
0.00000E+00
0.00000E+00
0.00000E+00
0.00000E+00
0.00000E+00
0.00000E+00
0.00000E+00
0.00000E+00
0.00000E+00
0.00000E+00
0.00000E+00
0.00000E+00
0.00000E+00
0.00000E+00
0.00000E+00
0.00000E+00
0.00000E+00
0.00000E+00
0.00000E+00
0.00000E+00
0.00000E+00
0.00000E+00
0.00000E+00
0.00000E+00
0.00000E+00
0.00000E+00
0.00000E+00
0.00000E+00
0.00000E+00
0.00000E+00
0.00000E+00
0.00000E+00
0.00000E+00
0.00000E+00
0.00000E+00
0.00000E+00
0.00000E+00
0.00000E+00
0.00000E+00
0.00000E+00
0.00000E+00
0.00000E+00
0.00000E+00
0.00000E+00
0.00000E+00
0.00000E+00
```

0.00000E+00
0.00000E+00
0.00000E+00
0.00000E+00
0.00000E+00
0.00000E+00
0.00000E+00
0.00000E+00
0.00000E+00
0.00000E+00
0.00000E+00
0.00000E+00
0.00000E+00
0.00000E+00
0.00000E+00
0.00000E+00
0.00000E+00
0.00000E+00
0.00000E+00
0.00000E+00
3.54323E+13
1.39802E+13
0.00000E+00
8.42005E+11
7.37483E+12
1.14079E+13
9.22063E+12
1.87176E+13
0.00000E+00
0.00000E+00
5.81405E+12
2.24560E+11
7.26197E+12
1.84440E+12
9.70668E+12
6.81691E+13
1.34235E+14
1.68061E+14
3.70698E+14
7.91448E+13
1.48568E+14
1.77044E+14
1.45542E+14
1.61375E+14
4.16290E+14
3.81858E+14
2.61602E+14
1.22627E+15
5.88323E+14
6.01867E+14
1.12253E+15
3.21902E+14
1.59777E+14
9.59479E+13

3.56834E+14
4.63104E+14
4.84998E+14
4.68019E+14
5.14809E+14
5.14607E+14
4.78261E+14
5.37184E+14
5.87165E+14
8.46124E+14
4.64373E+14
6.72433E+14
7.56141E+14
8.20507E+14
8.99717E+14
8.33247E+14
4.65555E+14
4.40570E+14
3.69819E+14
3.02764E+14
2.91491E+14
1.42743E+14
1.40409E+14
1.86590E+14
1.83823E+14
6.48736E+13
8.39301E+13
6.92676E+13
8.40952E+13
5.88835E+13
6.68578E+13
7.80158E+13
7.94474E+13
8.36210E+13
7.40420E+13
8.07234E+13
8.41183E+13
6.99647E+13
6.72511E+13
9.70156E+13
2.42721E+14
2.25834E+14
2.66899E+14
2.67326E+14
4.49069E+14
5.35710E+14
5.90354E+14
6.55611E+14
6.76918E+14
3.84201E+14
3.81732E+14
8.66501E+14
9.05708E+14
1.05720E+15

```
1.07579E+15
6.01950E+14
6.27657E+14
6.92258E+14
7.90249E+14
8.15442E+14
7.82716E+14
9.21132E+14
9.41873E+14
9.55982E+14
1.08504E+15
1.29848E+15
1.49379E+15
6.00456E+14
6.45399E+14
7.00549E+14
7.65512E+14
7.16953E+14
8.75261E+14
1.03854E+15
4.01964E+14
2.37435E+15
7.45025E+14
9.08017E+14
4.43533E+14
6.38733E+14
3.84381E+14
4.13346E+14
6.27725E+14
5.66044E+14
3.31033E+14
5.60994E+14
9.03191E+14
2.68485E+15
7.93873E+15
e t
done
end
=shell
    dir
    copy ft33f001 "${INPDIR}/ActLibtest.f33"
end
=origen
case {
       title="KRUSTYCONE_Depletion"

       lib{
              file="ft33f001"
       }
       mat{
              units="ATOMS-PER-BARN-CM"
              iso=[92235=8.206e-3 92238=3.2408e-2 42096=8.326e-3]
              volume=2248.19
       }
```

```
        time=[30]
        flux=[6.49672e16]
        print{
                nuc{ total=yes units=GRAMS }
        }
        save{
                file="test1.f71"
                steps=ALL
        }
}
end
```